In Vivo Predictive Dissolution: Analyzing the impact of Bicarbonate Buffer and Hydrodynamics on Dissolution

By

Brian Joseph Krieg

A dissertation submitted in partial fulfillment
of the requirements for the degree of
Doctor of Philosophy
(Pharmaceutical Sciences)
in the University of Michigan
2015

Doctoral Committee:

Research Professor Gregory E. Amidon, Co-Chair
Professor Gordon L. Amidon, Professor, Co-Chair
Professor Ronald G. Larson
Associate Professor Naír Rodríguez-Hornedo

Dedication

To my wife Jennifer and my mother Joyce

Acknowledgements

I would like to gratefully acknowledge all of my PhD committee members for their input and guidance to help strengthen my research. I could not ask for a better primary advisor than I had with Dr. Gregory Amidon. His knowledge and willingness to be available to discuss the work I was doing helped shape my research and made me a better scientist in the process. I would like to thank my secondary advisor, Dr. Gordon Amidon, for his guidance and for always encouraging me to follow the science in the research projects as well as making sure that I clearly and concisely stated my findings so they could have the biggest impact possible.

I would also like to thank Dr. Ronald Larson for all of his input and suggestions on the difficult mass transport problems that arose throughout the projects. This input ultimately led to a much better understanding of our hypotheses. I also would like to thank Dr. Naír Rodríguez-Hornedo who brought in a different perspective to the dissolution process and was always very passionate about the work being done.

Additionally, I would like to thank all of the collaborators during my time at the University of Michigan. I would like to thank Dr. Mohammad Taghavi for being such an excellent collaborator on the work in solving the mass transport analysis of bicarbonate in chapters 2 and 3. I would also like to thank Dr. Bertil Abrahamsson for his input and suggestions regarding the USP 4 dissolution work. Moreover, I would like to thank Dr. Erika Stippler and the USP for their help in guiding the bicarbonate project forward.

Furthermore, I would like to thank all of the lab members in both the labs of Dr. Greg Amidon and Dr. Gordon Amidon for the help they provided throughout my time in graduate

school. I would specifically like to thank Dr. Deanna Mudie, Dr. Hiro Tsume, and Dr. Arik Dahan who really helped to get me started in the lab and working on experiments.

I would like to gratefully acknowledge the financial support I received to help make the research I was doing possible. These sources of funding included the USP Fellowship, the Chingju Wang Sheu Graduate Student Fellowship, AstraZeneca Grant, and FDA Contract HHSF223201310144C.

Lastly, I would like to thank my family and friends for their support throughout my time in graduate school. Specifically my wife, Jennifer Krieg, and my mom, Joyce Baranek, who were always there to offer encouragement when I needed it and to help out in other areas of life that I would have neglected by being in Graduate School.

Table of Contents

List of Tables

List of Figures

Abstract

When a drug is given orally, one of the major factors that impacts safety and efficacy is dissolution rate. Two important *in vivo* parameters that impact dissolution that are not well accounted for in current dissolution methods are the physiological buffer species bicarbonate and hydrodynamics. This work explores important aspects of each of these.

Dissolution of pure drug using rotating disk dissolution methodology was used to evaluate the accuracy of several physically realistic simultaneous diffusion and chemical reaction schemes for CO2-bicarbonate buffer. Experimental results for ibuprofen, ketoprofen, indomethacin, 2-napthoic acid, benzoic acid, and haloperidol dissolution confirmed that the CO_2 hydration reaction is sufficiently slow that it plays an insignificant role in the hydrodynamic boundary layer. Therefore the reaction scheme of the CO2-bicarbonate buffer becomes $CO_2(aq) + H_2O \overset{k_d}{\leftarrow} H_2CO_3 \overset{K_{a1}}{\longleftrightarrow} H^+ + HCO_3^-$. Dissolution experiments were also performed in the USP 2 (paddle) apparatus using suspended ibuprofen particles and tablets to demonstrate that the CO2-bicarbonate transport analysis can be successfully applied to pharmaceutical dosage forms. This transport analysis allows for predictions of phosphate buffers that more closely simulate dissolution *in vivo*. In the case of weak acid and weak base BCS class 2 drugs phosphate buffer concentrations are typically 1-15mM at pH 6.5.

The role of hydrodynamics on particle dissolution was studied using the USP 4 (flow through) apparatus because it provides relatively well-defined fluid velocity profiles that may simulate *in vivo* conditions. Experimental results showed that increasing the fluid velocity

resulted in increased particle dissolution rates. The impact of fluid velocity can only be accurately predicted with knowledge of particle Reynolds number and the void space of the solid particles suspended in solution The suspensions studied were consistent with predictions assuming a void fraction of 0.25

The impact of hydrodynamics was also studied for erodible HPMC tablets using the USP 4 apparatus. I*n vitro* erosion studies using bulk fluid velocities that simulate average intestinal flow rates (~0.1cm/sec) resulted in erosion rates that were 2-4.5 times slower than erosion rates observed for the same formulations in humans. It was concluded that the USP 4 apparatus may not provide hydrodynamics that accurately simulate *in vivo* tablet erosion.

Chapter 1

The Impact of *In Vivo* Buffer and Hydrodynamic Parameters on *In Vitro* Dissolution

Abstract

A number of physiological parameters can impact the rate at which the drug dissolves *in vivo*. Two parameters that can play critical roles in the dissolution of oral drugs are the buffer species and the hydrodynamics. Bicarbonate is the main buffer present in the gastrointestinal tract and it can have a significant impact on the dissolution of ionizable drugs but current dissolution testing protocols do not accurately account for its effect on drug dissolution. Also, the hydrodynamics in the intestine can play a major role in dissolution and current *in vitro* testing methods typically do not account for this specifically with regards to fluid flow rate. This chapter will give a comprehensive overview of the literature that is currently available and discuss each of these factors. The role of bicarbonate buffer and fluid velocity in dissolution will be analyzed as well as how a better understanding of them can increase our knowledge to develop a more *in vivo* relevant dissolution methodology. The literature analysis will provide a background for both the experimental work and the transport analysis used to develop mathematical models to predict dissolution that can be used to improve our knowledge in the science of *in vivo* predictive dissolution.

Introduction

Dissolution testing is a key aspect for predicting the *in vivo* performance of an oral drug because the drug must go into solution before it will reach the systemic circulation. There are

numerous physiological conditions and physicochemical properties of the drug that have an effect on dissolution. Some of the most important factors that affect dissolution and their effect are listed in Table 1.1.

The conditions used in current dissolution testing methods do not accurately reflect the physiological environment that a drug encounters in the body. Having a dissolution methodology that can simulate conditions the drug and dosage form will see in the body before it is absorbed will create a valuable tool to evaluate a drug's performance *in vivo*. Two areas where current dissolution tests fail to achieve physiologically relevant conditions are the choice of buffer composition and strength as well as the hydrodynamic conditions the dosage form and drug will observe *in vivo*.

The primary buffer throughout the gastrointestinal tract is bicarbonate buffer. However, it is not commonly used as a buffer for dissolution testing because preparing bicarbonate buffer in the laboratory is a complicated process. It requires the control of carbon dioxide gas partial pressure ($CO_2(g)$). The carbon dioxide gas must be continuously pumped into the water because reacts with water to form bicarbonate. Without a constant supply of $CO_2(g)$, the carbon dioxide present in the aqueous system will be lost to the atmosphere and the buffer concentration will decrease. For this reason, the process of obtaining a bicarbonate buffer at equilibrium and at a physiologically relevant pH is time consuming and not an ideal method by which to perform dissolution testing.

In addition, this process is dependent on a number of chemical reactions taking place in the buffer solution and depends on the kinetics of these reactions. The rates of these chemical reactions add further complexity to bicarbonate buffer and this will be discussed in greater detail. It would be advantageous to use a more stable buffer that could more accurately depict

dissolution conditions in the gastrointestinal tract. A suitable substitute to bicarbonate buffer will provide a more practical way to achieve a physiologically relevant dissolution test. This will be accomplished by using predictions of dissolution rates of drugs in different buffers that match the dissolution rate in physiologically relevant bicarbonate buffer.

The first portion of this research will focus on characterizing the bicarbonate system through mathematical modeling using transport analysis to predict dissolution. The mathematical modeling will be verified experimentally by using rotating disk dissolution methodology. The mathematical model will then be applied to more practical buffers (e.g. Phosphate) to match the dissolution rates between more stable buffer systems and physiologically relevant concentrations of bicarbonate buffer that can then be verified experimentally. Lastly dissolution using the USP 2 apparatus will be investigated to see if the transport analysis can be applied to predict dissolution of drug particles in a non-static system with a diffusion layer thickness that is not clearly defined.

The hydrodynamic boundary layer has an important role in the mathematical modeling of the simultaneous diffusion and chemical reaction of particles. It is a convenient way in which to characterize the impact of hydrodynamic conditions that drug particles encounter and can be modeled using dimensionless numbers [1,2]. The current hydrodynamic conditions in standard USP dissolution apparatuses do not appear to accurately describe the stress and hydrodynamic conditions experienced by dosage forms and drug particles in the gastrointestinal tract. One way to better understand this is by considering physiologically appropriate flow rates and Reynolds numbers (Re) versus what is seen in current USP dissolution systems.

The second phase of this research will focus on developing an *in vitro* dissolution methodology that will incorporate more physiological hydrodynamic conditions (i.e.

Hydrodynamic boundary layer) to achieve conditions that resemble that of the gastrointestinal tract. This will be approached through the use dimensionless numbers (Sherwood number, Reynolds number, and Schmidt number) to identify experimental conditions that are more physiologically representative of the GI tract. The focus of this research will be concentrated on the USP 4 apparatus (flow through cell) as a potential system that permits adequate control of the hydrodynamics and specifically the fluid flow rate.

The review that follows discusses in detail the importance of buffer composition, bicarbonate buffer, and its role physiologically as well as the associated simultaneous diffusion and chemical reactions. This will lead to a discussion on how dissolution predictions will be modeled for the bicarbonate buffer system. Next, physiological modeling for the dissolution of particles with a focus on the hydrodynamic boundary layer will be examined as well as how dimensionless numbers can be incorporated to attain physiologically relevant dissolution conditions.

Physiological Importance and Relevance of Buffer Species: Bicarbonate Buffer

As shown in table 1.1, there are a number of *in vivo* parameters that affect the dissolution of drugs and an extensive study of these was reviewed by [3]Mudie et al. In terms of media throughout the gastrointestinal tract, efforts have been made to simulate fluid in the fed state (FESSIF) and fasted state (FASSIF) of the human intestine [3, 5, 4,] . These buffers typically contain bile salts, which have been shown to affect the solubility of drugs, based upon bile salt levels in the intestinal tract. The presence of bile acids in the GI tract alters the buffer capacity and can have a large impact on the dissolution rate of drugs [10]. The main buffer component used in these fluids is phosphate buffer. However, the concentration and buffer capacity of phosphate used experimentally does not give an accurate depiction of the buffer in the gastrointestinal tract.

Moreno et al. tested human intestinal fluid (HIF) against FASSIF and observed that HIF had a lower buffer capacity than FASSIF. The pH change caused by selected drugs was 5 times greater in HIF compared to FASSIF [6]. The buffer capacity of HIF was found to range from 4-13 mmol L^{-1}/pH in this study of the fasted state [13]. These values are roughly in the range of the reported values by Persson et al. who reported a buffer capacity of 2-3 mmol L^{-1}/pH in the fasted state and 13 – 15 mmol L^{-1}/pH in the fed state [7].

A difference in buffer capacity could have a large effect on the dissolution of drugs in the body. Past work in dissolution has shown that the properties of buffers and buffer concentrations can have a large effect on the dissolution of drugs [8,9,10,11]. In these studies, as the pH and buffer concentration are increased, the dissolution rate of weakly acidic drugs is also increased. McNamara and Amidon looked at the commonly used buffers acetate (pKa = 4.6), citrate (pKa=5.93), and phosphate (pKa=6.6) with respect to dissolution rates in each buffer at its maximum buffer capacity at pH 7-8 [10]. In the pH range of 7-8, the dissolution rate was found to be highest in the phosphate buffer and the lowest in acetate buffer [10]. The reason for this is that the buffer will reach its maximum buffering capacity when the pKa of the buffer becomes two units or more higher than the pKa of the drug [10].Therefore a strong emphasis needs to be placed on buffer species and concentration when evaluating the dissolution of ionizable drugs.

The main buffer in the small intestine of humans and other small animals is bicarbonate buffer. Bicarbonate plays a key role in neutralizing secreted acids in the mucosal layer which contributes to retaining a pH that is close to 7 [12]. This function is of particular relevance at the mucosal surface in the stomach and duodenum [12]. This occurs by bicarbonate reacting with HCl secretions to form carbonic acid which then can form carbon dioxide and water [13]. Bicarbonate is secreted throughout the GI lumen and it occurs at different rates throughout the GI tract [11,14].

For example, basal bicarbonate secretions have been shown at a steady rate of ~150 μmol cm^{-1} h^{-1} [1] in the proximal duodenum and ~25 μmol cm^{-1} h^{-1} in the distal duodenum [14]. The first step for the secretion of bicarbonate into the duodenum has been shown to occur through uptake of sodium bicarbonate into the enterocyte via a cotransporter [12]. Once in the enterocyte, bicarbonate will be secreted through exchange with Cl^- ions. In addition, bicarbonate can undergo paracellular migration. A simplified version of the secretion process of bicarbonate into the GI lumen and the diffusion of carbon dioxide from the lumen into the cells is illustrated in figure 1.1.

Bicarbonate concentrations vary based on location in the GI tract and other factors such as food and stress [14,15]. For example, the partial pressure of carbon dioxide has been shown to vary from 4% in arterial blood to up to 37% in the lumen during the duodenal fed state [15]. This variation in percent carbon dioxide in the body correlates with variations in the bicarbonate concentration (reaction description discussed in detail below). Therefore dissolution testing should be done at a wide variation of bicarbonate buffer concentrations to evaluate the impact of buffer concentration on drug dissolution.

McNamara et al. performed dissolution testing in systems with various percent carbon dioxide (5-20%) buffer compositions (and hence different bicarbonate buffer strengths) and compared these dissolution rates to FESSIF and FASSIF. McNamara et al. found that the dissolution rates obtained in FASSIF and FESSIF were greater for both weakly acidic drugs (indomethacin) and weakly basic drugs (dypyridamole) when compared to the bicarbonate buffer. Sheng et al. obtained similar results when using FASSIF and simulated intestinal fluid (SIF) without bile salts and with different phosphate concentrations. The dissolution study results of McNamara et al. and Sheng et al. correlate well with the data described above obtained by

Moreno et al. in which it was shown that the buffer capacity was higher for FASSIF than HIF. Thus current dissolution testing conditions must be reevaluated to obtain a more physiologically relevant buffer. In order to do so, more knowledge about the entire CO_2-bicarbonate buffer system must be obtained to accurately describe the impact this complicated buffer has on the dissolution of ionizable drugs.

The Reactions and Kinetics of the Bicarbonate Buffer System

Conversion of $CO_2(g)$ to $CO_2\ (aq)$

$$CO_2(g) \rightleftharpoons CO_2\ (aq) \qquad \text{(Rxn. 1.1)}$$

The first reaction to be considered is the first step in the process of preparing bicarbonate buffer in the lab which requires CO_2(g) conversion into its aqueous form. The solubility of CO_2(g) can be calculated using Henry's Law to calculate the concentration of carbon dioxide [$CO_2\ (aq)$] in the medium by using the partial pressure of CO_2(g) used in the different experiments. The Henry's law constant is dependent on the temperature of the system and the ionic strength. The effect of temperature can be described by equation 1.1

$$K_H(T) = Henry's\ law\ constant\ at\ Temperature\ T$$

$$K_H(\mathrm{T}) = K_H(T^\theta)\exp\left[-C\left(\frac{1}{T}-\frac{1}{T^\theta}\right)\right] \qquad \text{(Eq. 1.1)}$$

$K_H(T^\theta)$=3.4×10^{-2}; $T^\theta = 298\ K; T = Observed\ temperature;\ \ K;\ C = -2400\ K$

Harned and Davis also showed experimentally (see the table 2) that Henry's law Constant will be affected by the ionic strength, *I*, of the solution. Below are the equations to calculate K_H to correct for the presence of species that will affect the ionic strength of the solution [16].

$$K_H(\mathrm{T}) = \frac{[CO_2]\gamma_0}{P} = K_H\gamma_0 \qquad \text{(Eq. 1.2)}$$

$$K_H = \frac{K_H(\mathrm{T})}{\gamma_0} \qquad \text{(Eq. 1.3)}$$

$$log\gamma_0 + logK_H = logK_H(\mathrm{T}) \qquad \text{(Eq. 1.4)}$$

$$log\gamma_0 = pK_H - pK_H(\mathrm{T}) = bI \qquad \text{(Eq. 1.5)}$$

$$pK_H = pK_H(\mathrm{T}) + bI \qquad \text{(Eq. 1.6)}$$

$$b = constant = 0.10 \qquad \text{(Eq. 1.7)}$$

$$I = \frac{1}{2}\sum C_i\, z_i^2 \qquad \text{(Eq. 1.8)}$$

Experimentally, 0.9% NaCl may be used to obtain ionic strength near physiologic conditions.

$$I = \frac{1}{2}([Na^+] + [Cl^-]) = C$$

$$C = salt\ concentration = 0.9\%\ NaCl = 9\frac{g}{L} = 0.154M$$

$$bI = 0.10 * 0.154 = 0.0154$$

$$pK_H = pK_H^0(T) + bI$$

$$K_H = 10^{-pK_H} \qquad \text{(Eq. 1.9)}$$

Using equations 1.1-1.9 to calculate the Henry's law constant for 37°C and an ionic strength based on an isotonic solution gives a value of 0.02403. This value closely approximates the experimental values obtained shown in table 1.2 by Harned and Davis[17].

Based on the equations and experimental values for Henry's law constant, the solubility of carbon dioxide in water will decrease as the temperature and ionic strength increase. The Henry's law constant can be used along with the partial pressure of carbon dioxide (P(CO2)) being used to give the concentration of carbon dioxide in the buffer as shown below.

$$[\mathrm{CO_2}\ (aq)] = K_H P(\mathrm{CO_2}) \qquad \text{(Eq. 1.10)}$$

$$P(\mathrm{CO_2}) = \text{pressure of } \mathrm{CO_2} \text{ in atm}$$

Ex: 20% $\mathrm{CO_2}$ gives a value of 0.2 for $P(\mathrm{CO_2})$ in atm

The Reaction Between $\mathrm{CO_2}$ (aq) and $\mathrm{H_2O}$ (l)

The carbon dioxide in solution is free to react with water. This reaction ultimately leads to the formation of bicarbonate buffer. The complete reaction that takes place is shown below.

$$CO_2(aq) + H_2O \overset{K_c}{\rightarrow} H_2CO_3 \overset{K_{a1}}{\longleftarrow} H^+ + HCO_3^- \qquad \text{(Rxn. 1.2)}$$

Reaction 1.2 can be broken down into two parts to determine the overall reaction constant (K_a). The first part is the reversible reaction of the aqueous carbon dioxide to form carbonic acid as shown below.

$$CO_2(aq) + H_2O \overset{K_c}{\rightarrow} H_2CO_3 \qquad \text{(Rxn. 1.2a)}$$

The value for K_c is equal to the ratio for the hydration reaction of carbon dioxide and the dehydration of carbonic acid.

$$K_c = \frac{k_h}{k_d} \qquad \text{(Eq. 1.11a)}$$

$$K_c = \frac{[H_2CO_3]}{[CO_2(aq)]} \qquad \text{(Eq. 1.11b)}$$

The hydration (k_h) and dehydration rate constants (k_d) are significantly different and vary with temperature and ionic strength. The hydration rate constant (k_h) value varies from $0.06s^{-1}$ to $0.16s^{-1}$ and the dehydration rate constant's (k_d) value varies from $50s^{-1}$ to $80s^{-1}$ in literature in the range of 30-40^{o}C at different ionic strengths [18-21]. A comprehensive list of these values is given in table 1.3.

The concentration for carbonic acid at equilibrium is very low as evidenced by the values for the hydration rates and dehydration rates shown in the Table 1.3. Based on the constants given in Table 1.3, the hydration reaction is at least several hundred times slower than the dehydration reaction such that the concentration of carbonic acid in aqueous solutions is low relative to the other buffer species.

The Ionization of Carbonic Acid (H_2CO_3) to form Bicarbonate (HCO_3^-)

The first ionization constant of carbonic acid (K_{a1}) plays a role in determining the rate of the overall reaction.

$$H_2CO_3 \overset{K_{a1}}{\longleftarrow} H^+ + HCO_3^- \qquad \text{(Rxn. 1.2b)}$$

The value for K_{a1} is comprised of the forward reaction rate $(k_{a1f})$for the ionization of carbonic acid to form bicarbonate and the reverse reaction rate (k_{a1r}) where the bicarbonate ion reacts with a hydrogen ion to form carbonic acid.

$$K_{a1} = \frac{k_{af}}{k_{ar}} \qquad \text{(Eq. 1.12)}$$

$$K_{a1} = \frac{[H^+][HCO_3^-]}{[H_2CO_3]} \qquad \text{(Eq. 1.13)}$$

The value of K_{a1} is also affected by temperature and ionic strength. Table 1.4 presents values reported around 37°C.

There is little information regarding exact values for the forward and reverse reaction rates at 37°C. However, values for the reaction rate constants have been given by [26]Eigen and Hammes at 25 °C of $K_f = 8 \times 10^6$ and $K_r = 4.7 \times 10^{10}$. The values at 25 °C show that these rate constants are 6 to 10 orders of magnitude greater than the hydration (K_h) and dehydration rate (K_d) constants. This difference indicates that the hydration and dehydration reactions may be occurring too slowly to allow for an assumption of instantaneous chemical equilibrium. In comparison, the ionization reaction rates are so large that it can be assumed that the ionization of carbonic acid happens so rapidly that the chemical equilibrium is achieved instantaneously.

The Overall Reaction Constant K_a

In the literature, usually the entire reaction is assumed to be at equilibrium where K_c and K_{a1} are combined to give an overall pKa value (K_a). The chemical equilibrium and equation for equilibrium are shown below.

$$CO_2(aq) + H_2O \overset{K_c}{\longleftarrow} H_2CO_3 \overset{K_{a1}}{\longleftarrow} H^+ + HCO_3^-$$

$$K_a = K_c \cdot K_{a1} \qquad \text{(Eq. 1.14)}$$

$$CO_2(aq) + H_2O \overset{K_a}{\underset{\longleftarrow}{\longrightarrow}} H^+ + HCO_3^- \quad \text{(Rxn. 1.2c)}$$

$$K_a = \frac{[H_2CO_3]}{[CO_2(aq)]} \cdot \frac{[H^+][HCO_3^-]}{[H_2CO_3]} = \frac{[H^+][HCO_3^-]}{[CO_2(aq)]} \qquad \text{(Eq. 1.15)}$$

The K_a value has been studied at different temperatures and different ionic strength's. Using experimentally obtained data, it is possible to calculate K_a based on the temperature and ionic strength of the solution. An equation for the temperature effect was developed by Millero et al.

$$pK_a = -402.56788 + \frac{11656.46}{T} + 72.173\ \text{lnT} - 0.161325\ T + 7.5526 \times 10^{-5} T^2 \qquad \text{(Eq. 1.15)}$$

Corrections to adjust for ionic strength are given by [16]Butler .

$$pK_a = pK_a^0 - 1.0f(I) - bI \qquad \text{(Eq. 1.16)}$$

$$pK_{a1}^0 = constant\ given\ as\ a\ function\ of\ temperature\ without\ ionic\ strength\ dependence$$

$$f(I) = \left(\frac{I^{1/2}}{1+I^{1/2}} - 0.2I\right)\left(\frac{298}{t+273}\right)^{2/3} \qquad \text{(Eq. 1.17)}$$

$$t = temperature\ in\ \deg C$$

This function above for $f(I)$ can only be applied to a temperature range of 0 to 50° C. Applying these equations, the value for pK_a can be estimated based on the experimental conditions (eg: 37°C and a 0.9% NaCl solution) to be 6.04 which fits nicely with the experimental data given in table 1.5 for the overall reaction rate constant. Additionally this parameter was measured experimentally for our system and is consistent with this calculated value (see chapter 2)

The value for K_a is used below to calculate the bicarbonate concentration in solution.

$$K_a = \frac{[H^+][HCO_3^-]}{[CO_2(aq)]} \qquad \text{(Eq. 1.18)}$$

$$[H^+]\left[\text{HCO}_3^-\right] = K_a[CO_2\ (aq)] \qquad \text{(Eq. 1.19)}$$

$$\left[\text{HCO}_3^-\right] = \frac{K_a[CO_2\ (aq)]}{[\text{H}^+]} \qquad \text{(Eq. 1.20)}$$

Using the above equation, the bicarbonate concentration can be calculated in the bulk solution at equilibrium by monitoring [CO_2 (aq)] and [H^+]. A carbon dioxide monitor can be used to measure the percent carbon dioxide present in aqueous solution which can be converted to a value in atmospheric pressure (atm). The aqueous carbon dioxide concentration, $[CO_2\ (aq)]$, can then be found by multiplying this measured value by the Henry's Law constant under the experimental conditions of the system. In the above equation at equilibrium, K_a is constant and the $[H^+]$ can be monitored using a pH meter.

However, due to the solubility of carbon dioxide and the effect of hydrogen ions on the concentration of bicarbonate there are limitations in using bicarbonate buffer for dissolution. Dissolution testing at high bicarbonate buffer concentrations cannot realistically be performed at bulk solution pH values much below a pH of 5.5. This is shown in the Table 1.6 for the percent carbon dioxide needed to produce bicarbonate buffers of various strengths.

These values in Table 1.6 show that dissolution testing throughout the entire range of physiologically relevant pH in the small intestine (where weak acid dissolution primarily occurs) requires a wide range of %CO_2 in solution. The pH varies throughout the intestine and is lowest in the duodenal bulb which is closest portion to the stomach which will be receiving the low pH gastric secretions. The pH of the intestinal fluid is becomes higher as the fluid moves through the jejunum and the ileum. When the bulk pH is below 6, only very low concentrations of bicarbonate buffer can be made and below pH 5.5 creates situations where virtually no bicarbonate buffer can be produced because the solubility of CO_2(g) is too low to allow bicarbonate to form at these pH values. In addition, as the pH increases over 7, a buffer at low bicarbonate concentrations is difficult to prepare accurately because such a low partial pressure of CO_2(g) is required. This makes dissolution testing with physiological bicarbonate buffer

concentrations in the pH range of the small intestines (5-8) impractical. The pH values that are observed in the different portions of the small intestine are shown in Table 1.7. Table 1.7 shows an average pH range in the upper small intestines is 6 – 7. At these pH values, dissolution testing with physiologically relevant concentrations of bicarbonate buffer can be done.

Ionization of Bicarbonate (HCO_3^-) to form Carbonate CO_3^{-2}

The bicarbonate ion (HCO_3^-) can undergo ionization to form carbonate. However, at physiologically relevant pH the bicarbonate ion would not dissociate to form any significant concentrations of carbonate.

$$HCO_3^- \overset{K_{a2}}{\longleftrightarrow} H^+ + CO_3^{-2} \qquad \text{(Rxn. 1.2d)}$$

This reaction, like the bicarbonate reaction discussed above occurs essentially instantaneously [30]. The value for K_{a2} varies with temperature and ionic strength. The effect of temperature on K_{a2} was studied by Millero et al. and is shown below.

$$pK_{a2} = -122.4994 + \frac{5811.18}{T} + 20.5263 \ln T - 0.0120897\, T \qquad \text{(Eq. 1.21)}$$

Using the above equation, the value for pK_{a2} at 37° C is 10.249. The effect of Ionic strength can also be taken into account. The Davies equation can be modified to calculate the value of K_{a2} as shown below [16].

$$pK_{a2} = pK_{a2}^0 - 2.0 f(I) \qquad \text{(Eq. 1.22)}$$

The final value for pK_{a2} after taking temperature and physiological ionic strength (assuming isotonic conditions) into account is 9.94.

$$CO_2(aq) + H_2O \overset{K_C}{\longleftarrow} H_2CO_3 \overset{K_{a1}}{\longleftrightarrow} H^+ + HCO_3^- \overset{K_{a2}}{\longleftrightarrow} H^+ + CO_3^{-2} \qquad \text{(Rxn. 1.2e)}$$

The value for pK_{a2} is sufficiently greater than the pK_a so that at physiologically relevant pH values, essentially no carbonate will form.

Carbonic Anhydrase catalytic effect and physiologic relevance:

The presence of the enzyme carbonic anhydrase has been shown to catalyze the hydration and dehydration of CO_2. Carbonic anhydrase is a zinc containing metalloenzyme that has an acid form and a basic form with a pKa ~7 [31]. There are 11 known carbonic anhydrase isoenzymes that have been found to be present in mammals [32]. A number of these carbonic anhydrase isoenzymes are throughout the gastrointestinal tract (CA I,II,III,IV, and VI).
The enzymatic activity of carbonic anhydrase and the effect it has on hydration and dehydration has been studied extensively. Roughton and Booth showed that the activity of the enzyme increases as pH increases [33]. However, as Khalifah states, the equilibrium constants would not change, only the forward and reverse rate constants k_h and k_d would change [34]. This means that the uptake and output of carbon dioxide are equally catalyzed by carbonic anhydrase. This was discussed by Roughton and Booth and can be viewed as shown below.

$$K_c = \frac{k_h}{k_d} = \frac{\frac{K_{cat_h}}{K_{m_h}}}{\frac{K_{cat_d}}{K_{m_d}}} \qquad \text{(Eq. 1.23)}$$

$$K_{cat} = The\ turnover\ number$$

$$K_m = the\ Michaelis\ Constant$$

The ratio $\frac{K_{cat}}{K_m}$ provides a way to compare how effective an enzyme is towards a substrate. A ratio on the order of magnitude of 10^8 means every collision between carbonic anhydrase and carbon dioxide will result in the formation of a complex that will lead to bicarbonate being formed. The turnover number varies with each enzyme and pH and CA II has the largest at $1x10^6$ s^{-1} [35]. Additionally, Koeing and Brown obtained a $\frac{K_{cat_h}}{K_{m_h}}$ value for carbonic anhydrase of $2.1x10^8$ while Khalifah obtained a value $1.35x10^8$ [37] [36]. These large values of turnover numbers

and $\frac{K_{cat_h}}{K_{m_h}}$ for carbonic anhydrase demonstrate that this enzyme can convert carbon dioxide into its product essentially instantaneously. With these values, the rate limiting step in the presence of carbonic anhydrase becomes the diffusion of the molecules and not the reaction of carbon dioxide with water to produce carbonic acid.

However, of the isoenzyme's listed above, the one that seems to be most plausible for catalyzing the hydration/dehydration reaction of carbon dioxide in the gastrointestinal tract liquid media is CA VI. This isoenzyme is located in the human salivary glands and CA VI is the only isoenzyme among the isoforms that is secreted which allows for the case to be made that carbonic anhydrase is present in the luminal fluid of the intestines [38,39]. The other isoenzymes are located in the cyptoplasm, mitochondria, or are membrane associated [32]. These isoenzymes would theoretically not have a direct effect on the hydration/dehydration of carbon dioxide in the intestinal fluid. However, they would play a role in the overall bicarbonate equilibrium.

It has been reported that 10-14 mg of the CA VI isoenzyme are swallowed every day [38]. The concentration of CA VI fluctuates depending on the health of the person and disease state (eg: gastrointestinal disorders). In healthy patients, the average concentration of CA VI in saliva was found to be 23 mg/liter [38]. This suggests that CA VI could be present in the gastrointestinal tract. Parkkilla et al. also showed that CA VI is able to survive the highly acidic conditions of the stomach. Parkkilla et al. exposed CA VI enzyme to a pH of 2.2 for up to 30 minutes and showed there to be little reduction in enzyme activity. Since CA VI could survive the acidic conditions in the stomach, then it may be active in the fluid of the small intestine and available to catalyze the hydration/dehydration reaction of carbon dioxide. However, the presence of carbonic anhydrase has not been confirmed in the intestinal tract. Therefore the hydration and dehydration reactions are assumed to occur at their non-catalyzed rates in the lumenal fluid of

the intestines. This will be an important point to consider when evaluating dissolution experiments in the CO_2-bicarbonate buffer system and applying a mathematical model that uses a simultaneous diffusion and chemical reaction approach.

Modeling diffusion and simultaneous chemical reaction to predict dissolution rates

Background on Rotating Disks Dissolution and Diffusion Layer Gradients

Mathematical modeling will be implemented following the model formulated by Mooney et al. [40,8] that assumes simultaneous diffusion and chemical reaction in the hydrodynamic boundary layer (or diffusion layer) adjacent to the dissolving surface of the tablet using a rotating disk. The model permits the estimation of the pH at the surface of the tablet by taking into account the properties of the drug and buffer system while assuming simultaneous diffusion and chemical reaction in the hydrodynamic boundary layer. These properties include the pH of the buffer, pKa of the drug and buffer, drug solubility, and the diffusion coefficient of all of the species involved. In this model the dissolution of a drug is assumed to take place by a diffusion layer-controlled process [8].

This model has been applied to rotating disk hydrodynamics which has been characterized in terms of dissolution and diffusion layer thickness [41]. The hydrodynamic boundary layer exists because as the liquid flows along the solid surface its velocity is decreased due to friction [42]. This decrease in velocity near the solid surface creates a boundary layer where the fluid's velocity will change abruptly [42]. Within this layer transport occurs primarily by diffusion based on the concentration of all of the species present. This diffusion layer controlled process takes place through a boundary layer of a constant thickness across the solid surface [42]. The diffusion layer is a valid assumption based on the bulk solution being a homogenous well mixed mixture where no concentration gradients are present [43]. Levich characterized this

boundary layer thickness based on the liquid's physical properties, velocity, and diffusion coefficient of the solid being dissolved [41,42]. Levich applied this theory to obtain the boundary layer thickness that is seen with a rotating disk by using equation 1.24.

$$h = 1.61 D^{1/3} \omega^{-1/2} v^{1/6} \qquad \text{(Eq. 1.24)}$$

$$D = diffusion\ coefficient\ of\ the\ drug$$

$$v = kinematic\ viscosity\ of\ the\ solution$$

$$w = rotational\ speed\ of\ the\ disk\ (radians/second)$$

The correlation between the diffusion layer thickness and flux is evident by examining the equation for flux in a rotating disk system (equation 1.25). It is a function of all of the same variables with the addition of the solubility of the drug.

$$J = 0.62 D^{\frac{1}{3}} v^{-\frac{1}{6}} w^{\frac{1}{2}} \Delta C \qquad \text{(Eq. 1.25)}$$

$$\Delta C = difference\ between\ the\ solubility\ of\ the\ drug\ and\ the\ concentration\ in\ the\ bulk$$

The above equation assumes that no natural convection is occurring and that the system is operating under laminar hydrodynamic conditions [44].

Reactions and Equations for Obtaining flux in a buffered system

The reactions that are taken into account in the simultaneous diffusion and chemical reaction model developed by Mooney et al. are shown below [8]:

$$H^+ + OH^- \overset{K_w}{\leftrightarrow} H_2O \qquad \text{(Rxn. 1.3)}$$

$$HA \overset{K_a^A}{\leftrightarrow} H^+ + A^- \qquad \text{(Rxn. 1.4)}$$

$$HA + OH^- \overset{K_1^*}{\leftrightarrow} H_2O + A^- \qquad \text{(Rxn. 1.5)}$$

$$HA + B \overset{K_2}{\leftrightarrow} BH^+ + A^- \qquad \text{(Rxn. 1.6)}$$

$$BH^+ \overset{K_a^B}{\leftrightarrow} H^+ + B \qquad \text{(Rxn. 1.7)}$$

$$BH^+ + OH^- \overset{K_3^*}{\leftrightarrow} H_2O + B \qquad \text{(Rxn. 1.8)}$$

In reactions 1.3-1.8, HA is the unionized form of the drug and BH^+ is the unionized form of the buffer. Any change that is caused by chemical reactions in the diffusion layer will lead to a change in one of the products or reactants in the reactions given above [8]. Fick's laws can be applied to all of the elements involved in the above reactions to give the differential equations shown below.

$$\frac{\delta[HA]}{\delta t} = D_{HA}\frac{\delta^2[HA]}{\delta X^2} + \Phi_1 = 0 \qquad \text{(Eq. 1.26)}$$

$$\frac{\delta[A^-]}{\delta t} = D_A\frac{\delta^2[A^-]}{\delta X^2} + \Phi_2 = 0 \qquad \text{(Eq. 1.27)}$$

$$\frac{\delta[H^+]}{\delta t} = D_H\frac{\delta^2[H^+]}{\delta X^2} + \Phi_3 = 0 \qquad \text{(Eq. 1.28)}$$

$$\frac{\delta[OH^-]}{\delta t} = D_{OH}\frac{\delta^2[OH^-]}{\delta X^2} + \Phi_4 = 0 \qquad \text{(Eq. 1.29)}$$

$$\frac{\delta[B]}{\delta t} = D_B\frac{\delta^2[B]}{\delta X^2} + \Phi_5 = 0 \qquad \text{(Eq. 1.30)}$$

$$\frac{\delta[BH^+]}{\delta t} = D_{BH}\frac{\delta^2[BH^+]}{\delta X^2} + \Phi_6 = 0 \qquad \text{(Eq. 1.31)}$$

In this model, these equations are assumed to be at steady state. Using the above equations and reactions, a number of mass balance relations can be made to obtain a cubic polynomial equation to solve for the pH at the surface of the tablet in a rotating disk. This equation can easily be solved with computer software or using Newton's method. A higher pH at the surface of the tablet for weak acid drugs corresponds to a faster dissolution rate.

As reaction 1.4 illustrates, an ionizable drug acts to buffer the pH at the dissolving surface. In order to better understand how different drugs behave as self buffers, figure 1.2 shows the relative flux of drugs as pH is increased in an unbuffered dissolution medium. Figure 1.2 shows that the pH will not affect the dissolution rate of a highly soluble drug (benzoic acid)

unless it reaches a very high pH value. This is because benzoic acid is so soluble that it is able to buffer the pH at the surface of the tablet very well and resist the changes in pH. The opposite is seen with a very insoluble drug (indomethacin). A large increase in the relative dissolution rate is observed with indomethacin at a much lower pH because its solubility is sufficiently low that it is not able to buffer the surface pH as well, allowing the pH at the surface to rise and approach the bulk pH, thereby increasing dissolution rate.

The impact of adding a buffer into the bulk solution is examined in Figure 1.3. Figure 1.3 compares the pH gradient in the diffusion layer of ibuprofen when a 50mM phosphate buffer concentration is present in a pH 6.50 bulk solution to the gradient when no buffer is present in the bulk solution at pH 6.50. The high concentration of phosphate buffer helps to maintain a fairly constant pH across the diffusion layer so the pH at the surface is similar to the pH in the bulk solution. However, when no buffer is present, there is a sharp decrease in pH due to the drug forming H^+ ions at its surface that are not being consumed by a buffer species. Therefore the surface pH is much less than the bulk pH when no buffer is present for a dissolving weak acid drug.

Solving for the pH at the surface allows for all of the other unknown surface concentrations to be calculated. These calculated surface concentrations allow for the total flux of the drug to be predicted.

$$Total\ Flux = -J^{total} = -\frac{1}{h}[D_{HA}[HA]_0 + D_H([H^+]_0 - [H^+]_h) + D_{OH}([OH^-]_h - [OH^-]_0) + D_B([B]_h - [B]_0)] \quad \text{(Eq. 1.32a)}$$

$$Total\ Flux = -J^{total} = -(J_{HA} + J_H + J_{OH} + J_B) \quad \text{(Eq. 1.32b)}$$

Theoretical predictions using the film model have been shown to be accurate for various drugs (with different physicochemical properties) over a range of buffer concentration and pH ranges [8].

The work presented so far assumes a buffer with only one pKa. However, this is usually not the case with buffers such as bicarbonate and phosphate. To determine the impact of buffers with multiple pKa's on drug dissolution, Aunins et al. [9] did work with polyionizable buffers. One of the buffer's that was studied in this work was phosphate buffer which is commonly used in dissolution testing and is the main buffer component of FASSIF and FESSIF. Aunins et al. applied the same model to include the different reactions and mass balances that occur with a buffer that has more than one pKa like phosphate. The accuracy of including these additional parameters was studied by Aunins et al. by comparing predictions to experimental data and good agreement was found depending on the drug, buffer concentration, and pH of the solution. In addition, this model was compared to the more simplistic model for a monoprotic buffer. When compared, these models predicted nearly identical values as long as the pH of the solution was not within the range of the smallest or largest pKa. In the case of phosphate buffer, which has three pKa's (1.86, 6.60, 11.5), the first and third pKa would only change the shape of the dissolution predictions over the buffer concentration used if the pH used was relatively low or high [9]. This result indicates that the monoprotic buffer system would be appropriate to be used for predictions for physiologically relevant dissolution testing based on the pH of the small intestine (see table 8) where dissolution primarily occurs. Figure 1.4 specifically examined this by comparing the monoprotic and triprotic model predictions at pH 6.5 for ibuprofen over a range phosphate buffer concentration. Figure 1.4 shows that the same prediction for flux is obtained using either model at each buffer concentration. Therefore the simpler monoprotic film model will be used when predicting experimental dissolution results.

Figure 1.5 applied the monoprotic model for phosphate buffer to show predictions of flux for ibuprofen at different phosphate buffer concentrations and different bulk pH values. The

figure illustrates the major role that both bulk pH and buffer concentration play as the drug is dissolving. In order to develop an *in vivo* predictive dissolution test, these *in vitro* parameters must be as close to physiologically relevant as possible. If not, the results could be significantly different from what is occurring in intestinal tract. This makes bicarbonate buffer and the ability to predict how it impacts the dissolution of drugs so important.

Applying the model to Bicarbonate buffer:

The overall equilibrium constant (pKa = 6.04) for bicarbonate buffer and the pH range for the dissolution experiments allows for the assumption that a monoprotic buffer model can be applied to bicarbonate. However, one problem with using the film model proposed by Mooney et al. is that it may not adequately take into account the reaction kinetics of the bicarbonate buffer system in the aqueous diffusion layer. The model discussed above does not take into account the forward and reverse rate constants of each reaction. Instead it assumes the reactions are at equilibrium and it uses the overall equilibrium constant. However, as previously discussed, the uncatalyzed reaction rate for the hydration of carbon dioxide to carbonic acid is a very slow process relative to the ionization reactions. This means the assumption of equilibrium within the bulk solution may not translate into what is actually occurring in the diffusion layer. A similar situation was examined by Mooney et al. in which the drug phenylbutazone, which has non-instantaneous ionization kinetics, was studied. In this study Mooney et al. showed that non-instantaneous ionization kinetics of the drug can affect the observed dissolution rate [45]. In the pH range of 5-8 (roughly that seen throughout the intestines) the dissolution rate of d-phenylbutazone was noticeably slower than phenylbutazone. The ionization of each compound is not spontaneous but the stronger bond between carbon and deuterium was hypothesized by

Mooney et al. to slow the reaction to a greater extent [45]. This would make the forward rate constants for d-phenylbutazone smaller [45].

If the time the diffusing molecule spends in the diffusion layer is much less than the reaction time, then the reaction would presumably only be occurring in the bulk solution[45]. A way for determining whether a reaction will take place in the diffusion layer is to compare the average lifetime of a diffusing molecule in the diffusion layer using the equation by Higuchi for the residence time in the diffusion layer [46]. The average lifetime in the diffusion layer is based on its thickness, the diffusivity of the molecule, and the rotational speed of the rotating disk [45]. The reaction time depends on the first order rate constant and it defines the time needed for the reaction to be 63% complete [45].

$$t_D = \frac{h^2}{2D_i} = \frac{1.3\nu^{1/3}}{D_i^{1/3}w} \qquad \text{(Eq. 1.33)}$$

$$t_D = avaerage\ lifetime\ of\ a\ diffusiing\ molecule\ in\ the\ diffusion\ layer$$

$$t_r = \frac{1}{k} \qquad \text{(Eq. 1.34)}$$

$$t_r = reaction\ time$$

$$k = first\ order\ rate\ constant$$

Predicting extreme cases of the bicarbonate buffer reaction kinetics

Based on the hydration rate of carbon dioxide, it is possible that the hydration of carbon dioxide does not occur in the diffusion layer. In fact, Roughton and Booth showed that no bicarbonate ion is present after 1 second in a carbon dioxide saturated solution at 0^oC. Using Roughton's value of $0.131s^{-1}$ at 37^oC, Parsons describes that only 50% of the reaction would take place in 5.3 seconds and it would take 35 seconds for the reaction to be 99% complete. These times are significantly longer than the calculated time in the diffusion layer for CO_2 of 0.5 second or less depending on the thickness of the diffusion layer. Thus, the hydration reaction in

the absence of any catalyst may not be going to completion in the aqueous diffusion layer around the tablet during the dissolution test. If the hydration reaction does not occur within the diffusion layer, this would have a large affect on the chemical equilibrium in the diffusion layer. Therefore the film model of Mooney and Stella would need to be adjusted to take into account the slow reaction kinetics of the hydration reaction in order to accurately predict the dissolution of drugs. How exactly this is done and the steps that need to be taken will be examined in further detail in chapters 2-4. One hypothesis was that the only buffer reactions taking place in the diffusion layer would be the ionization reaction of carbonic acid to form bicarbonate.

$$H_2CO_3 \overset{K_{a1}}{\longleftrightarrow} H^+ + HCO_3^-$$

Based on the chemical equilibrium that was previously discussed, the pKa of the above reaction would be 3.55. This pKa is much smaller than if the hydration of carbon dioxide was assumed to be going to completion in the diffusion layer (pKa =6.04). However, the only time the hydration/dehydration reaction could be assumed to be at equilibrium is when the reaction time is very large (i.e. in the bulk solution) or if a catalytic species such as the enzyme carbonic anhydrase were present to speed up these reactions. This difference in overall equilibrium constants could have a large effect on the predictions of the dissolution rate depending on drug physicochemical properties. Additionally, it could act as an upper and lower limit for predicted dissolution rates using bicarbonate buffer. Figure 1.6 shows the predicted flux (dissolution rate) of ibuprofen is ~6 times slower when assuming no hydration/dehydration is occurring in the diffusion layer compared to when the hydration/dehydration reactions are assumed to be instantaneous.

The predictions in figure 1.6 also show that there is a clear difference in the flux when dissolution is performed in bicarbonate buffer (both models) and when dissolution is performed

in phosphate buffer. This is consistent with literature where a difference in dissolution rates in bicarbonate buffer and in 50 mM phosphate buffer was observed by both McNamara et al. and Sheng et al. This difference will be the focus of chapters 2-4 where a third model will be identified to take into account the slow reactions involved in the formation of bicarbonate buffer. This model will be shown to accurately predict dissolution in bicarbonate buffer and predict equivalent phosphate buffer concentrations.

The importance of being able to incorporate physiologically relevant media in dissolution testing can become evident when determining the dissolution profile of a new drug product or evaluating the bioequivalence of reference and generic drug products. The significance of dissolution media and bioequivalence has been studied by Alvarez et al. In their study the current USP recommended dissolution testing protocol for drug products was analyzed and compared to *in vivo* results. These drug products were shown to not be equivalent *in vivo*. However, the USP *in vitro* dissolution protocol was not able to determine the differences between brand name and generic drugs that were shown to occur *in vivo* [47]. Applying a more physiologically relevant buffer in dissolution testing should better simulate *in vivo* conditions and this will be one of the aspects studied in chapter 4. As the data will show, the buffer species and buffer concentration are critical parameters but not the only physiologic parameters that would need to be incorporated to provide an *in vivo* predictive dissolution test. However, a better buffer system should aid in predicting *in vivo* bioequivalence and assist in guiding decisions with new drug products.

Hydrodynamic Considerations for Physiologic Conditions and Parameters:

Hydrodynamics in the gastrointestinal tract are governed primarily by peristalsis. Peristalsis involves the motor patterns in the gastrointestinal tract where the lumen undergoes

partial or total occlusion as content moves through the gastrointestinal tract [48]. *In vivo* studies have been performed using MRI to look at the contraction amplitudes within the intestine [49]. When these contractions are not strong enough to completely occlude the lumen, backflow of the digesta in the lumen may occur [50]. Abrahamsson et al. observed that greater occlusion in the stomach led to increased rates of mixing. Froelich et al. showed that the mean minimal cross sectional diameter was 9.95mm and the mean maximal diameter was 20.5mm. These contractions and peristalsis occur because of the intake of calcium into smooth muscle cells and the contractions have been shown to occur at a rate of 10.96/minute [49, 48]. For matter in the intestine to be transported down the intestine, the contractions must create enough pressure to overcome the fluid friction that is present in the gastrointestinal tract [50]. Flow rates and velocities have been measured throughout the gastrointestinal tract using MRI based imaging. These values are shown in the table 1.8.

The values in table 1.8 can be applied to the diffusion layer thickness equation to obtain a similar hydrodynamic boundary layer for particles in a dissolution test. A similar theory could be applied to dimensionless numbers such as the Re number. The Re number compares the effects of viscous and inertial forces. Laminar flow is assumed to be present in the gastrointestinal tract based on low Re numbers that are obtained when looking at the properties of the fluid and flow velocities in the GI tract [50]. Abrahamsson et al. used these properties to predict Re numbers around a 1cm tablet to vary between 0.01-30 in the stomach [53]. However, these Re numbers are difficult to accurately predict because it depends on the physical conformation, the extent and mode of the contraction, and the properties of the fluid in the gastrointestinal tract [50].

In the body, a dosage form will undergo both normal and shear stress [53]. Dosage forms have been shown to undergo destruction within the stomach due to contractions [54]. These destructive forces vary depending on whether a person is in the fed or fasted state [54]. The greatest destructive forces occur in the fed state [54]. The force a tablet undergoes due to shear stress is difficult to measure however. Using data from the human stomach, Abrahamsson et al. predicted shear stress values as high as 500 dyne/cm^2 and an average of 10-70 dyne/cm^2.

Modeling the Hydrodynamic Boundary Layer of Particles

Theories and Equations:

As discussed previously in reference to the rotating disk, the diffusion layer thickness affects the dissolution rate of compounds. *In vivo* dissolution typically involves the disintegration of tablet dosage forms leading to the dissolution of particles. The diffusion layer thickness can be assumed to be constant for very large particles (approaching infinite curvature) or tablets that undergo little change in size (eg. Rotating disk) during the dissolution process [55]. Modeling of the hydrodynamic boundary layer (or diffusion layer) of particles may be based on the Noyes Whitney equation to describe dissolution.

$$\frac{dm}{dt} = k_{diss}(C_s - C_t) = A\,k_{mass}(C_s - C_t) = A\,k_{mass}\Delta C \qquad \text{(Eq. 1.35)}$$

$k_{diss} = the\ dissolution\ rate\ coefficient$ (cm^3/sec)

$k_{mass} = the\ mass\ transfer\ coefficient$ (cm/sec)

$A = solid\ surface\ area$(cm^2)

$C_s = solubility\ at\ the\ solid\ surface$(mass/cm^3)

$C_t = the\ drug\ concentration\ in\ the\ bulk$ (mass/cm^3)

The mass transfer coefficient in the Noyes Whitney equation is equal to the diffusion coefficient of the drug divided by the diffusion layer thickness.

$$k_{mass} = \frac{D_{eff}}{h_{app}} \qquad \text{(Eq. 1.36)}$$

$$\frac{dm}{dt} = A\, k_{mass} \Delta C = \frac{AD_{eff}\,\Delta C}{h_{app}} \qquad \text{(Eq. 1.37)}$$

The effect of the mass transfer coefficient on spherical particle dissolution has been modeled by Hixson and Crowell, Higuchi and Hiestand, Niebergall et al, and Wang and Flanagan. The Hixson and Crowell model is equivalent to the Noyes Whitney equation shown above. In this model, it is assumed that the mass transfer coefficient is a constant and that the diffusion layer thickness is a constant [56]. This equation is shown below.

$$\frac{dm}{dt} = K(C_s - C_t) \qquad \text{(Eq. 1.38)}$$

$$K = constant$$

Higuchi and Hiestand modeled the dissolution of spherical particles assuming that dissolution is diffusion controlled, the bulk solution concentration is negligible at all times, and particle shape was assumed to be a sphere [57]. In addition, the diffusion layer thickness was assumed to be equivalent to the particle radius (or greater) which is shown in their model for particle dissolution [57].

$$\frac{dm}{dt} = D4\pi r^2 \frac{dC}{dr} \qquad \text{(Eq. 1.39)}$$

Equation 1.39 (Higuchi and Hiestand equation) shows that dissolution is dependent on the radius of the dissolving particle.

The Niebergall et al. model differs from the other two models by describing the diffusion layer thickness to be proportional to the square root of the particle diameter [55]. This is shown in equations 1.40 and 1.41.

$$h_{app} = kd^{1/2} \qquad \text{(Eq. 1.40)}$$

$$k = constant$$

$$d = diameter$$

$$\frac{dm}{dt} = \frac{DA}{k\sqrt{d}}\,\Delta C \qquad \text{(Eq. 1.41)}$$

Wang and Flanagan derived a variation of the Noyes Whitney equation where the diffusion layer thickness is based on the radius of curvature of the dissolving surface which gave equation 1.42 shown below [58].

$$\frac{dm}{dt} = A\,D_{eff}\left(\frac{1}{\alpha} + \frac{1}{r_p}\right)\Delta C \qquad \text{(Eq. 1.42)}$$

$$r_p = radius\ of\ particle\ curvature$$

$$\alpha = constant$$

According to Wang and Flanagan, the value of α in this equation, $\left(\frac{1}{\alpha} + \frac{1}{r_p}\right)$, is a constant. This equation shows that as the radius goes to zero (when α >> r), the diffusion layer thickness depends on the particle radius. When the radius is large (when r>> α), the diffusion layer thickness is dependent on the constant α.

The idea of a constant diffusion layer thickness above a critical particle size was proposed by Hintz and Johnson. According to the Hintz and Jonson model, the diffusion layer thickness is equal to the radius of the particle until it reaches a critical value when it becomes constant [59,2] . Multiple studies have been done to evaluate the critical particle size at which a constant diffusion layer thickness applies and what constant diffusion layer thickness fits the data the best. Hintz and Johnson theorized the diffusion layer thickness is equal to 30μm for particles with a radius larger than 30μm and becomes equal to the radius of the particle when the radius is less than 30μm through fitting dissolution data obtained using a rotating paddle on various sizes of disks of compressed drug. Sheng et al. looked at the diffusion layer thickness for the BCS Class II drug fenofibrate using the Paddle method at both 50 RPM and 100 RPM. The test was performed on suspensions of varying particle size to observe the affect of particle size. When the

paddle was rotated at 100 RPM, the diffusion layer thickness was found to have a constant value of 43.5μm for particles with radius's greater than 23.7μm [60]. However, when the paddle was rotated at 50 RPM, the diffusion layer thickness continued to slowly increase as the radius of the particle increased [60]. The Sheng et al. results differ somewhat from the Hintz and Johnson model because the dissolution rate obtained is smaller than what would be expected based on the Hintz and Johnson model. A comparison of these models is shown in n figure 1.8.

Diffusion Layer Thickness and Dimensionless Numbers:

The mass transfer coefficient and diffusion layer thickness can be expressed through the use of dimensionless numbers [2]. The dimensionless numbers of most relevance for characterizing dissolution are the Reynolds number (Re) and the Schmidt number (Sc). The Re number compares the ratio of momentum forces to viscous forces. In a laminar flow (low Re numbers with no disruption to parallel flow) case, the viscous forces dominate. For turbulent flow (high Re numbers where there is chaotic flow), inertial forces dominate. Sc is a ratio of kinetic viscosity and molecular diffusivity and is assumed to be constant (under experimental conditions) [61].

$$\boldsymbol{Re} = \boldsymbol{d} \times \mathbf{v} \times \boldsymbol{\rho}/\boldsymbol{\nu} \qquad \text{(Eq. 1.43)}$$

d = sphere diameter

v = Linear Velocity

ρ = fluid density

ν=fluid viscosity

$$\boldsymbol{Sc} = \boldsymbol{\upsilon} \times \boldsymbol{\rho}/\boldsymbol{D_{eff}} \qquad \text{(Eq. 1.44)}$$

$$D_{eff} = effective\ diffusion\ coefficient\ of\ the\ drug$$

The Sherwood number (Sh) is a combination of the Re and Sc numbers that is used to equate the differing characteristics observed in mass transfer through molecular diffusion and

fluid flow [1,2]. The Sherwood number defined in equation 1.45 is based on data from Ranz and Marshall. Ranz and Marshall looked at the evaporation of drops in terms of mass and heat transfer and fit the data to a ratio of Re and Sc. It was assumed that when the Re number was equal to zero, the mass transfer would need to have a value of two to obtain the vapor diffusivity in air [1]. Using this assumption and the experimentally fitted data, equation 1.45 was obtained.

$$Sh = 2 + 0.6Re^{1/2}Sc^{1/3} \qquad \text{(Eq. 45)}$$

The mass transfer coefficient can be defined in terms of dimensionless numbers [1,2].

$$k_{mass} = \frac{D_{eff}\,Sh}{d_p} \qquad \text{(Eq. 46)}$$

$$d_p = particle\ diameter$$

Using the above equations, it is possible to relate the mass transfer coefficient above to the effective diffusion layer and put it in terms that would take into account the particle size and fluid velocity experienced by the particles. The dimensionless numbers defined above are incorporated into the diffusion layer thickness and the mass transfer coefficient.

$$\frac{dm}{dt} = A\,D_{eff}\frac{Sh}{d_p}\Delta C \qquad \text{(Eq. 1.47)}$$

Equation 1.47 allows for the dissolution rate to be expressed in terms of experimental parameters that can be inserted into the Re and Sc numbers for the Sh number definition. These parameters include the velocity the particle experiences *in vivo* and can be adjusted to meet physiologically relevant properties and allow for a more accurate dissolution tests to be performed based on conditions in the GI tract. Therefore large fluid velocities observed in a USP 2 apparatus make the value for Sh much larger which leads to a small diffusion layer thickness that is much smaller than what would be expected physiologically. This is shown in figure 1.7.

Based on the Sh values, the diffusion layer thickness can be calculated for and compared to the other models proposed by Hintz and Johnson and Sheng et al. When the diffusion layer thickness is calculated using dimensionless numbers (assuming fluid velocity in the intestine (0.13cm/s)), the initial thickness is similar to both the Sheng et al. (at 100 RPM) and the Hintz and Johnson model. However, the diffusion layer thickness does continue to vary with radius and will not become a constant for particles less than 100 μm. A comparison of these models is shown in figure 1.8.

Conditions in Different Dissolution Apparatus':

As described above, the physiological conditions in the gastrointestinal tract vary. When the agitation around a tablet and/or drug particles is increased, the rate of dissolution will increase. However, if the agitation is large, drugs with different properties may exhibit similar dissolution rates even though they behave differently in the body [62]. Therefore, it would be advantageous to have a dissolution apparatus that can mimic physiologic hydrodynamic conditions. The apparent diffusion layer thickness for particles of different size derived above can be used along with physiological parameters to create a dissolution test that is more physiologically relevant in a hydrodynamic sense. For example, the relative velocity that a particle experiences in the GI tract could be used in an apparatus and applied to a suspension of particles. This would create a situation where the particles would have hydrodynamic conditions similar to the GI tract and therefore have a diffusion layer thickness similar to particles in the GI tract. A similar situation could be obtained through the use of the Reynolds number. If a physiologically relevant Re number could be achieved in a dissolution apparatus, the diffusion layer thickness would be expected to be comparable to the expected value in the body.

USP 2 Apparatus (Paddle Method):

When choosing an apparatus for dissolution testing of particles, the most common method is the USP apparatus 2 (Paddle) method. However, it does not appropriately depict physiologic conditions based on the known hydrodynamic environment of the system. As described above, the Re numbers experienced throughout the Gastrointestinal tract are quite low (0.01 – 30). However, the Re numbers in the USP 2 paddle apparatus are much larger. Figure 9 shows how much the Re numbers vary depending on the rotational speed and that they are on the order of magnitude of $5x10^3 – 1x10^4$ using the equation shown below.

$$Reynolds\ number\ for\ the\ paddle\ method = Re = \frac{Ur}{v}\ \text{(Eq. 1.48)}^{63}$$

$$U = representative\ fluid\ velocity$$

$$r = dimension\ of\ the\ paddle$$

$$v = viscosity\ of\ the\ fluid$$

In addition to the high Re numbers, there is a large the variation in agitation and shear rates throughout the USP 2 apparatus. It has been observed that, at a rotational speed of 50 RPM, the agitation rate varies and reaches a minimum at the bottom of a USP vessel when using the paddle method [64,65]. The USP 2 apparatus shows that the shear rates throughout the vessel are heterogeneous and that the lowest shear strain can be seen in areas where a tablet would be located [65]. The highest shear rates occurred around the impeller and at the walls while the lowest are seen between the shaft of the impeller and the wall of the dissolution apparatus [65]. Shear rate quantities are affected by rotational speed (the distribution stays constant) and were as high as $185s^{-1}$ with a rotational speed of 100 RPM [65]. The variability in the hydrodynamics of the USP 2 apparatus does not make it an ideal system for physiologically relevant dissolution testing. This heterogeneous stress in the USP 2 system has been looked at with respect to a tablet and it has

been shown to cause uneven dissolution across the tablet's surface [66]. This would affect particles as well as they would be undergoing different conditions throughout the apparatus.

USP 4 Apparatus (flow through cell)

The USP 4 apparatus (flow through cell) is a possible alternative to be used for obtaining more physiologically relevant dissolution because of the experimental conditions it provides. The flow rate can be varied to a large extent to mimic those seen in the body and Re numbers can be obtained that fit the estimated values by Abrahamsson et al. The properties seen in the flow through cell vary with the width of the flow through cell and the fluid flow rate [67]. By varying the size of the flow through cell and the flow rate, Cammarn et al. obtained Re numbers that varied in the range of 3.7 – 292. As experimental conditions lead to increased Re numbers in the USP 4 apparatus, Cammarn et al. showed that the dissolution rate increased [61]. This data was taken from Cammarn et al. and made into a plot (Figure 1.10) to show the relationship between the experimental Re number and the observed dissolution rate.

The flow in the USP 4 flow through cell can be made much more homogenous than that seen in the paddle method when the appropriate conditions are used. Shiko et al. observed that a homogenous flow could be obtained in a 12mm cell using a flow rate of 4-8 ml/min but the flow will start to deviate when the flow rate is increased to 16 ml/min. However, when a 22.6 mm cell is used, the flow becomes heterogeneous starting at a flow rate of 8 ml/min and the 16 ml/min flow rate is much more heterogeneous than that seen in the 12mm cell [67]. Additionally, the flow characteristics can be affected by the presence of no beads, open column (a single bead), or a packed bed where the fluid enters the flow through cell. Kakhi showed that an open column or packed bed increases the area for flow by an order of magnitude when compared to a situation with no beads present. The flow is similar in both the open and packed bed conformation

because it is flat and symmetrical in each case [68]. In addition, the shear stress profile is quite similar and it is proposed that differences in dissolution observed by the open and packed bed would not be related to the fluid dynamics of the vessel [68]. This creates a better defined system for dissolution testing with properties that could produce hydrodynamic conditions more similar to those seen in the gastrointestinal tract.

The flow rates used in the flow through cell can be converted to linear velocity and applied to the derived equation for diffusion layer thickness by applying the equation of Cammarn et al. for linear velocity in a flow through cell.

$$Linear\ velocity = \frac{U}{\rho A} \qquad \text{(Eq. 1.49)}$$

$$U = flow\ rate$$

$$\rho = media\ density$$

$$A = area\ for\ flow$$

area for flow = A = cross sectional area of the cell − cross sectional area of the tablet/particles

Applying Equation 1.49 will allow for fluid velocities to be achieved within the flow-through cell dissolution apparatus which can more closely match physiologically relevant conditions. This will help in creating a more appropriate hydrodynamic condition and corresponding hydrodynamic boundary layer (i.e. diffusion layer thickness) that drug particles will experience *in vivo* and should provide a more realistic set of conditions in which to evaluate dissolution rate.

Conclusion

The effect of buffer species and concentration as well as the hydrodynamics employed in dissolution testing play a major role in the dissolution rate of drugs. The purpose of this research is to increase the physiological relevance of dissolution testing with respect to each of these aspects. This will provide greater reliability in characterizing how a drug product will act in the

gastrointestinal tract. In addition, the mathematical modeling of buffer and diffusion layer thickness of particles should offer insight into what parameters should be used for the current buffer and apparatus used for dissolution testing. This will assist in providing a more meaningful way for determining bioequivalence for generic drugs.

Chapters 2-4 will address the complex bicarbonate buffer system. This will be done by considering the reaction kinetics involved with the buffer and applying these to a model to accurately describe their affect on the chemical reactions that occur at the surface of the tablet and within the diffusion layer during dissolution. The successful modeling, when applied to pure drug in a rotating disk system, will allow for the experimental exploration of the model to other buffer systems and dosage forms in the USP 2 dissolution apparatus. This will allow for qualifications to be made on the effectiveness of physiologically relevant buffers to provide meaningful dissolution results that are predictive of *in vivo* results

Chapters 5-6 will address dissolution and erosion studies in the USP 4 apparatus. These chapters will address incorporating the velocities a dissolving particle or eroding tablet will see *in vivo* into an *in vitro* study and how this can impact each of the respective processes. Accurate modeling of the effect velocity has on the diffusion layer thickness of particles will allow for physiologically relevant parameters to be used to approximate the rate at which particles will dissolve in the GI tract.

Two of the most important factors for a dissolving drug *in vivo* are the dissolution media and the hydrodynamics. If modeling bicarbonate buffer effects and hydrodynamic effects on the diffusion layer separately are successful, then this would enhance our knowledge of two critical factors in dissolution testing and will give a more complete view of drug dissolution in the intestinal tract.

Tables

Table 1. 1 Physiological and physicochemical factors that affect dissolution rate in the body and their corresponding Parameters in the body.

Factor	Affect on Dissolution Rate	Physiologically Relevant Data
Drug Properties: Solubility	↑ Solubility ↑ dissolution rate	The physiological properties can have an impact on each of the drug properties listed
pKa	Depends on the pH of the system	
Diffusion Coefficient	Larger diffusion coefficient corresponds to a ↑ dissolution rate	
pH	Weak acid: ↑ pH ↑ dissolution rate Weak base: ↑ pH ↓ dissolution rate	[3] pH range in GI Tract (stomach through intestine) 1.5 – 8.0
Volume of the fluid	↑ volume causes a ↓ in the bulk concentration and ↓ dissolved drug effect on the bulk solution which leads to an ↑ dissolution rate	Stomach (ml): Fasted state [4] 13-72, [3] 300; Fed state [4] 534-859, [5] 500; Small intestine (ml): fasted state [4] 45-319, [4] 200; Fed state [4] 20-256, [5] 1000;
Buffer Species	Can ↑ dissolution rate of an ionizable by limiting pH change at the surface of the drug particle or tablet depending on buffer pKa	Bicarbonate is the buffer species present in the gastrointestinal tract
Buffer concentration	↑ Buffer concentration ↑ dissolution rate for ionizable drugs	[6] Bicarbonate Concentrations (mM): Stomach: 9 – 20; Duodenum: 3-15; Jejunum: 2-20, 30; Ileum: 40, 50, 70, 74, 75;
Presence of bile salts	↑ drug solubility/wetting effect	[3] Concentrations (mM): Duodenum: fasted state = 6.4±1.2; fed state = 14.5±9.4; Upper Jejunum: fasted state = 5 fed state = 15 Lower Jejunum: fasted state = 6;
Hydrodynamics	Motility and contractions affect stress placed on the tablet/particles	[7] Contractions occur at a rate ~11/minute in the small intestine
Flow rate	↑ Flow rate ↑ dissolution rate	[8] Stomach (ml/min): 4.8 - 34.8 [9] Small intestine (ml/min): 1.62 – 30.96

Table 1. 2. Measured values from literature and estimated values of Henry's Law Constant for Carbon Dioxide at different temperature and ionic Strength

Solvent	Temperature (^{o}C)	Henry's Law Constant
Water	35	0.02678 [17]
Water	40	0.02407 [17]
0.2 M NaCl Solution	35	0.02553 [17]
0.2 M NaCl Solution	40	0.02289 [17]
Isotonic solution (0.0154 M)	37	0.02403 *

*Estimated using the van't Hoff Equation for temperature dependence and ionic strength dependence from Butler[16]

Table 1. 3. Experimental values from literature obtained for the hydration and dehydration rate constant of carbonic acid, carbon dioxide and water.

Temperature (^{o}C)	Solvent	K_h (s^{-1})	K_d (s^{-1})
38	Buffer mixture with Gaseous CO_2	0.161 [19]	
40	Water	0.143 [94]	
38	Phosphate Buffer	0.062 [95]	
37	Water	0.145 [23]	49.5 [23]
32.5	HCl and Sodium Bicarbonate Mixture (made to ionic strength of 0.65 with NaCl)	0.057 [18]	50.2 [18]
36.7	Water		80 [20]
36.9	HCl and Sodium Bicarbonate Mixture		49.04 [21]
37	HCl and Potassium Bicarbonate Mixture (0.1 M Ionic Strength)		72 [22]

Table 1. 4. Experimental values from literature obtained at different experimental conditions for the equilibrium constant K_{a1} (ratio of the forward and reverse ionization reaction).

Temperature (^oC)	Solvent	K_{a1}	pKa1
35	Buffer with NaCl (Ionic Strength =0.143)	2.816×10^{-4} [24]	3.55
35	Aqueous Solution	1.67×10^{-4} [25]	3.78
38	Aqueous Solution	1.59×10^{-4} [25]	3.80

Table 1. 5. Experimental values from literature obtained at different experimental conditions for the overall equilibrium reaction constant $\boldsymbol{K_a}$

Temperature (^oC)	Solvent	pK_a
35	Aqueous Solution	6.3094 [17]
35	Aqueous Solution	6.3086 [27]
35	Aqueous solution made to ionic strength 0.1 with NaCl	6.0683 [27]
35	Aqueous solution made to ionic strength 0.2 with NaCl	6.0091 [27]
40	Aqueous Solution	6.2978 [17]
40	Aqueous solution made to ionic strength 0.1 with NaCl	6.0529 [27]
40	Aqueous solution made to ionic strength 0.2 with NaCl	5.9935 [27]
38	Phosphate buffer with sodium bicarbonante (ionic strength = 0.12)	6.09 [28]
32.5	HCl and Sodium Bicarbonate Mixture (made to ionic strength of 0.65 with NaCl)	5.9354 [18]
37	Isotonic solution (ionic strength =0.154)	6.045 Calculated

Table 1. 6. % CO_2 needed to produce various bicarbonate buffer concentrations at a range of physiologic pH values.

pH	5.0 %CO_2	10 %CO_2	15 %CO_2	20 %CO_2	40 %CO_2	60 %CO_2
5	**0.11**	**0.22**	**0.33**	**0.44**	**0.88**	**1.31**
5.5	**0.35**	**0.69**	**1.04**	**1.39**	**2.77**	**4.16**
6	**1.10**	**2.19**	**3.29**	**4.38**	**8.77**	**13.15**
6.5	**3.47**	**6.93**	**10.40**	**13.86**	**27.72**	**41.58**
7	**10.96**	**21.92**	**32.87**	**43.83**	**87.66**	**131.49**
7.5	**34.65**	**69.30**	**103.95**	**138.61**	**277.21**	**415.82**

Table 1. 7. pH values inside the different portions of the intestinal tract (recreated from [29]Dressman et al 1998).

Location	Fasted State pH	Fed state pH
Mid-distal duodenum	4.9	5.2
	6.1	5.4
	6.3	5.1
	6.4	
Jejunum	4.4-6.5	5.2-6.0
	6.6	6.2
Ileum	6.5	6.8-7.8
	6.8-8.0 (range)	6.8-8.0
	7.4	7.5

Table 1. 8. Experimentally determined flow rates and velocities of fluid in the GI tract

Measured Value Location	Flow Rate (ml/min)	Velocity
[51]Stomach	Fully open pylorus = 4.8 Peak retropulsive velocity= 34.8	Peak velocity = 0.74 cm/s
[52]Small intestine	Range = 1.62 – 30.96 Average = 11.28	Mean velocity = 0.129 cm/s
[50]Ileum and Jejunum	Fasted state = 0.73 Fed state = 3.0	-

Figures

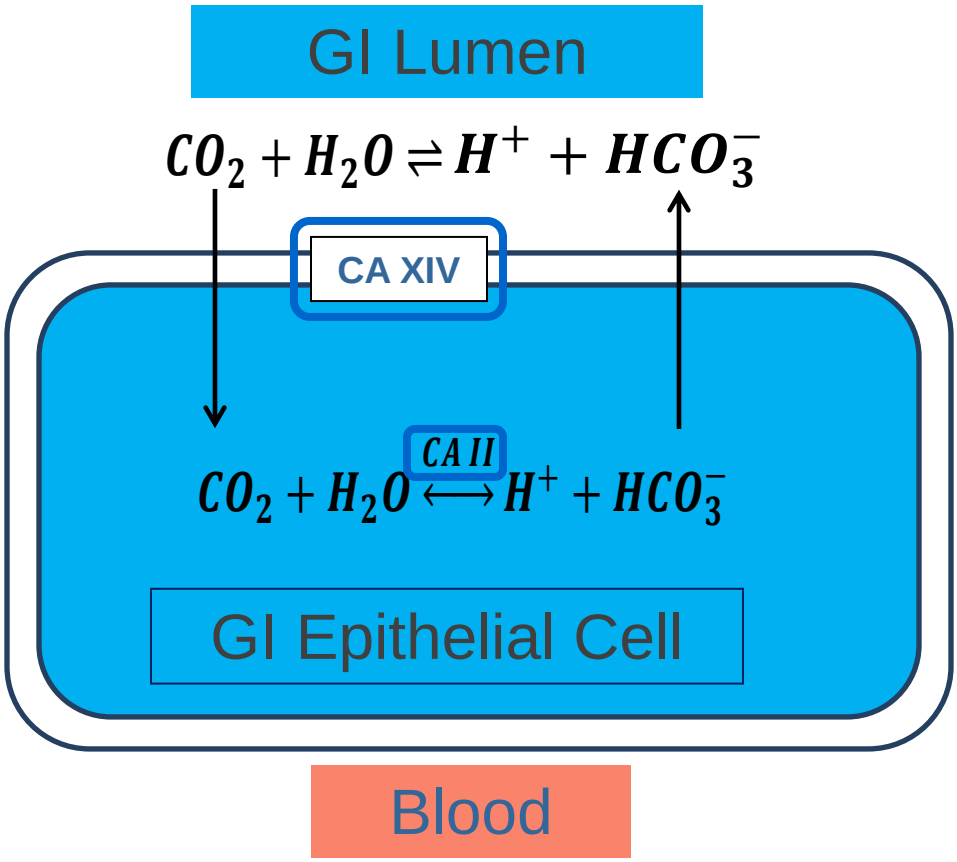

Figure 1. 1. Jacob stewarts cycle depiction for the formation of bicarbonate in the GI epithelial cells and in the GI lumen.

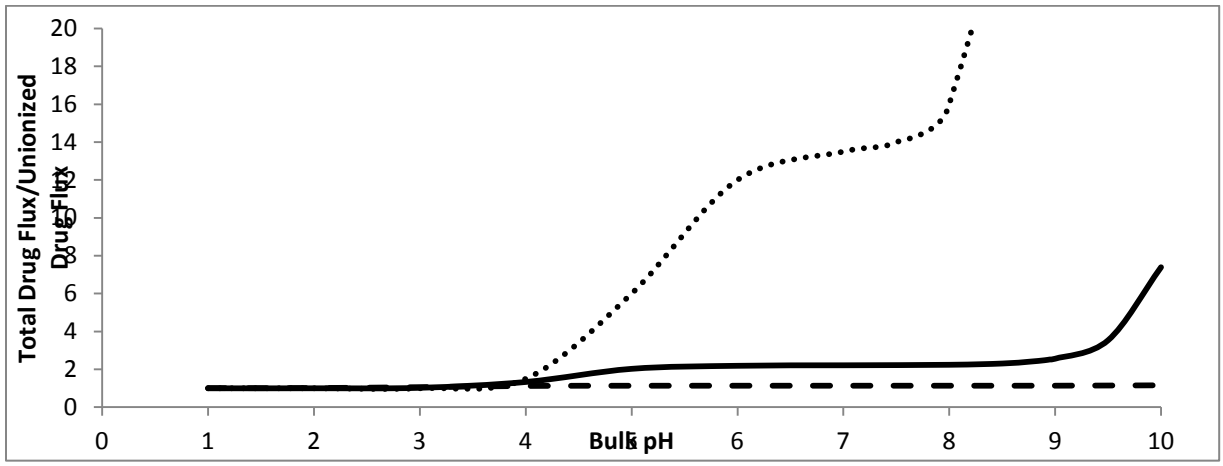

Figure 1. 2. The relative flux (total drug flux/unionzed drug flux) of weak acid drugs with varying physicvochemical properties at different bulk pH values . Predictions for indomethacin (⋯⋯) ; Predictions for Ibuprofen (———); Predictions for Benzoic Acid (– –) at different pH's.

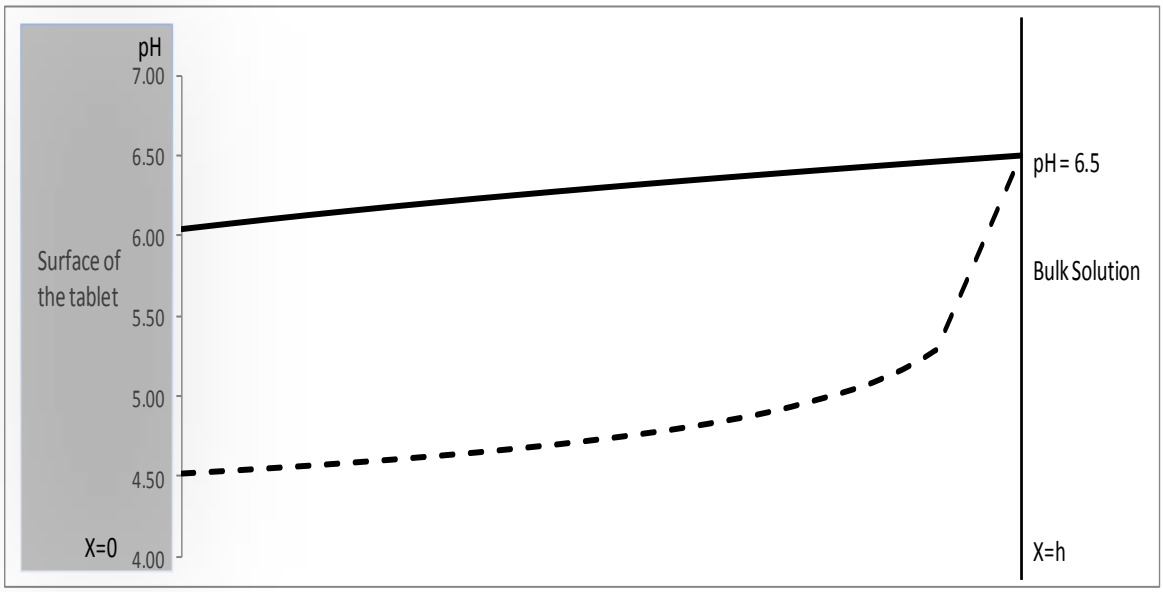

Figure 1. 3. A comparison of the predicted pH gradient in the diffusion layer of a 50mM phosphate buffer at pH 6.5 versus when no buffer is present at pH 6.5. Predictions for 50mM phosphate buffer (———); Predictions when no buffer is present (– –)

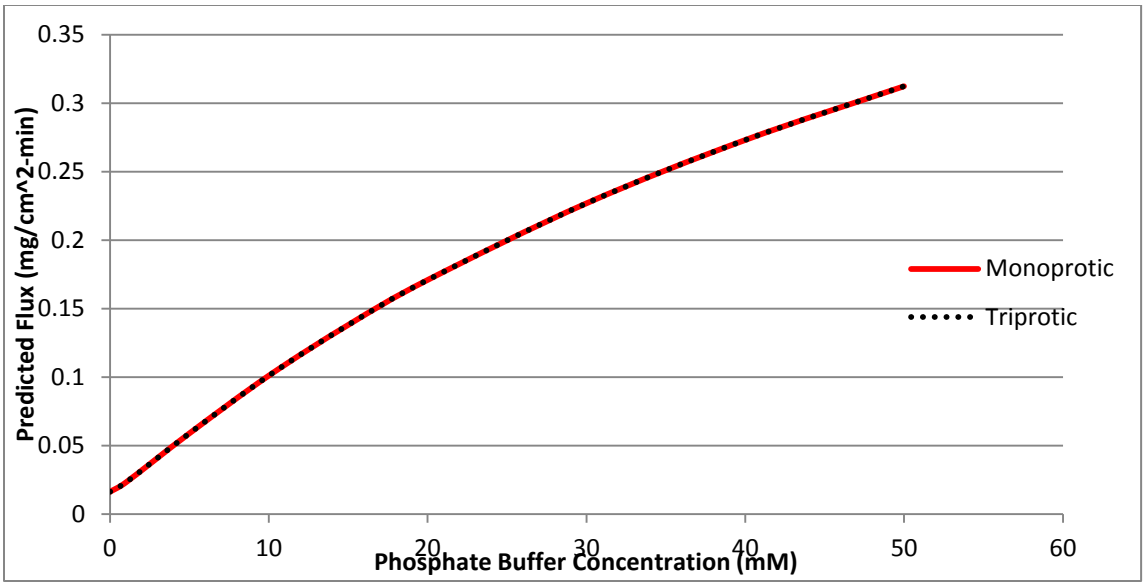

Figure 1. 4. Comparing predictions of ibuprofen flux over a wide variation in phosphate buffer concentration at pH 6.5 when using a monoprotic and triportic buffer system model. Predicted ibuprofen flux made using the monoprotic buffer model (——); Predicted ibuprofen flux using the triprotic buffer model (·····);

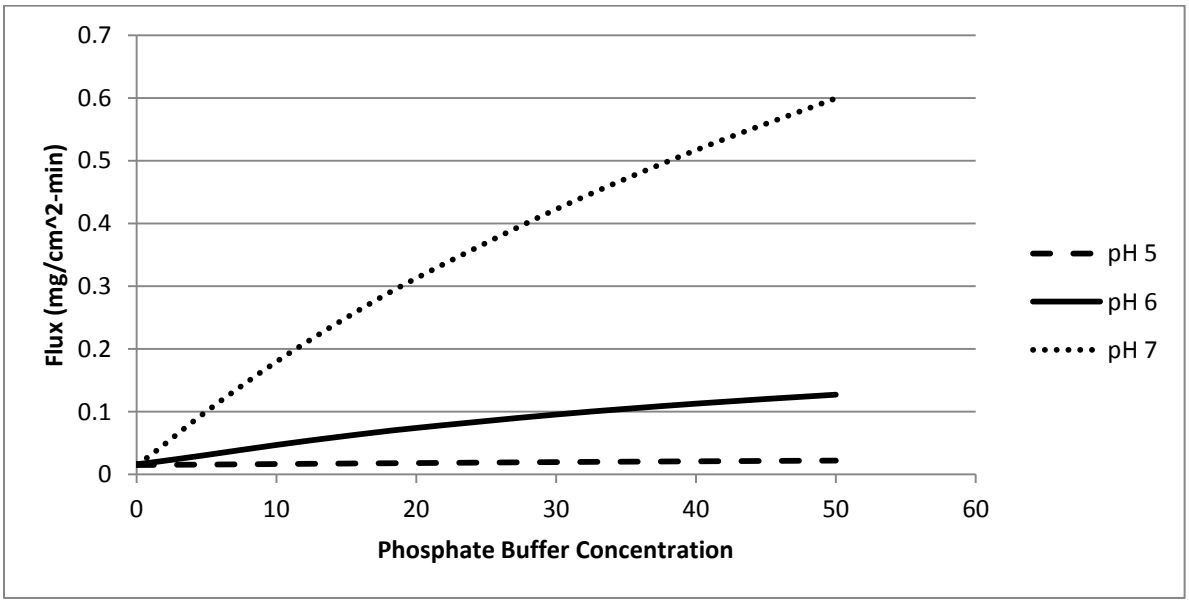

Figure 1. 5. Predicted flux of ibuprofen vs. phosphate buffer concentration. Predictions at bulk pH 5.0 (– –); Predictions at bulk pH 6.0 (——); predictions at bulk pH 7.0 (·····).

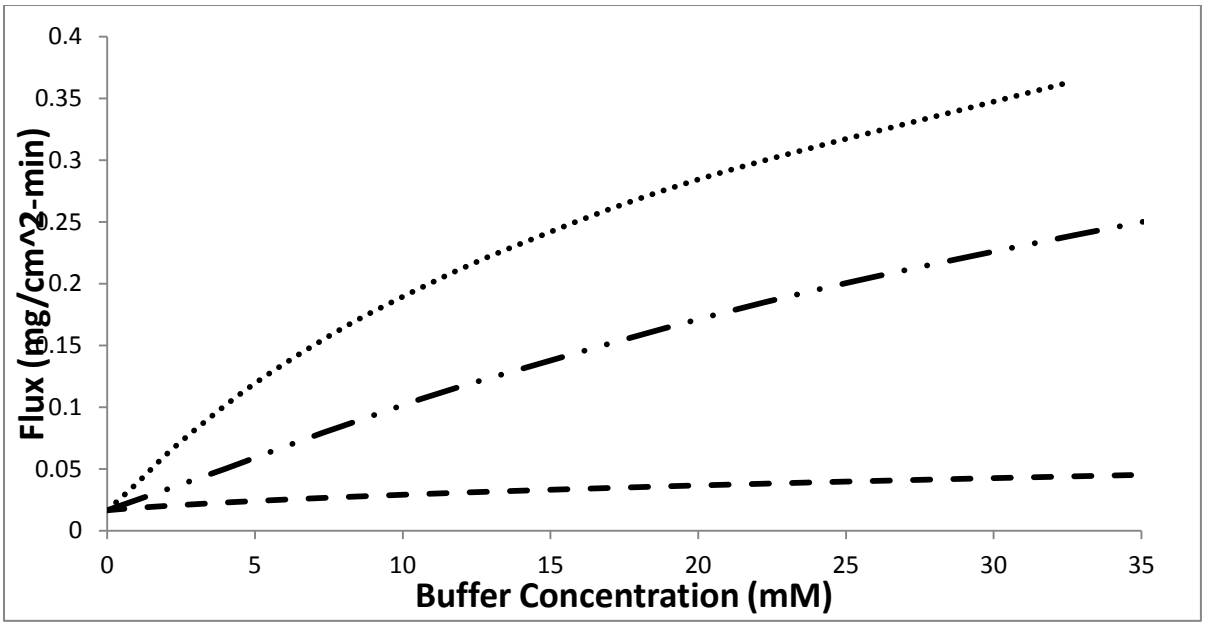

Figure 1. 6. Predicted dissolution rate of ibuprofen in bicarbonate buffer and in phosphate buffer at different buffer concentrations. Predictions in bicarbonate when the hydration/dehydration reaction of carbon dioxide with water is instantaneous (·····); Predictions in bicarbonate when the hydration/dehydration reactions do not occur (– –); Predictions in Phosphate (—— · ·)

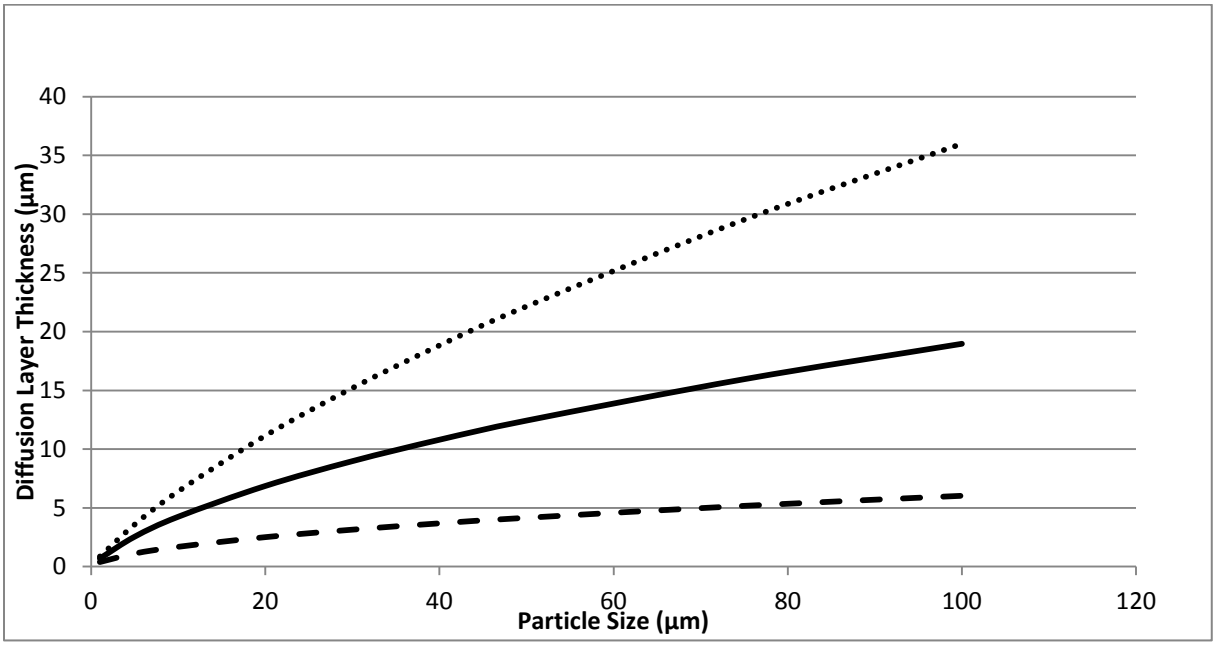

Figure 1. 7. Comparison of diffusion layer thickness predictions using Ranz and Marshall Sh# based on stomach fluid velocity, intestinal fluid velocity, and the USP 2 apparatus fluid velocity. Predictions based on the fluid velocity in the intestine (·····), Predictions based on fluid velocity in the stomach (——); Predictions based on the fluid velocity observed in a USP 2 Apparatus (– –);

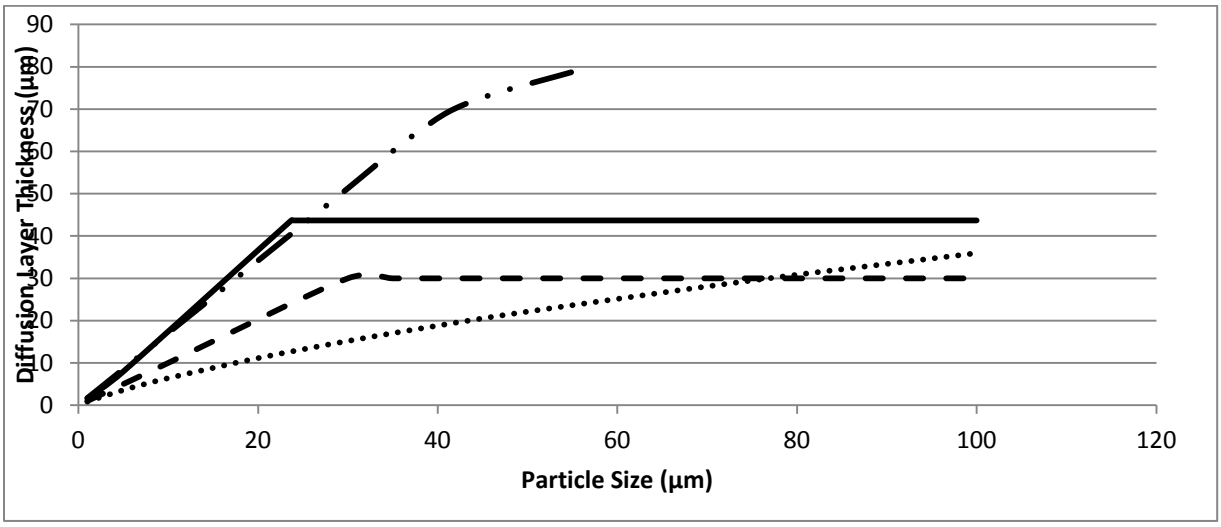

Figure 1. 8. Comparison of the diffusion layer thickness at different particle size radius' based on the different approaches to predicting diffusion layer thickness. Predictions using the Sheng et al. Model using a USP 2 apparatus at 50 RPM(— · ·) and 100 RPM(———), Predictions using the Hintz and Johnson model (– –) Predictions using dimensionless numbers following sugano and the Ranz and Marshall Sh# (·····).

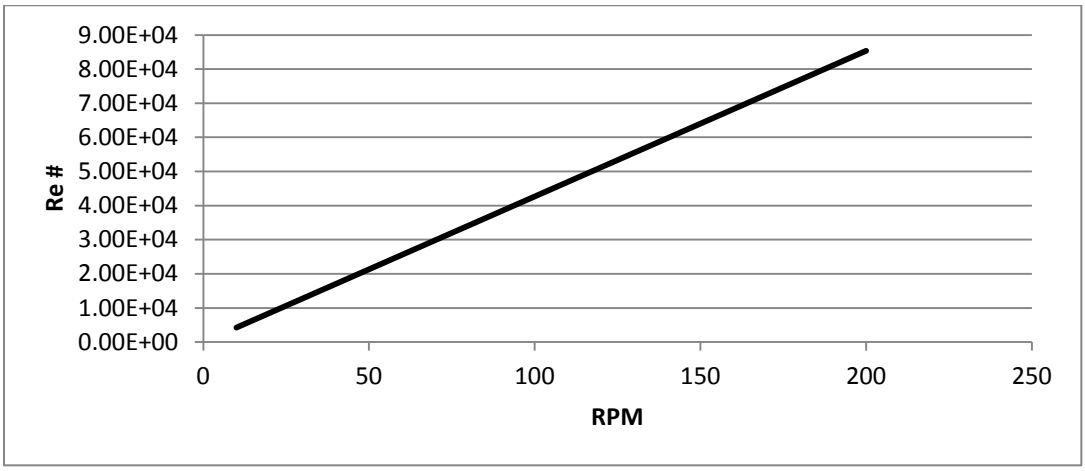

Figure 1. 9. Plot of Re numbers obtained in a USP 2 apparatus assuming the tablet is undergoing the maximum velocity at the impeller tip.

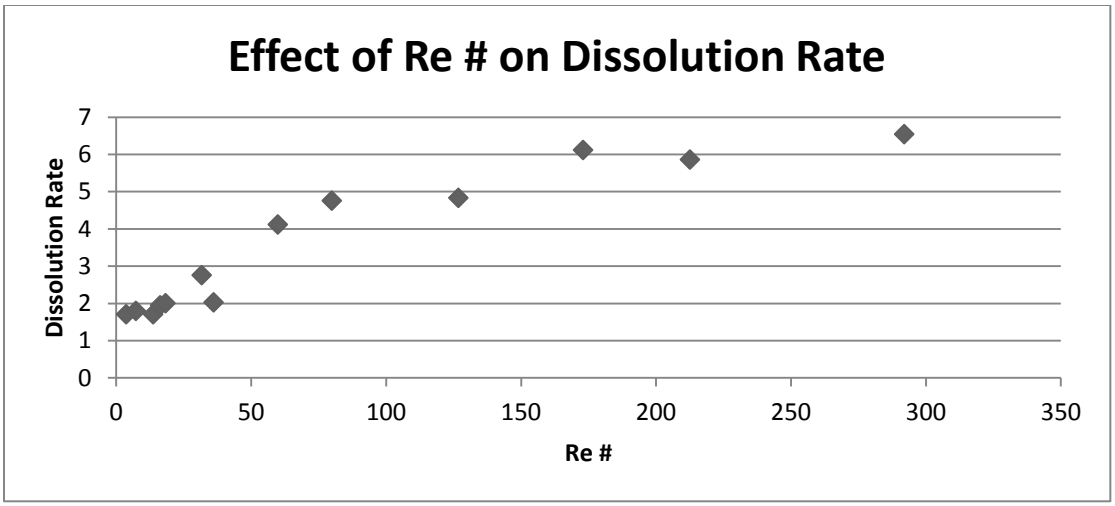

Figure 1. 10. Experimental dissolution rates obtained in a flow through system vs the Re numbers in the apparatus based on the experimental parameters. (data from Cammarn et al[61])

References

1. Ranz WE, Marshall WR 1952. Evaporation From Drops: Part II. Chemical Engineering Progress 48(4):173 - 180.
2. Sugano K 2008. Theoretical comparison of hydrodynamic diffusion layer models used for dissolution simulation in drug discovery and development. International Journal of Pharmaceutics 363(1-2):73-77.
3. Mudie DM, Amidon GL, Amidon GE 2010. Physiological Parameters for Oral Delivery and in Vitro Testing. Mol Pharmaceutics 7(5):1388-1405.
4. Galia E, Nicolaides E, Horter D, Lobenberg R, Dressman JB 1998. Evaluation of various dissolution media for predicting in vivo performance of class I and II drugs. Pharmaceutical research 15(May):698.
5. Lindahl A, Ungell A, Knutson L, Lennernas H 1997. Characterization of Fluids from the Stomach and Proximal Jejunum in Men and Women. Pharmaceutical Research 14(4):497-502.
6. Moreno MPdlC, Oth M, Deferme S, Lammert F, Tack J, Dressman J, Augustijns P 2006. Characterization of fasted-state human intestinal fluids collected from duodenum and jejunum. Journal of pharmacy and pharmacology 58(8):1079-1089.
7. Persson EM, Gustafsson A-S, Carlsson AS, Nilsson RG, Knutson L, Forsell P, Hanisch G, Lennernäs H, Abrahamsson B 2005. The Effects of Food on the Dissolution of Poorly Soluble Drugs in Human and in Model Small Intestinal Fluids. Pharmaceutical Research 22(12):2141-2151.
8. Mooney K, Mintun M, Himmelstein K, Stella V 1981. Dissolution kinetics of carboxylic acids II: Effect of buffers. J Pharm Sci 70(1):22-32.
9. Aunins JG, Southard MZ, Myers RA, Himmelstein KJ, Stella VJ 1985. Dissolution of Carboxylic Acids III. The Effect of Polyionizable Buffers. Journal of Pharmaceutical Sciences 74(12):1305 - 1316.
10. McNamara DP, Amidon GL 1988. Reaction plane approach for estimating the effects of buffers on the dissolution rate of acidic drugs. Journal of Pharmaceutical Sciences 77(6):511-517.
11. Sheng J. 2007. Toward an In Vitro Bioequivalence Test. Pharmaceutical Sciences, ed., Ann Arbor: University of Michigan.
12. Allen A, Flemstrom G 2005. Gastroduodenal Mucus Bicarbonate Barrier: Protection Against Acid and Pepsin. Am J Physiol Cell Physiol 288:C1-C19.
13. Fiddian-Green RG, Pittenger G, Whitehouse WM 1982. Back-Diffusion of CO_2 and its influence on the intramural pH in the Gastric Mucosa. Journal of Surgical Research 33:39-48.
14. Hogan DL, Ainsworth MA, Isenberg JI 1994. Review Article: Gastroduodenal Bicarbonate Secretion. Aliment Pharmacol Ther 8:475-488.
15. McNamara DP, Whitney KM, Goss SL 2003. Use of a physiologic bicarbonate buffer system for dissolution characterization of ionizable drugs. Pharmaceutical Research 20(10):1641-1646.
16. Butler JN. 1991. Carbon Dioxide Equilibria and Their Applications. ed., Reading, Mass: Addison Wesley.
17. Harned HS, DavisJr R 1943. The Ionization Constant of Carbonic Acid in Water and the Solubility of Carbon Dioxide in Water and Aqueous Salt Solutions from 0 to 50 deg C. Journal of the American Chemical Society 65:2030 -2037.
18. Soli AL, Byrne RH 2002. Carbon Dioxide System Hydration and Dehydration Kinetics and the Equilibrium CO2/H2CO3 Ratio in Aqueous NaCl Solution. Marine Chemistry 78:65 - 73.

19. Roughton FJW 1935. Recent Work on Carbon Dioxide Transport By the Blood. Physiol Rev 15:241 -296.
20. Roughton FJW 1941. The Kinetics and Rapid Thermochemistry of Carbonic Acid. J Biol Chem 129:2930 - 2934.
21. Berger RL, Stoddart LC 1965. Combined Calorimeter and Spetrophotometer for Observing Biological Reactions. The Review of Scientific Instruments 36(1):78 - 84.
22. Eigen M, Hammes G. 1963. In Nord FF, editor Elementary Steps in Enzyme Reactions Advances in Enzymology, ed.: John Wiley & Sons. p 1 - 38.
23. Gutknecht J, Bisson MA, Tosteson FC 1977. Diffusion of Carbon Dioxide through Lipid Bilayer Membranes: Effects of Carbonic Anhydrase, Bicarbonate, and Unstirred Layers. Journal of General Physiology 69:779-794.
24. Lindskog S, Coleman JE 1973. The Catalytic Mechanism of Carbonic Anhydrase (metalloenzymes/enzyme mechanism/hydration of CO_2). Proc Nat Acad Sci USA 70(9):2505-2508.
25. Kivela A 2003. Carbonic Anhydrase in Normal and Neoplastic Gastrointestinal Tissues: With Special Emphasis on Isoenzymes I, II, IX, XII, and XIV. Academic Dissertation.
26. Roughton FJW, Booth VH 1946. The Effect of Substrate Concentration, pH and other Factors upon the Activity of Carbonic Anhydrase. J Biochem 40:319 - 330.
27. Khalifah RG 1973. Carbon Dioxide Hydration Activity of Carbonic Anhydrase: Paradoxical Consequences of the Unusually Rapid Catalysis. Proc Nat Acad Sci USA 70(7):1986 - 1989.
28. Sly WS, Hu PY 1995. Human Carbonic Anhydrases and Carbonic Anhydrase Deficiencies. Annu Rev Biochem 64:375 - 401.
29. Koenig SH, Brown RD 1981. Exchange of Labeled Nuclei in the CO_2 - HCO_3^- - Solvent System Catalyzed By Carbonic Anhydrase. J Biophys 35:59 - 78.
30. Khalifah RG 1971. The Carbon Dioxide Hydration Activity of Carbonic Anhydrase. I. Stop-Flow Kinetic Studies on the Native Human Isoenzymes B and C. The Journal of Biological Chemistry 246(8):2561 - 2573.
31. Parkkila S, Parkkila A, Lehtola J, Reinila A, Sodervik H, Rannisto M, Rajaniemi H 1997. Salivary Carbonic Anhydrase Protects Gastroesophageal Mucosa from Acid Injury. Digestive Diseases and Sciences 42(5):1013 - 1019.
32. Nishimori I, Onishi S, Vullo D, Innocenti A, Scozzafava A, Supuran CT 2007. Carbonic Anhydrase Activators: The first Activation study of the human secretory isoform VI with amino acids and amines. Bioorganic & Medicinal Chemistry 15:5351 - 5357.
33. Mooney KG, Mintun M, Himmelstein K, Stella V 1981. Dissolution kinetics of carboxylic acids I: Effect of pH under unbuffered conditions. J Pharm Sci 70(1):13-22.
34. Levich VG. 1962. Physicochemical Hydrodynamics. ed., New jersey: Prentice Hall.
35. Grijseels H, Crommelin DJA, Blaey CJD 1981. Hydrodynamic Approach to Dissolution Rate. Pharmaceutisch Weekblad - Scientific Edition 3:129 -144.
36. Ozturk SS, Palsson BO, Dressman JB 1988. Dissolution of ionizable drugs in buffered and unbuffered solutions. Pharmaceutical research 5(May):272.
37. Grijseels H, van Bloois L, Crommelin DJA, de Blaey CJ 1983. Dissolution at porous interfaces II. A study of pore effects through rotating disk experiments. Int J Pharm 14:299.
38. Mooney KG, Rodriguez-Gaxiola M, Mintun M, Himmelstein KJ, Stella VJ 1981. Dissolution Kinetics of Phenylbutazone Journal of Pharmaceutical Sciences 70(12):1358-1365.
39. Higuchi T, Lee HK, Pitman IH 1971. Farm Aikak 80:55.
40. Álvarez C, Núñez I, Torrado JJ, Gordon J, Potthast H, García-Arieta A 2011. Investigation on the possibility of biowaivers for ibuprofen. Journal of Pharmaceutical Sciences 100(6):2343-2349.
41. Huizinga JD, Lammers WJEP 2009. Gut Peristalsis is Governed by a Multitude of Cooperating Mechanisms. Am J Physiol Gastrointest Liver Physiol 296(G1 - G8).

42. Froehlich JM, Patak MA, Weyman CV, Juli CF, Zollikofer CL, Wentz K 2005. Small Bowel Motility Assessment With Magnetic Resonance Imaging. Journal of Magnetic Resonance Imaging 21:370 - 375.
43. Lentle RG, Janssen PWM 2008. Physical Characteristics of Digesta and Their influence on Flow and Mixing in the Mammalian Intestine: a review. J Comp Physiol B 178:673 - 690.
44. Abrahamsson B, Pal A, Sjöberg M, Carlsson M, Laurell E, Brasseur JG 2005. A Novel in Vitro and Numerical Analysis of Shear-Induced Drug Release from Extended-Release Tablets in the Fed Stomach. Pharmaceutical Research 22(8):1215-1226.
45. Kamba M, Seta Y, Kusai A, Ikeda M, Nishimura K 2000. A unique dosage form to a value weight the mechanical destructive force in the gastrointestinal tract. International Journal of pharmaceutics 208:61-70.
46. Niebergall PJ, Milosovich G, Goyan JE 1963. Dissolution Rate Studies II: Dissolution of Particles Under Conditions of Rapid Agitation. J Pharm Sci 52(3):236 - 241.
47. Hixson AW, Crowell JH 1931. Dependence of Reaction Velocity upon Surface and Agitation I Theoretical Consideration. Industrial & Engineering Chemistry 23(8):923 - 931.
48. Higuchi WI, Hiestand EN 1963. Dissolution rates of finely divided drug powders I. Effect of a distribution of particle sizes in a diffusion-controlled process. J Pharm Sci 52:67-71.
49. Wang J, Flanagan DR 1999. General Solution for Diffusion-Controlled Dissolution of Spherical Particles 1. Theory. J Pharm Sci 88(7):731 - 738.
50. Hintz RJ, Johnson KC 1989. the effect of particle size distribution on dissolution rate and oral absorption. Int J Pharm 51:9-17.
51. Sheng JJ, Sirois PJ, Dressman JB, Amidon GL 2008. Particle Diffusional Layer Thickness in a USP Dissolution Apparatus II: A Combined Function of Particle Size and Paddle Speed. Journal of Pharmaceutical Sciences 97(11):4815-4829.
52. Cammarn SR, Sakr A 2000. Predicting dissolution via hydrodynamics: salicylic acid tablets in flow-through cell dissolution. International Journal of pharmaceutics 201:199-209.
53. Hamlin WE, Ballard BE, Wagner JG, Nelson E 1962. Loss of sensitivity in distinguishing real differences in dissolution rates due to increasing intensity of agitation. Journal of Pharmaceutical Sciences 51(5):432-&.
54. Mauger J, Ballard J, Brockson R, De S, Gray V, Robinson D 2003. Intrinsic Dissolution Performance Testing of the USP Dissolution Apparatus 2(Rotating Paddle) Using Modified Salicylic Acid Calibrator Tablets: Proof of Principle. Dissolution Technologies:6-15.
55. Mirza T, Joshi Y, Liu Q, Vivilecchia R 2005. Evaluation of Dissolution Hydrodynamics in the USP, Peak™ and Flat-Bottom Vessels Using Different Solubility Drugs. Dissolution Technologies.
56. Kukura J, Baxter JL, Muzzio FJ 2004. Shear distribution and variability in the USP Apparatus 2 under turbulent conditions. International Journal of Pharmaceutics 279(1-2):9-17.
57. Morihara M, Aoyagi N, Kaniwa N, Katori N, Kojim S 2002. Hydrodynamic Flows Around Tablets in Different Pharmacopeial Dissolution Tests. Drug Development & Industrial Pharmacy 28(6):665-662.
58. Shiko G, Gladden LF, Sederman AJ, Connolly PC, Butler JM 2011. MRI Studies of the Hydrodynamics in a USP 4 Dissolution Testing Cell. Journal of Pharmaceutical Sciences 100(3):976-991.
59. Kakhi M 2009. Mathematical modeling of the fluid dynamics in the flow-through cell. International Journal of Pharmaceutics 376(1-2):22-40.
60. Dressman JB, Amidon GL, Reppas C, Shah VP 1998. Dissolution testing as a prognostic tool for oral drug absorption: immediate release dosage forms. Pharmaceutical Research 15(Jan):11.
61. Schiller C, Frohlich CP, Giessmann T, Siegmund W, Monnikes H, Hosten N, Weitschies W 2005. Intestinal fluid volumes and transit of dosage forms as assessed by magnetic resonance imaging. Alimentary Pharmacology and Therapeutics 22(10):971-979.
62. Jantratid E, Janssen N, Reppas C, Dressman JB 2008. Dissolution Media Simulating Conditions in the Proximal Human Gastrointestinal Tract: An Update. Pharmaceutical Research 25(7):1663-1676.

63. Gutzeit A, Patak MA, Weymarn Cv, Graf N, Doert A, Willemse E, Binkert CA, Froehlich JM 2010. Feasibility of Small Bowel Flow Rate Measurement With MRI. Journal of Magnetic Resonance Imaging 32:345-351.
64. Mills GA, Urey HC 1940. The Kinetics of Isotopic Exchange Between Carbon Dioxide, Bicarbonate Ion, Carbonate Ion and Water. J Am Chem Soc 62:1019 - 1026.
65. Pinsent BRW, Pearson L, Roughton FJW 1956. The Kinetics of Combination of Carbon Dioxide With Hydroxide Ions. Trans Faraday Soc 52:1594 - 1598.
66. Garg LS, Maren TH 1972. THE RATES OF HYDRATION OF CARBON DIOXIDE AND DEHYDRATION OF CARBONIC ACID AT 37 °. Biochim Biophys Acta, 261:70 - 76.
67. Rossi-Bernardi L, Berger RL 1968. The Rapid Measurement of pH by the Glass Electrode: The Kinetics of Dehydration of Carbonic Acid at 25^{o} and 37^{o}. The Journal of Biological Chemistry 243(6):1297 - 1302.
68. Nassanen R 1947. Potentiometric Study on the First Ionization of Carbonic Acid in Aqueous Solutions of Sodium Chloride. Acta Chemica Scandinavica 1:204 - 209.
69. Wissbrun KF, French DM, Patterson AP 1954. The True Ionization Constant of Carbonic Acid in Aqueous Solution from 5^{o} to 45^{o}. J Phys Chem 58:693 - 695.
70. Harned HS, Bonner FT 1945. The First Ionization of Carbonic Acid in Aqueous Solutions of Sodium Chloride. J Am Chem Soc 67:1026 - 1031.
71. Magid E, Turbeck BO 1968. The Rates of the Spontaneous Hydration of CO_2 and the Reciprocal Reaction in Neutral Aqueous Solutions Between 0^{o} and 38^{o}. Biochim ET Biophys Acta, 165:515 - 524.
72. Pal A, Indireshkumar K, Schwizer W, Abrahamsson B, Fried M, Brasseur JG 2004. Gastric flow and mixing studied using computer simulation. Proceedings of the Royal Society B: Biological Sciences 271(1557):2587-2594.

Chapter 2

In Vivo Predictive Dissolution: Transport Analysis of the CO2, Bicarbonate *In Vivo* Buffer System

Abstract

Development of an oral *in vivo* predictive dissolution medium for acid drugs with a pKa in the physiological range (eg: BCS Class IIa) requires transport analysis of the complex *in vivo* CO2/bicarbonate buffering system. In this chapter the bicarbonate buffer system using hydrodynamically defined rotating disk dissolution will be examined. Transport analysis of Drug flux was predicted using the film model approach of Mooney et al[1] based on equilibrium assumptions as well as accounting for the slow hydration reaction, $CO_2 + H_2O \rightarrow H_2CO_3$. The accuracy of the models was compared with experimentally determined results using the rotating disk dissolution of ibuprofen, indomethacin, and ketoprofen. The weak acid drugs were studied at a variety of experimental conditions to analyze the ability of the model to predict dissolution in bicarbonate buffer at conditions the drugs may encounter *in vivo*. The equilibrium and slow hydration reaction rate models predict significantly different dissolution rates. The experimental results are more accurately predicted by accounting for the slow hydration reaction under a variety of pH and hydrodynamic conditions. While the complex bicarbonate buffering system requires further consideration given its dynamic nature *in vivo*, a simplifying irreversible reaction transport (IRR) analysis accurately predicts *in vitro* rotating disk dissolution rates of several carboxylic acid drugs. This IRR transport model provides further insight into bicarbonate buffer

and can be useful in developing more physiologically relevant buffer systems for dissolution testing.

Introduction

When a drug product is administered orally, the absorption may be limited by the rate at which the drug dissolves in the gastrointestinal tract. For BCS Class II low solubility drugs, dissolution can be the rate limiting step [2]. The composition of the intestinal fluid plays a critical role in determining this rate. One of the main components of intestinal fluid is the bicarbonate buffer species that controls lumenal pH. Buffers can have a large effect on the dissolution of ionizable drugs by affecting the pH at the solid liquid interface (surface) of the dissolving drug [1,3,4,5,6].

Bicarbonate (HCO_3^-) is secreted by epithelial cells and the pancreas into the small intestine where it is the main buffer in the lumen and acts to maintain a relatively constant pH in the intestinal tract. Bicarbonate is thought to follow the Jacobs Stewart Cycle in the small intestine[7-9]. Bicarbonate (HCO_3^-) present in the intestinal lumen can react with hydrogen ions (H^+) to form carbonic acid (H_2CO_3) which then produces carbon dioxide (CO_2 (aq)) and water (H_2O) through the dehydration reaction. This process is reversible (see Rxn 2 below) and carbon dioxide can diffuse into the intestinal cells or react with water to form carbonic acid through the hydration reaction. Carbonic acid can also ionize to form hydrogen ions and bicarbonate. In the intestinal cells, the same reversible process can occur, resulting in the formation of CO_2 (aq) and HCO_3^- . The HCO_3^- formed in the intestinal cells can be transported back into the intestinal lumen. The concentration of each of the species formed is dependent on the corresponding equilibrium constants.

Concentrations of aqueous carbon dioxide and bicarbonate are directly related in the luminal fluid of the GI tract [10,11,12]. In the stomach of healthy humans, the percent CO_2 typically ranges between 4-10 % CO_2 (30-76 mmHg) and similar values are observed in the proximal jejunum [12,13]. McGeese and Hastings measured an average of 13.2 % (100 mmHg) CO_2 in the jejunum at an average pH of 6.5 [14]. In the proximal duodenum, where there is a lower pH, these values are typically significantly higher and can be as high as 66% CO_2 (500 mmHg) [15]. These $\%CO_2$ levels can be compared to normal atmospheric conditions which are approximately 0.04%. The stomach secretes about 400 mmol of H^+ per day[16] (17mmol/h) which enters the duodenum. Therefore bicarbonate must be secreted at a rate in the duodenum that is high enough to neutralize the incoming H^+. This increase in bicarbonate and H^+ will result in an increase in the concentration of CO_2 partial pressure in the duodenum. Bicarbonate secretions have been shown to range from approximately 150-600 µmol cm^{-1} h^{-1} (~6mmol/h) in the proximal duodenum to approximately 25-200 µmol cm^{-1} h^{-1} (~2mmol/h) in the distal duodenum depending on the H^+ concentration [11]. The differences in the H^+ stomach secretions and duodenal bicarbonate secretions results in the pH of the proximal duodenum fluctuating up to 5 pH units transiently[16].

An important consideration in more fully understanding the bicarbonate system are the individual reaction rates associated with the equilibrium constants K_c and K_{a1} in Rxn 1 below. In particular, the hydration and dehydration reactions associated with K_c are six to ten orders of magnitude slower than the reaction rates associated with K_{a1}. The enzyme carbonic anhydrase is present in the intracellular fluid and membranes of the epithelial cells of the intestinal tract [8,17]. It functions to significantly accelerate the hydration and dehydration reactions in these regions. However, there is no evidence that carbonic anhydrase is secreted or present in the luminal fluid.

Therefore, it is likely that the hydration and dehydration reactions occur at their slow rates in the bulk lumenal fluid.

Understanding the role of bicarbonate buffer and the reactions involved in its formation is essential to understanding the dissolution of weak acid and weak base drugs in the intestinal tract and, ultimately, to creating a more physiologically relevant dissolution medium. While the impact that certain buffers have on a dissolving drug has been modeled accurately and is well understood, there has been little consideration to the effect of bicarbonate buffer on drug dissolution in the intestine [1,3,4,5,18]. There have been several studies characterizing the effect bicarbonate buffer has on drug dissolution and attempts have been made at modeling the process[5,10,19-21] . However, a thorough examination of how the CO_2 reaction chemistry of bicarbonate buffer affects drug dissolution has not been explored though this is an area that has been studied rigorously and applied in geology and other sciences[22-26]. It is anticipated that a better understanding of the impact of bicarbonate buffer on the pH at the surface of a dissolving ionizable drug will provide the foundation for creating buffer systems that more closely resemble *in vivo* conditions and dissolution.

The significant role the slow hydration and dehydration rates have on the formation of bicarbonate and its ability to function as a buffer and alter the pH at the surface of dissolving drug (i.e at the solid liquid interface) has been investigated in this study. The simultaneous convective diffusion and chemical reaction within the boundary layer model assuming either: (a) instantaneous chemical equilibrium, or (b) slow hydration and dehydration will be compared to experimental results using the defined hydrodynamics of the rotating disk dissolution system for weak acid drugs. Our analysis and experimental results demonstrate that the slow irreversible reaction rate (IRR) model best matches the experimental rotating disk dissolution rate of the

weak acid drugs studied. This analysis can be helpful in developing buffering systems that are more physiologically relevant for *in vivo* dissolution predictions and testing. A similar analysis may be applied to weak base and amphoteric drugs. This analysis has been successfully applied to weak base drugs and this is detailed in chapter 3

Reactions and Kinetics of the Bicarbonate Buffer System:

Conversion of $CO_2(\boldsymbol{g})$ to CO_2 $(\boldsymbol{aq})$

Bicarbonate buffer can be produced experimentally by controlling the partial pressure of CO_2 (g) equilibrated with water as shown in reaction 2.1.

$$CO_2(g) \overset{K_H}{\underset{\leftarrow}{\rightarrow}} CO_2(aq) + H_2O \overset{K_C}{\underset{\leftarrow}{\rightarrow}} H_2CO_3 \overset{K_{a1}}{\underset{\longleftarrow}{\longrightarrow}} H^+ + HCO_3^- \qquad \text{(Rxn. 2.1)}$$

$$CO_2(aq) + H_2O \overset{K_a}{\underset{\leftarrow}{\rightarrow}} HCO_3^- + H^+ \qquad \text{(Rxn. 2.2)}$$

Chapter one described each of these reactions and reaction rates in detail. Reaction 1 outlines the entire chemical reaction process that leads to the formation of bicarbonate in the dissolution media and reaction 2.2 outlines the chemical equilibrium in the bulk solution. Therefore the bicarbonate concentration can be written as a function of the partial pressure of carbon dioxide (P_{CO2}) using K_H, assuming equilibrium.

$$\left[HCO_3^-\right] = \frac{KaK_HP_{CO_2}}{[H^+]} \qquad \text{(Eq. 2.1)}$$

The values for P_{CO2} and $[H^+]$ can be adjusted to yield a desired bicarbonate buffer concentration. At low pH values the total buffer concentration, when CO_2 (aq) concentration is included, is relatively high due to high CO_2 (g) partial pressures found *in vivo* in the duodenum. Due to solubility limitations of carbon dioxide and the effect of $[H^+]$ on the concentration of bicarbonate, the presence of bicarbonate is most significant for pH values in the range: $5.5 \leq$ pH

≤ 7.5. For pH below 5.5, only very dilute bicarbonate buffer concentrations can be produced even at high CO_2 (g) partial pressures. At pH values above 7.5, only low CO_2(g) values are required to achieve relevant bicarbonate buffer concentrations though the buffer capacity is substantially reduced. The relationship between CO_2(g), CO_2(aq), $[H^+]$, and $[HCO_3^-]$ is shown in Figure 2.1. Typical physiologic conditions of pH and carbon dioxide levels result in total buffer concentrations (CO_2(aq) + $[HCO_3^-]$) in the duodenum and jejunum in the range of 3-20 mM as shown in Figure 2.1. Figure 2.1 also compares the total buffer concentration to the bicarbonate concentration as a function of pH. The bicarbonate concentration present is significantly less than the total buffer concentration especially at low pH values.

Simultaneous Diffusion and Reaction Model

Dissolution of drugs from a solid surface are generally accurately predicted by considering the simultaneous diffusion and chemical reactions as described by Mooney et al. [1, 27]. Applying this to a rotating disk dissolution apparatus permits the estimation of pH at the surface of a compacted drug by taking into account the properties of the drug and buffer system and assuming simultaneous and instantaneous diffusion and chemical reaction in the hydrodynamic boundary layer near the surface of the rotating disk. Levich characterized this boundary layer thickness for a rotating disk based on liquid viscosity, rotational speed, and diffusion coefficient [28,29]:

$$h = 1.61 D^{1/3} \omega^{-1/2} \upsilon^{1/6} \qquad \text{(Eq. 2.2)}$$

When the Levich theory is applied to rotating disk drug dissolution, h is the thickness of the diffusion layer, D is the diffusion coefficient of the drug in the dissolving medium (aqueous buffer), υ is the kinematic viscosity (water = 0.007 cm^2/s) and ω is the rotational speed (100RPM = 10.47 radians/sec). The diffusion layer thickness is a constant for each specific drug under

fixed conditions of rotational speed (see Table 1). Following Mooney and coworkers[1], the simultaneous diffusion and chemical reaction model assuming instantaneous reaction was applied to the bicarbonate buffer system.

Applying a simultaneous diffusion and reaction model to bicarbonate buffer

The reaction rate for the hydration of carbon dioxide to carbonic acid is a slow process as described above. If the time the diffusing molecule spends in the diffusion layer is less than the reaction time, then the reaction would primarily be occurring only in the bulk solution and not in the diffusion layer [30]. The average residence time of a molecule in the diffusion layer is determined by diffusion layer thickness and the diffusivity of the molecule[30] (Equation 2.3). The reaction time depends on the first order rate constant and it defines the time needed for the reaction to be 63% complete [30] (Equation 2.4). Equations 2.3 and 2.4 can be used to assess the extent that a reaction will go to completion within the diffusion layer:

$$t_D = \frac{h^2}{2D_i} = \frac{1.3v^{1/3}}{D_i^{1/3}w} \qquad \text{(Eq. 2.3)}$$

where t_D is the average residence time of a diffusing molecule in the diffusion layer. The reaction time, t_r, is given by equation 2.4 where k is the first order rate constant.

$$t_r = \frac{1}{k} \quad \text{(Eq. 2.4)}$$

If the hydration reaction between CO_2 (aq) and H_2O does not occur sufficiently fast, the reaction will not go to completion in the diffusion layer and the flux of bicarbonate throughout the diffusion layer will be less than predicted. Table 2.1 compares the ratio of t_r (~$8s^{-1}$) and t_D at different diffusion layer thickness values (based on ibuprofen) calculated at different rotational speeds. These values were calculated according to the Levich equation for boundary layer

thickness at the surface of a rotating disk (Eq. 2.2). The table shows that $t_r > t_D$ even at large diffusion layer thickness values (low RPM) and that t_r can vary between an order of magnitude to two orders of magnitude greater than t_D. This analysis indicates that the hydration reaction is occurring to a very limited extent in the diffusion layer while the dehydration reaction appears sufficiently fast that it may be assumed to be occurring rapidly enough that this difference in reaction rates will impact the buffer capacity of bicarbonate in the diffusion layer. It is worth noting that these differences are relevant in the diffusion layer but not in the bulk aqueous phase where all the reactions occur sufficiently fast to be considered instantaneous and Rxn 2 and K_a apply because the reaction time is unlimited.

As the results will show, this slow reaction has a large effect on the experimental flux in comparison to predictions applying the instantaneous reaction film model[1] to bicarbonate buffer. Initially, two different chemical equilibrium approaches were applied. The first approach was to assume that all of the reactions in the formation of bicarbonate buffer are sufficiently fast so that the chemical equilibrium that is assumed to occur in the bulk solution (and displayed in Rxn. 2.2) can be applied to the boundary layer in the film model (pKa = 6.04; Bulk Chemical Equilibrium Model). When applying the bulk chemical equilibrium (BCE) model, CO_2 is the nonionized form of the buffer and HCO_3^- is the ionized form of the buffer. The second approach assumed that both the hydration and dehydration reaction are so slow in comparison to the ionization reactions that the formation of bicarbonate is dependent only on Rxn. 2.3 (pKa1 = 3.55, Carbonic Acid Ionization Model).

$$H_2CO_3 \overset{K_{a1}}{\longleftrightarrow} H^+ + HCO_3^- \qquad Rxn.\,2.3$$

In the case of the carbonic acid ionization (CAI) model, H_2CO_3 is the nonionized form of the buffer and HCO_3^- is the ionized form. It is notable that the concentration of CO_2(aq) is 300

times greater than carbonic acid. Therefore, the total buffer concentration used in the CAI model is less than that used in the BCE model which includes the CO_2 (aq) concentration. However, the results show that these two assumptions do not accurately describe experimental results. Therefore a modification to the transport analysisis that incorporates the slow reaction rates for the hydration and dehydration reactions is necessary.

Incorporating Reaction Rates into a Simultaneous Diffusion and Chemical Reaction Model

The experimental results (see below) indicate that when reactions occur non-instantaneously, the film model needs to account for the slow reactions. There are multiple species reacting in the diffusion layer during the dissolution of a weak acid or weak base drug which makes adding reaction rates into the film model challenging. Therefore, to follow the same steps using the simultaneous diffusion and chemical reaction model, two assumptions were made to simplify the process. The first assumption is that only the hydration and dehydration reaction rates need to be considered and all other reactions can be assumed to take place instantaneously. The second assumption is that since the hydration reaction (k_h) happens very slowly, it can be assumed to not be taking place at all in the diffusion layer (though it will occur in the bulk solution) and the only reaction rate that needs to be included in the modeling process is the dehydration reaction rate (k_d). These assumptions describe a situation where the protons formed at the surface of the dissolving weak acid drug will react with HCO_3^- to form H_2CO_3 which can then form CO_2 and H_2O through an irreversible chemical reaction (Irreversible reaction model, IRR). This assumption, when applied to the film model changes the resulting equation for calculating the surface pH. The surface pH is no longer independent of reaction rates and diffusion layer thickness because the dehydration reaction rate and the diffusion layer thickness remain included in the equation for surface pH. The experimental results show that

using the irreversible reaction model (IRR model) allows for accurate predictions of drug flux in bicarbonate buffer. The derivation of the IRR model is presented in the appendix and the cubic equation needed to solve for surface pH and drug flux are shown in appednix equations 33 and 34d.

Materials and Methods

Ibuprofen (Albermarle, Lot#11550-0005), indomethacin (Alexis Biochemicals $\geq 98\%$, Lot# L25666, and ketoprofen (Sigma Aldrich, Lot# 044K0790) were used as received and all other chemicals used were of analytical grade. Distilled water was used for all experiments. Mineral oil USP grade was used for the titration experiment to prevent the escape of $CO_2(g)$. All dissolution runs were performed in a jacketed beaker at 37^{o}C. Two runs were done for each experimental condition described below. Samples were analyzed using a UV spectrophotometer (Agilent Technologies, Model# 61103A). The samples were obtained using a flow through system that recycled the analyzed solution back into the dissolution vessel. The standard curves were also made using the UV flow through system.

Ibuprofen solubility was measured by agitating a suspension of ibuprofen particles in 50mM acetate buffer at pH 4.5 while being kept at 37^{o}C. The pH of the saturated solution at 37^{o}C was measured to be 4.5. Samples were taken from the solutions and filtered before they were diluted with 50mM acetate buffer at pH 4.5. The measured solubility was 0.150 mg/ml and based on the the pH-solubility profile this solubility is in good agreement with an intrinsic solubility of 0.068mg/ml used in this paper and reported by Karl et al.[31]

The intrinsic solubility of indomethacin was measured by agitating a suspension of indomethacin particles in 0.1N hydrochloric acid solution while being kept at 37^{o}C. Samples were taken from the solutions and filtered before they were diluted with 0.1N hydrochloric acid.

The intrinsic solubility of ketoprofen was measured by agitating a suspension of ketoprofen particles in 0.1N hydrochloric acid solution while being kept at 37^{o}C. Samples were taken from the solutions and filtered before they were diluted with pH 6.7 25mM phosphate buffer.
The pKa of the bicarbonate buffer was measured by adjusting 100% dry compressed air and 100% carbon dioxide (at appropriate ratios to give physiologically relevant conditions) in a 100 ml 0.9%NaCl solution in a jacketed beaker at 37^{o}C. Solid NaOH and a 5N NaOH solution were used to adjust the buffer pH to ~7.0. Next, the sources of the gas mixture were eliminated from the solution and USP grade mineral oil (heated to 37^{o}C) was added to the buffer solution where it produced an oil layer on top of the aqueous buffer to limit the escape of carbon dioxide gas. 1.0M HCL solution was added in 0.1ml increments to the aqueous phase and the pH was monitored until it dropped to ~5.0. In addition, the %CO_2 in the aqueous phase was monitored throughout using a CO2 monitor (YSI 8500 CO_2 monitor).

For the dissolution experiments in bicarbonate buffer, different concentrations of bicarbonate buffer were prepared by adjusting quantities of 100% dry compressed air and 100% carbon dioxide in a 0.9%NaCl solution at appropriate ratios to make pgysiologically relevant concentrations of bicarbonate buffer. See Table 3 for the experimental parameters used for the dissolution tests The %CO_2(aq) in solution was determined using a CO_2 monitor (YSI 8500) and pH was monitored using a pH meter (Beckman Φ 40). The mixture of carbon dioxide gas and air was continuously pumped in throughout the dissolution runs to maintain bulk equilibrium. Solid sodium hydroxide and sodium hydroxide solution was added to adjust pH. The volume of the bicarbonate buffer dissolution medium for ibuprofen and indomethacin was 100ml and for ketoprofen it was 200ml. Differences in volume used for the experiments were made according to the solubility and predicted flux of each drug to achieve desirable experimental conditions

(sink conditions and adequate sensitivity for UV analysis). All experiments were carried out at 100RPM. However, dissolution tests for ibuprofen were also done at rotational speeds of 50, 250, and 500RPM. Ibuprofen was also performed at bulk pH values 5.5, 6.0 and 7.0 (see table3 for buffer concentration at each pH).

The flux of the drug was predicted by applying the mathematical models outlined in this paper and the parameters that are given in Table 2 using MATLAB (MathWorks).

Results

Bicarbonate Buffer Measured pKa

Figure 2.2 shows the measured pH as a function of the amount of 1.0M HCl added during the titration and the experimental buffer capacity (dn/dpH) as a function of pH. This titration data suggests that the pKa of the bulk solution is ~ 6. A statistical analysis was performed by comparing the residual sum of squares and the result was a best fit bulk pKa of 6.04. This value was used for calculating the bulk bicarbonate buffer concentrations for all of the rotating disk dissolution experiments. Additionally, this was the pKa that was used in the BCE model for predicting drug flux in bicarbonate buffer. One factor to note is that bicarbonate concentration is continuously changing throughout the titration because the $\%CO_2$ increases as the pH decreases. However, it was observed in the bulk solution that CO_2 (aq) acts as a buffer component and therefore the total buffer concentration remains relatively constant. The measured value of 6.04 for the pKa of the overall reaction (Rxn. 2.2) is consistent with experimentally determined values in the literature which were given in chapter 1.

Ibuprofen Results

Figure 2.3 shows the predicted impact of rotational speed (change in diffusion layer thickness) on the surface pH and the relative buffering ability of bicarbonate based on the

different model approaches for ibuprofen. Assuming instantaneous hydration/dehydration reactions (BCE model: pKa =6.04) predicts bicarbonate to have the greatest buffer capacity and highest surface pH. When it is assumed that the hydration/dehydration reactions do not occur at all in the diffusion layer (CAI model: pKa 3.55), bicarbonate is predicted to have a low buffer capacity and low predicted surface pH. Assuming carbonic acid undergoes the irreversible dehydration reaction (IRR model) the predictions of buffer capacity and surface pH fall between the BCE and CAI models. Additionally, Figure 2.3 shows that the predicted surface pH decreases using the IRR model as the rotational speed increases. The thickness of the diffusion layer has no effect on surface pH for the BCE and CAI models because it is assumed that chemical equilibrium is achieved instantaneously in each case.

Figure 2.4 shows the calculated Damkohler numbers (Diffussion time/reaction time = $\frac{\frac{h^2}{2D}}{\frac{1}{k}}$) for the dehydration and hydration reactions as a function of diffusion layer thickness. This plot is consistent with figure 2.3, because as the diffusion layer thickness decreases, the reaction time becomes the rate limiting step in the case of the dehydration reaction. This explains why the IRR model starts to converge with the CAI model in figure 2.3 as the diffusion layer thickness decreases. In the case of the hydration reaction, the Damkohler number is always at least an order of magnitude less than one which is consistent with the assumption that it does not contribute to buffering the pH in the diffusion layer.

Figure 2.5 shows the experimental and predicted results for the flux of ibuprofen in bicarbonate buffer at different rotational speeds. As will be seen with all of the experimental data, the BCE model overestimates the effect bicarbonate buffer has on increasing the surface pH and the flux of ibuprofen. The CAI model underestimates the effect of bicarbonate buffer and the flux of ibuprofen. The flux predictions for the BCE and CAI models in Figure 4 are

influenced only by the changing diffusion layer thickness as the rotational speed is changed because the surface pH is constant and independent of diffusion layer thickness (see figure 2.3). The predicted flux in the IRR model also depends on diffusion layer thickness but in a more complicated fashion. The surface pH is dependent on the residence time of the diffusing species, H_2CO_3, and this impacts the consumption of H+ through the irreversible dehydration reaction (see Figure 2.3 and Appendix: Eq. 33). The IRR model more accurately predicts the effect of a changing diffusion layer thicknessas as well as the diffusing species residence time in the diffusion layer on the ability of bicarbonate to buffer the pH at the surface of the dissolving drug.

Figure 2.6 shows the predicted and experimental flux of ibuprofen in bicarbonate buffer over a range of buffer concentrations at pH 6.5. There is a large difference in flux predictions when comparing the BCE versus CAI models. The experimental flux of ibuprofen in bicarbonate buffer falls between predictions assuming instantaneous hydration/dehydration reactions (BCE model) or no hydration/dehydration reactions (CAI model). When the hydration reaction is assumed to not occur and the dehydration reaction rate is incorporated into the mathematical analysis (IRR model), the predicted flux matches the experimental flux very well.

Figure 2.7 shows the effect bulk pH has on the flux of ibuprofen in 10-11mM bicarbonate buffer at pH values of 6, 6.5, and 7 as well as 3.5mM bicarbonate buffer at pH 5.5. The experimental flux shows little variation as bulk solution pH is changed. The BCE model overestimates the effect that bulk pH and bicarbonate buffer have on increasing the pH at the surface of the dissolving drug and the flux of ibuprofen. The CAI model underestimates the effect that bulk pH and bicarbonate buffer have on increasing the pH at the surface of the dissolving drug and the flux of ibuprofen. The flux of ibuprofen in bicarbonate buffer over different bulk pH values is accurately predicted using the IRR model.

Ketoprofen Results

Figure 2.8 shows the experimental and predicted flux of ketoprofen in bicarbonate buffer over a range of buffer concentrations at pH 6.5. The predictions show that an increase in buffer concentration results in a significant increase in the flux. In comparison to ibuprofen, the solubility of ketoprofen is similar but it has a lower drug pKa. Therefore ketoprofen acts as a similar self-buffer to ibuprofen but will be impacted by increasing buffer concentrations more under the experimental conditions. As was seen with ibuprofen, the experimental flux of ketoprofen in bicarbonate buffer is not predicted accurately by the BCE and CAI models and is only accurately predicted when the dehydration reaction rate is incorporated by applying the IRR model.

Indomethacin Results

Figure 2.9 shows the experimental and predicted flux of indomethacin in bicarbonate buffer over a range of buffer concentrations at pH 6.5. In comparison to ibuprofen and ketoprofen, the solubility of indomethacin is much lower. Therefore indomethacin does not serve as an effective self-buffer which leads to the surface pH approaching the bulk pH at low buffer concentrations. As was seen for with the other weak acid drugs, the experimental flux of indomethacin in bicarbonate buffer is not predicted accurately by the BCE or CAI models and is only accurately predicted by applying the IRR model.

To provide further confirmation for the accuracy of the IRR model, previous experimental work involving rotating disk dissolution in bicarbonate buffer was evaluated. A specific example is work by McNamara et al. [10] that also looked at the weak acid drug indomethacin using rotating disk dissolution. Their work focused on dissolution at different bicarbonate buffer concentrations (different bulk P_{CO2}) at a bulk pH of 6.8. Figure 2.10 shows

that the IRR model gives accurate predictions for the flux of indomethacin that was interpolated from the rotating disk experiments of McNamara et al. (Figure 3 in their paper) using the parameters in Table 6 as well as the pKa for indomethacin that was reported in their paper (pKa = 4.17).

Discussion

The results show that the ability of bicarbonate to buffer the surface pH of a dissolving drug is dependent on the hydration/dehydration reaction kinetics. The boundry layer IRR model predicts the pH at the surface of the dissolving drug and allows for accurate predictions of drug flux consistent with the mass transport analysis. The success of the boundry layer IRR model indicates that H_2CO_3 will form CO_2 and H_2O through an irreversible reaction in the diffusion layer while undergoing its instantaneous, reversible ionization reaction to form bicarbonate. The IRR model, in effect, means that bicarbonate buffer behaves differently at the solid surface and in the boundary layer of a dissolving drug than it does in the bulk dissolution medium where the hydration/dehydration reaction is at equilibrium. In effect, bicarbonate has a "dynamic buffer capacity" represented by the IRR model at the dissolving surface and boundary layer where the hydration reaction can be assumed to not occur while it has the standard buffer capacity expected of bicarbonate buffer in the bulk.

Based on drug solubility and drug pKa, each drug studied has a different self-buffering effect at its dissolving surface. The results show that the IRR model accurately predicts surface pH and drug flux even when large differences in drug properties exist. For example, indomethacin has an intrinsic solubility ~100 times lower than ibuprofen and ketoprofen but this does not impact the accuracy of the predictions. Additionally, the ibuprofen and indomethacin data from this paper and from McNamara et al. shows the robustness of the IRR model to

changes in experimental conditions and the accuracy of the IRR model to be replicated in different laboratories. The IRR model can accurately account for surface pH changes when the bulk pH and diffusion layer thickness is altered. When the diffusion layer thickness decreases, less time is available for the protons that have formed H_2CO_3 to undergo the dehydration reaction and form CO_2 and H_2O. This changes the ability of bicarbonate to function as a buffer and it becomes similar to a situation where only the ionization reaction occurs. Therefore changing the rotational speed of the disk will change the surface pH and this can be well accounted for by the IRR model. The impact on surface pH that results from the changing diffusion layer thickness in the IRR model is one of the many factors taken into account in the cubic equation (Appendix: Equation 33) that calculates the pH at the surface of the dissolving drug. The only difference between the CAI and the IRR models is the mass transfer coefficient for the flux of carbonic acid: IRR = $\sqrt{k_d D_{H_2CO_3}}$ and CAI = $\frac{D_{H_2CO_3}}{h}$. When the ratio of the mass transfer coefficients equals one (h = 5.4 μm) then the pH at the surface becomes equal to the CAI model because the irreversible reaction is no longer consuming protons that will allow for an increase in the buffer capacity beyond the CAI model. Conversely, figures 3 and 4 show that as the diffusion layer thickness becomes larger, the proton consumption caused by the irreversible chemical reaction increases which allows for the IRR model to provide a similar buffer effect that is seen in the BCE model, However, this effect would only occur at unrealistically large diffusion layer thickness values.

Although bicarbonate is the buffer present in the GI tract, using it as a buffer in dissolution testing is challenging because of long preparation times and hydrodynamic concerns (i.e. presence of air and CO_2 gas bubbles in the apparatus) that make it less than ideal. However, the accuracy of the IRR model in predicting drug flux in bicarbonate buffer using known

physicochemical parameters allows for the possibility of predicting a more physiologically relevant buffer based on the physicochemical properties of the drug. Aunins et al. demonstrated that the dissolution of of weak acid drugs can be accurately predicted in standard buffers (i.e.: phosphate) using the standard film model[3]. The accuracy of these models creates the basis for the development of an *in vitro* dissolution buffer system with more standard buffers that would be more predictive of the *in vivo* buffer conditions. However, the work done in this paper and by Aunins et al. applies only to rotating disk dissolution with fixed experimental conditions in the bulk solution. A dissolving ionizable dosage form could have an effect on the bulk pH or introduce additional ionic or buffering species that could impact experimental and predicted dissolution rates . Additionally, the dynamic nature of the *in vivo* environment with dynamic intestinal secretion of bicarbonate, the absorption of water, and transit through the intestine continues to make prediction of *in vivo* dissolution complex.

Conclusions

Applying the boundary layer model with the assumption of instantaneous bulk chemical equilibrium (BCE model) does not accurately predict the buffer capacity of bicarbonate in the diffusion layer of a dissolving drug. Assuming that the hydration and dehydration reactions happen instantaneously overestimates the ability of bicarbonate to buffer the pH at the surface of the dissolving drug. On the other hand, assuming that both the dehydration and hydration reactions are too slow to occur in the diffusion layer (CAI model) underestimates the impact of bicarbonate buffer in the diffusion layer and at the surface of the tablet.

The predicted and experimental flux in bicarbonate buffer indicates the importance of the reaction kinetics in the bicarbonate buffer system. The effect of the slow hydration reaction in the diffusion layer has a significant impact on the buffer capacity of bicarbonate at the surface

of a dissolving drug and drug dissolution. The assumption that CO_2 does not react with H_2O in the diffusional boundary layer, and thus assuming that H_2CO_3 undergoes an irreversible chemical reaction forming CO_2 and H_2O in addition to its ionization reaction (pKa=3.55), accurately predicts the effect that bicarbonate buffer has on the pH in the diffusion layer. The IRR model is intermediate between the BCE and CAI models and most accurately describes the experimental results. In effect, bicarbonate has: (a) a "dynamic buffer capacity" represented by the IRR model at the dissolving surface where the hydration reaction can be assumed to not occur and, (b) the standard buffer capacity expected of bicarbonate buffer in the bulk where the hydration reaction can be assumed to occur sufficiently quickly to appear to be instantaneous (ie. is at equilibrium). The irreversible reaction in the diffusion layer where H_2CO_3 forms CO_2 and H_2O allows protons to be consumed and assists in buffering the pH at the surface of the tablet. The protons consumed by the irreversible reaction is a function of the time H_2CO_3 spends in the diffusion boundary layer and is therefore dependent on the thickness of the diffusion layer. Unlike the film models, assuming instantaneous chemical equilibrium (BCE and CAI), the pH at the surface in the IRR model is a function of diffusion layer thickness.

The IRR model has been shown to accurately predict the rotating disk dissolution rate of the weak acid drugs studied. More experimental work is needed to assess its applicability to weak bases and amphoteric drugs. However, for ionizable drugs, the pH at the surface is a key component in determining the rate at which the drug will dissolve, and the IRR model is accurate at predicting surface pH under various experimental conditions examined in this paper. Therefore, the IRR model may be used to identify buffers that more closely resemble the bicarbonate buffer of the luminal fluid and provide an approach for the development of more relevant *in vivo* dissolution media.

Appendix

Irreversible Reaction (IRR) model for the dissolution of weak acid drugs (HA = unionized form of the weak acid drug; A^- = ionized form of the weak acid drug) in bicarbonate buffer. Below are the the equilibrium reactions before the irreversible dehydration reaction assumption is introduced:

$$H^+ + OH^- \overset{K_W}{\underset{\rightarrow}{\leftarrow}} H_2O$$

$$HA \overset{K_a^A}{\underset{\rightarrow}{\leftarrow}} H^+ + A^-$$

$$HA + OH^- \overset{K_1^*}{\underset{\rightarrow}{\leftarrow}} H_2O + A^-$$

$$HA + HCO_3^- \overset{K_2}{\underset{\rightarrow}{\leftarrow}} H_2CO_3 + A^-$$

$$CO_2 + H_2O \overset{K_c}{\underset{\rightarrow}{\leftarrow}} H_2CO_3$$

$$H_2CO_3 \overset{K_{a1}}{\underset{\rightarrow}{\longleftarrow}} HCO_3^- + H^+$$

$CO_2 + OH^- \overset{K_{a2}}{\underset{\rightarrow}{\longleftarrow}} HCO_3^-$ is not considered because research has shown that this reaction would not play a role at the pH the experiments were performed at [32].

Chemical equilibrium constant equations:

$$K_w = [H^+][OH^-] \text{ (Eq. A1)}$$

$$K_a^A = \frac{[A^-][H^+]}{[HA]} \text{ (Eq. A2)}$$

$$K_1 = \frac{[A^-]}{[HA][OH^-]} = \frac{K_a^A}{K_W} \text{ (Eq. A3)}$$

$$K_2 = \frac{[A^-][H_2CO_3]}{[HA][HCO_3^-]} = \frac{K_a^A}{K_{a2}^B} \text{ (Eq. A4)}$$

$$K_c = \frac{[H_2CO_3]}{[CO_2]} = \frac{k_h}{k_d} \text{ (Eq. A5)}$$

$$K_{a1} = \frac{[HCO_3^-][H^+]}{[H_2CO_3]} = \frac{k_{a1f}}{k_{a1r}} \text{ (Eq.A6)}$$

Differential equations defining the flux of the different species:

$$\frac{\delta[HA]}{\delta t} = D_{HA}\frac{\delta^2[HA]}{\delta X^2} + \emptyset_1 = 0 \text{ (Eq. A7)}$$

$$\frac{\delta[A^-]}{\delta t} = D_A\frac{\delta^2[A^-]}{\delta X^2} + \emptyset_2 = 0 \text{ (Eq. A8)}$$

$$\frac{\delta[H^+]}{\delta t} = D_H\frac{\delta^2[H^+]}{\delta X^2} + \emptyset_3 = 0 \text{ (Eq. A9)}$$

$$\frac{\delta[OH^-]}{\delta t} = D_{OH}\frac{\delta^2[OH^-]}{\delta X^2} + \emptyset_4 = 0 \text{ (Eq.A10)}$$

$$\frac{\delta[HCO_3^-]}{\delta t} = D_{HCO_3}\frac{\delta^2[HCO_3^-]}{\delta X^2} + \emptyset_5 = 0 \text{ (Eq. A11)}$$

$$\frac{\delta[H_2CO_3]}{\delta t} = D_{H_2CO_3}\frac{\delta^2[H_2CO_3]}{\delta X^2} + \emptyset_6 = 0 \text{ (Eq. A12)}$$

$$\frac{\delta[CO_2]}{\delta t} = D_{CO_2}\frac{\delta^2[CO_2]}{\delta X^2} + \emptyset_7 = 0 \text{ (Eq. A13)}$$

Defining ∅ 1-7 for the differential equations:

$$\emptyset_1 = -k_{af}^A[HA] + k_{ar}^A[H^+][A^-] - k_{1f}[HA][OH^-] + k_{1r}[A^-] - k_{2f}[HA][HCO_3^-] + k_{2r}[H_2CO_3][A^-]$$

$$\emptyset_2 = k_{af}^A[HA] - k_{ar}^A[H^+][A^-] + k_{1f}[HA][OH^-] - k_{1r}[A^-] + K_{2f}[HA][HCO_3^-] - k_{2r}[H_2CO_3][A^-]$$

$$\emptyset_3 = k_{af}^A[HA] - k_{ar}^A[H^+][A^-] + k_{a1f}[H_2CO_3] - k_{a1r}[H^+][HCO_3^-]$$

$$\emptyset_4 = -k_{1f}[HA][OH^-] + k_{1r}[A^-]$$

$$\emptyset_5 = -K_{2f}[HA][HCO_3^-] + K_{2r}[H_2CO_3][A^-] + k_{a1f}[H_2CO_3] - k_{a1r}[H^+][HCO_3^-]$$

$$\emptyset_6 = k_{2f}[HA][HCO_3^-] - k_{2r}[H_2CO_3][A^-] + k_h[CO_2] - k_d[H_2CO_3] - k_{a1f}[H_2CO_3] + k_{a1r}[H^+][HCO_3^-]$$

$$\emptyset_7 = -k_h[CO_2] + k_d[H_2CO_3]$$

Setting up relations for ∅ and the diffusion terms based on assumptions from mooney et al. 1981:

The first relation is that the amount of components reacting as acids must equal the amount of components acting as bases.

$$\emptyset_4 + \emptyset_5 = \emptyset_1 + \emptyset_3 \quad \text{(Eq. A14)}$$

Eq. 14 based on the definitions for phi above:

$$\left(-k_{1f}[HA][OH^-] + k_{1r}[A^-]\right) + \left(-k_{2f}[HA][HCO_3^-] + k_{2r}[H_2CO_3][A^-] + k_{a1f}[H_2CO_3] - ka1rH+HCO3- = -kafAHA+KarAH+A--k1fHA[OH-]+k1rA--k2fHA[HCO3-]+k2r[H2CO3]A-+kafAHA-karAH+A-+ka1fH2CO3-ka1rH+HCO3- \quad \text{(Eq. A15)}$$

The like terms cancel on each side of the above equation which leads to Eq.15 becoming: $0 = 0$

The second assumption is that the acid drug in solution is neither created nor destroyed.

$$\emptyset_1 + \emptyset_2 = 0 \quad \text{(Eq. A16)}$$

Eq. 16 based on the definitions for phi above:

$$0 = \left(-k_{af}^A[HA] + k_{ar}^A[H^+][A^-] - k_{1f}[HA][OH^-] + k_{1r}[A^-] - k_{2f}[HA][HCO_3^-] + k_{2r}[H_2CO_3][A^-]\right) + \left(k_{af}^A[HA] - k_{ar}^A[H^+][A^-] + k_{1f}[HA][OH^-] - k_{1r}[A^-] + k_{2f}[HA][HCO_3^-] - k_{2r}[H_2CO_3][A^-]\right)$$

Equation 16 allows for the relation made in equation 17 based on the assumption of steady state.

$$D_{HA}\frac{\delta^2[HA]}{\delta X^2} + D_A\frac{\delta^2[A^-]}{\delta X^2} = 0 \quad \text{(Eq. A17)}$$

The third assumption is that since k_h is so small (~0.1-0.16s^{-1}) it is going to be assumed that it is not playing a role in formation of any H_2CO_3in the diffusion layer. Therefore H_2CO_3 is undergoing an irreversible chemical reaction to form CO_2 and H_2O in addition to the reversible ionization reaction that forms H^+ and HCO_3^-. The change in carbon dioxide concentration has no effect on the other buffer components leading to the Irreversible Reaction Model (IRR Model).

$$CO_2(aq) + H_2O \overset{k_d}{\leftarrow} H_2CO_3 \overset{K_1}{\underset{\leftarrow}{\rightarrow}} H^+ + HCO_3^-$$

Therefore it is assumed that the only two buffer components are H_2CO_3 and HCO_3^-. The change in bicarbonate is based only upon the change in carbonic acid. This assumption leads to equation 18:

$$D_{HCO_3}\frac{\delta^2[HCO_3^-]}{\delta X^2} - k_{2f}[HA][HCO_3^-] + k_{2r}[H_2CO_3][A^-] + k_{a1f}[H_2CO_3] - k_{a1r}[H^+][HCO_3^-] +=$$

$$-(D_{H_2CO_3}\frac{\delta^2[H_2CO_3]}{\delta X^2} + k_{2f}[HA][HCO_3^-] - k_{2r}[H_2CO_3][A^-] - k_{a1f}[H_2CO_3] +$$

$$k_{a1r}[H^+][HCO_3^-] - k\ \ [H_2CO_3]) \quad \text{(Eq. A18)}$$

All of the like terms cancel and equation 18 simplifies to equation 19.

$$D_{HCO_3}\frac{\delta^2[HCO_3^-]}{\delta X^2} = -(D_{H_2CO_3}\frac{\delta^2[H_2CO_3]}{\delta X^2} - k\ \ [H_2CO_3]) \quad \text{(Eq. A19).}$$

At this point, all of the second order differential equations can be solved. For all of the terms that are diffusion controlled the boundary conditions and general solution are shown below.

$$D_C\frac{\delta^2[C]}{\delta X^2} = 0 \quad \text{(Eq. A20)}$$

$$Boundary\ Conditions:$$

$$at\ x = h; \quad C = C_h$$

$$at\ x = 0; \quad C = C_0$$

The general solution to the second order differential is shown below.

$$c = \frac{(C_h - C_o)x}{h} + C_0 \qquad \text{(Eq. A21)}$$

H_2CO_3 is not only diffusion controlled because it also undergoes an irreversible chemical reaction. The boundary conditions are the same for the species but its general solution is different.

$$D_{H_2CO_3}\frac{\delta^2[H_2CO_3]}{\delta X^2} - k\ \ [H_2CO_3] = 0 \qquad \text{(Eq. A22)}$$

$$D_{H_2CO_3}\frac{\delta^2[H_2CO_3]}{\delta X^2} = k\ \ [H_2CO_3]$$

$$Boundary\ Conditions:$$

$$at\ x = h; \quad C = [H_2CO_3]_h$$

$$at\ x = 0; \quad C = [H_2CO_3]_0$$

The general solution to the second order differential for carbonic acid is shown below.

$$\frac{\left(-[H_2CO_3]_0 e^{-\frac{\sqrt{k_d}}{\sqrt{D_{H_2CO_3}}}h} + [H_2CO_3]_h\right) e^{\frac{\sqrt{k_d}}{\sqrt{D_{H_2CO_3}}}x}}{e^{\frac{\sqrt{k_d}}{\sqrt{D_{H_2CO_3}}}h} - e^{-\frac{\sqrt{k_d}}{\sqrt{D_{H_2CO_3}}}h}} - \frac{\left([H_2CO_3]_h - [H_2CO_3]_0 e^{\frac{\sqrt{k_d}}{\sqrt{D_{H_2CO_3}}}h}\right) e^{-\frac{\sqrt{k_d}}{\sqrt{D_{H_2CO_3}}}x}}{e^{\frac{\sqrt{k_d}}{\sqrt{D_{H_2CO_3}}}h} - e^{-\frac{\sqrt{k_d}}{\sqrt{D_{H_2CO_3}}}h}} \qquad \text{(Eq. A23a)}$$

The diffusion coefficient of carbonic acid is a constant ($D_{H_2CO_3}$=14.6 x 10^{-6}cm^2/s) and so is the dehydration rate constant ($k_d = 50s^{-1}$). The diffusion layer thickness changes based on the Levich equation but it is on the order of 0.001-0.005. Therefore $e^{-\frac{\sqrt{k_d}}{\sqrt{D_{H_2CO_3}}}h}$ is so small (~4 x 10^{-5}) in comparison to $e^{\frac{\sqrt{k_d}}{\sqrt{D_{H_2CO_3}}}h}$ (~2.5 x 10^4) that it can be assumed that $e^{-\frac{\sqrt{k_d}}{\sqrt{D_{H_2CO_3}}}h}$ and

$-[H_2CO_3]_0 e^{-\frac{\sqrt{k_d}}{\sqrt{D_{H_2CO_3}}}h}$ (~ 10^{-7}-10^{-9})and $[H_2CO_3]_h e^{-\frac{\sqrt{k_d}}{\sqrt{D_{H_2CO_3}}}h}$ (~ 10^{-9}-10^{-10}) is equal to zero and equation 23a becomes Eq. 23b.

$$\frac{[H_2CO_3]_h e^{\frac{\sqrt{k_d}}{\sqrt{D_{H_2CO_3}}}x}}{e^{\frac{\sqrt{k_d}}{\sqrt{D_{H_2CO_3}}}h}} - \frac{\left([H_2CO_3]_0 e^{\frac{\sqrt{k_d}}{\sqrt{D_{H_2CO_3}}}h}\right) e^{-\frac{\sqrt{k_d}}{\sqrt{D_{H_2CO_3}}}x}}{e^{\frac{\sqrt{k_d}}{\sqrt{D_{H_2CO_3}}}h}} \quad \text{(Eq. A23b)}$$

In order to apply the rest of the assumptions to the film model, the derivative to all of the general solutions must be obtained in order to define all of the species in terms of flux.

Taking the derivative of all of the diffusion controlled species gives the equation below:

$$\frac{\partial[C]}{\partial X} = \frac{(C_h - C_o)}{h} \quad \text{(Eq. A24)}$$

Equation 24 must be multiplied by the diffusion coefficient to give the flux of the species.

$$D\frac{\partial[C]}{\partial X} = D\frac{(C_h - C_o)}{h} \qquad \text{(Eq. A25)}$$

Taking the derivative of the general solution for H_2CO_3 (Eq. 23b) gives equation 26.

$$\frac{[H_2CO_3]_h\sqrt{k_d}e^{\frac{\sqrt{k_d}}{\sqrt{D_{H_2CO_3}}}x}}{\sqrt{D_{H_2CO_3}}e^{\frac{\sqrt{k_d}}{\sqrt{D_{H_2CO_3}}}h}} - \frac{[H_2CO_3]_0\sqrt{k_d}e^{-\frac{\sqrt{k_d}}{\sqrt{D_{H_2CO_3}}}x}}{\sqrt{D_{H_2CO_3}}} \qquad (Eq.\,A26)$$

In order to solve for the flux from x=h to x=0, the h and x must be inserted into equation 26.

At x= 0

$$\frac{[H_2CO_3]_h\sqrt{k_d}e^{\frac{\sqrt{k_d}}{\sqrt{D_{H_2CO_3}}}0}}{\sqrt{D_{H_2CO_3}}e^{\frac{\sqrt{k_d}}{\sqrt{D_{H_2CO_3}}}h}} - \frac{[H_2CO_3]_0\sqrt{k_d}e^{-\frac{\sqrt{k_d}}{\sqrt{D_{H_2CO_3}}}0}}{\sqrt{D_{H_2CO_3}}}$$

$e^{\frac{\sqrt{k_d}}{\sqrt{D_{H_2CO_3}}}0}$ is equal to 1 which simplifies the above equation:

$$\frac{[H_2CO_3]_h\sqrt{k_d}}{\sqrt{D_{H_2CO_3}}e^{\frac{\sqrt{k_d}}{\sqrt{D_{H_2CO_3}}}h}} - \frac{[H_2CO_3]_0\sqrt{k_d}}{\sqrt{D_{H_2CO_3}}}$$

$\sqrt{D}e^{\frac{\sqrt{k_d}}{\sqrt{D_{H_2CO_3}}}h}$ (~ 0.4) $\gg [H_2CO_3]_h\sqrt{k_d}$ (~10^{-4}- 10^{-5}) that $\frac{[H_2CO_3]_h\sqrt{k_d}}{\sqrt{D}e^{\frac{\sqrt{k_d}}{\sqrt{D_{H_2CO_3}}}h}}$ is considered to be zero

which leaves:

$$-\frac{[H_2CO_3]_0\sqrt{k_d}}{\sqrt{D_{H_2CO_3}}}$$

At x= h

$$\frac{[H_2CO_3]_h\sqrt{k_d}e^{\frac{\sqrt{k_d}}{\sqrt{D_{H_2CO_3}}}h}}{\sqrt{D_{H_2CO_3}}e^{\frac{\sqrt{k_d}}{\sqrt{D_{H_2CO_3}}}h}} - \frac{[H_2CO_3]_0\sqrt{k_d}e^{-\frac{\sqrt{k_d}}{\sqrt{D_{H_2CO_3}}}h}}{\sqrt{D_{H_2CO_3}}}$$

$e^{-\frac{\sqrt{k_d}}{\sqrt{D_{H_2CO_3}}}h}$ is so small (~4 x 10^{-5}) that it can be assumed that it and

$-[H_2CO_3]_0\sqrt{k_d}e^{-\frac{\sqrt{k_d}}{\sqrt{D_{H_2CO_3}}}h} = 0$

$$\frac{[H_2CO_3]_h\sqrt{k_d}}{\sqrt{D_{H_2CO_3}}}$$

Therefore $\frac{\partial[H_2CO_3]}{\partial x}$ from x=h (bulk solution) to the surface of the tablet (x=0) is

$$\frac{\partial[H_2CO_3]}{\partial x} = \frac{\sqrt{k_d}}{\sqrt{D_{H_2CO_3}}}([H_2CO_3]_h - [H_2CO_3]_0) \quad (Eq. A27)$$

If you multiply each side by the diffusion coefficient of carbonic acid, then that will give the flux of carbonic acid.

$$D_{H_2CO_3}\frac{\partial[H_2CO_3]}{\partial x} = ([H_2CO_3]_h - [H_2CO_3]_0)\sqrt{D_{H_2CO_3}k_d} \quad (Eq. A28)$$

It is assumed that electric neutrality is maintained at every point in the diffusion layer so the positively charged species flux must be equal to the negatively charged species flux.

$$\sum z_i J_i = 0 \quad \text{(Eq. 29)}$$

$$D_H\frac{([H^+]_h - [H^+]_0)}{h} = D_{OH}\frac{([OH^-]_h - [OH^-]_0)}{h} + D_A\frac{([A^-]_h - [A^-]_0)}{h} + D_{HCO_3}\frac{([HCO_3^-]_h - [HCO_3^-]_0)}{h} \quad \text{(Eq. A30)}$$

Another assumption is that since no boundary or internal sources of buffer exist, then the total buffer flux must be equal to 0.

$$D_{HCO_3}\frac{([HCO_3^-]_h - [HCO_3^-]_0)}{h} + ([H_2CO_3]_h - [H_2CO_3]_0)\sqrt{D_{H_2CO_3}k_d} = 0 \quad \text{(Eq. A31)}$$

$$D_{HCO_3}\frac{([HCO_3^-]_h - [HCO_3^-]_0)}{h} = -([H_2CO_3]_h - [H_2CO_3]_0)\sqrt{D_{H_2CO_3}k_d} \quad \text{(Eq. A32)}$$

Equation 32 can be used to find the concentration of bicarbonate at the surface of the tablet. First it must be put in terms of known values and H^+ at the surface of the tablet as shown below.

$$D_{HCO_3}([HCO_3^-]_h - [HCO_3^-]_0) = -([H_2CO_3]_h - [H_2CO_3]_0)h\sqrt{D_{H_2CO_3}k_d}$$

$$-D_{HCO_3}[HCO_3^-]_0 - [H_2CO_3]_0\left(h\sqrt{D_{H_2CO_3}k_d}\right) = -[H_2CO_3]_h\left(h\sqrt{D_{H_2CO_3}k_d}\right) - D_{HCO_3}[HCO_3^-]_h$$

$$[H_2CO_3]_0 = \frac{[HCO_3^-]_0[H^+]_0}{K_{a1}}$$

$$D_{HCO_3}[HCO_3^-]_0 + \frac{[HCO_3^-]_0[H^+]_0}{K_{a1}}\left(h\sqrt{D_{H_2CO_3}k_d}\right)$$

$$= [H_2CO_3]_h\left(h\sqrt{D_{H_2CO_3}k_d}\right) + D_{HCO_3}[HCO_3^-]_h$$

$$[HCO_3^-]_0\left(K_{a1}D_{HCO_3} + [H^+]_0\left(h\sqrt{D_{H_2CO_3}k_d}\right)\right)$$

$$= K_{a1}\left([H_2CO_3]_h\left(h\sqrt{D_{H_2CO_3}k_d}\right) + D_{HCO_3}[HCO_3^-]_h\right)$$

$$[HCO_3^-]_0 = \frac{K_{a1}\left([H_2CO_3]_h\left(h\sqrt{D_{H_2CO_3}k_d}\right) + D_{HCO_3}[HCO_3^-]_h\right)}{\left(K_{a1}D_{HCO_3} + [H^+]_0\left(h\sqrt{D_{H_2CO_3}k_d}\right)\right)}$$

The above equation can be inserted into equation 30 where electric neutrality is assumed in the diffusion layer.

$$D_H\frac{([H^+]_h - [H^+]_0)}{h} =$$

$$D_{OH}\frac{([OH^-]_h - [OH^-]_0)}{h} + D_A\frac{([A^-]_h - [A^-]_0)}{h} +$$

$$\frac{D_{HCO_3}}{h}\left([HCO_3^-]_h - \left(\frac{K_{a1}\left([H_2CO_3]_h\left(h\sqrt{D_{H_2CO_3}k_d}\right) + D_{HCO_3}[HCO_3^-]_h\right)}{\left(K_{a1}D_{HCO_3} + [H^+]_0\left(h\sqrt{D_{H_2CO_3}k_d}\right)\right)}\right)\right) \quad \text{(Eq. A30b)}$$

The chemical equilibrium in equations 1 and 2 were used to define all of the species at the surface of the tablet (x=0) in either terms of $[H^+]_0$ or $[HA]_0$.

$$D_H\frac{([H^+]_h - [H^+]_0)}{h} = \frac{D_{OH}}{h}\left([OH^-]_h - \frac{K_w}{[H^+]_0}\right) + \frac{D_A}{h}\left([A^-]_h - \frac{[HA]_0K_a^A}{[H^+]_0}\right) + \frac{D_{HCO_3}}{h}\left([HCO_3^-]_h -\right.$$

$$Ka1H2CO3hhDH2CO3kd + DHCO3HCO3 - hKa1DHCO3 + H + 0hDH2CO3kd \quad \text{(Eq. A30c)}$$

The pH at the surface can be calculated by applying the boundary conditions to equation 30c.

Boundary Conditions at X = h (bulk solution):

$[HA] = [HA]_h \cong 0$

$[A^-] = [A^-]_h \cong 0$

$[H^+] = [H^+]_h \ (known)$ = Bulk pH

$[OH^-] = [OH^-]_h \ (known)$ = Known based on bulk pH and chemical equilibrium

$[HCO_3^-] = [HCO_3^-]_h \ (known)$ = Experimental Buffer Concentration

$[H_2CO_3] = [H_2CO_3]_h \ (known)$ = Experimental Buffer Concentration

$[CO_2] = [CO_2]_h \ (known)$ = Analyzed with a CO_2 monitor.

Boundary Conditions at X = 0 (surface of the drug):

$[HA] = [HA]_0 \quad (Weak\ acid\ intrinsic\ Solubility)$

$[A^-] = [A^-]_0 \ (Unknown)$

$[H^+] = [H^+]_0 \ (Unknown)$

$[OH^-] = [OH^-]_0 \ (Unknown)$

$[HCO_3^-] = [HCO_3^-]_0 \ (Unknown)$

$[H_2CO_3] = [H_2CO_3]_0 \ (Unknown)$

$[CO_2] = [CO_2]_0 \ (Unknown)$

$$D_H \frac{([H^+]_h - [H^+]_0)}{h} =$$

$$\frac{D_{OH}}{h}\left([OH^-]_h - \frac{K_w}{[H^+]_0}\right) + \frac{D_A}{h}\left(-\frac{[HA]_0 K_a^A}{[H^+]_0}\right) +$$

$$\frac{D_{HCO_3}}{h}\left([HCO_3^-]_h - \left(\frac{K_{a1}([H_2CO_3]_h(h\sqrt{D_{H_2CO_3}k_d}) + D_{HCO_3}[HCO_3^-]_h)}{\left(K_{a1}D_{HCO_3} + [H^+]_0(h\sqrt{D_{H_2CO_3}k_d})\right)}\right)\right) \quad \text{(Eq. A30d)}$$

Multiplying equation 30d by h and subtracting the right side of the equation from the left side results in the following cubic equation to solve for $[H^+]_0$.

$$p[H^+]_0^3 + q[H^+]_0^2 + r[H^+]_0 + s = 0 \quad \text{(Eq. A33)}$$

$$\boldsymbol{p} = D_H\left(h\sqrt{D_{H_2CO_3}k_d}\right)$$

$$\boldsymbol{q} = -D_H[H^+]_h\left(h\sqrt{D_{H_2CO_3}k_d}\right) + D_{OH}[OH^-]_h\left(h\sqrt{D_{H_2CO_3}k_d}\right)$$

$$+ D_{HCO_3}[HCO_3^-]_h\left(h\sqrt{D_{H_2CO_3}k_d}\right) + K_{a1}D_{HCO_3}D_H$$

$$\boldsymbol{r} = -K_{a1}D_{HCO_3}D_H[H^+]_h + K_{a1}D_{HCO_3}D_{OH}[OH^-]_h - D_{OH}K_w\left(h\sqrt{D_{H_2CO_3}k_d}\right)$$

$$- D_A[HA]_0K_a^A\left(h\sqrt{D_{H_2CO_3}k_d}\right) - D_{HCO_3}^2K_{a1}[HCO_3^-]_h$$

$$- D_{HCO_3}[H_2CO_3]_hK_{a1}\left(h\sqrt{D_{H_2CO_3}k_d}\right) + D_{HCO_3}^2K_{a1}[HCO_3^-]_h$$

$$\boldsymbol{s} = -K_{a1}D_{HCO_3}D_{OH}K_w - K_{a1}D_{HCO_3}D_A[HA]_0K_a^A$$

The total drug flux is dependent on the interfacial pH.

$$D_{HA}\frac{([HA]_h-[HA]_0)}{h} + D_A\frac{([A^-]_h-[A^-]_0)}{h} = total\ drug\ flux \quad \text{(Eq. A34a)}$$

$[HA] = [HA]_h \cong 0$

$[A^-] = [A^-]_h \cong 0$

$$D_{HA}\frac{-[HA]_0}{h} + D_A\frac{-[A^-]_0}{h} = total\ drug\ flux \quad \text{(Eq. A34b)}$$

$$D_{HA}\frac{-[HA]_0}{h} - \frac{D_A}{h}\frac{[HA]_0K_a^A}{[H^+]_0} = total\ drug\ flux \quad \text{(Eq. A34c)}$$

Assuming the diffusion coefficient of the ionized form of the drug is equal to the unionized form of the drug simplifies equation 34c to equation 34d.

$$-D_{HA}\frac{[HA]_0}{h}\left(1 + \frac{K_a^A}{[H^+]_0}\right) = total\ drug\ flux \quad \text{(Eq. A34d)}$$

Tables

Table 2. 1. The effect diffusion layer thickness (Ibuprofen used for h calculation) has on the time CO_2 spends in the diffusion layer (t_D) and how it compares to the reaction time (t_r = 8s)

h (μm)	t_D	t_r/t_D
61 (50 RPM)	0.76	11
43 (100 RPM)	0.38	21
27 (250 RPM)	0.15	53
19 (500 RPM)	0.076	106
14 (1000 RPM)	0.04	212

Table 2. 2. Drug and buffer properties applied to the simultaneous diffusion and reaction model

Species	Solubility (M)	pKa	Diffusion Coefficient (cm^2/s)
Ibuprofen	3.30×10^{-4} [31]	4.43 [31]	7.93×10^{-6} [b]
Indomethacin	5.963×10^{-6} [c]	4.27 [33]	6.8×10^{-6} [34]
Ketoprofen	5.303×10^{-4} [c]	4.02[35,36]	9.3×10^{-6} [3]
Bulk Bicarbonate		6.04 [c]	14.6×10^{-6} [37]
Carbonic Acid		3.55[38]	14.6×10^{-6} [37]
Carbon Dioxide	0.02403		24.9×10^{-6} [39]

Values were taken from literature, estimated using the Wilke-Chang equation (b), or measured experimentally (c). Table 3 average values (d)

Table 2. 3. Rotating disk dissolution experimental parameters applied to the weak acid drugs examined

Drug			Ibuprofen		Indomethacin	Ketoprofen
Bulk pH	5.5	6.0	6.5	7.0	6.5	6.5
Percent CO2	50	45	7-8, 14-16*, 21-22	5	7-8, 14-16, 21-22	7-8, 14-16, 24-26
Total Buffer concentration $[CO_2(aq)]+[HCO3^-]$ (mM)	15.5	20.7	6.5-7.5, 13-15*, 19.5-20.5	12.2	6.5-7.5, 13-15, 19.5-20.5	6.5-7.5, 13-15, 22-24
Bicarbonate Concentration [HCO3-] (mM)	3.5	9.9	5-5.5, 10-11*, 14.5-15.5	11	5-5.5, 10-11, 14.5-15.5	5-5.5, 10-11, 16.5-18.0
RPM	100	100	50, 100, 250, 500	100	100	100

* = the concentration used for the ibuprofen experiments at 50, 250 and 500 RPM. For ibuprofen at pH 6.5 and 100 RPM all buffer concentrations listed were used.

Figures

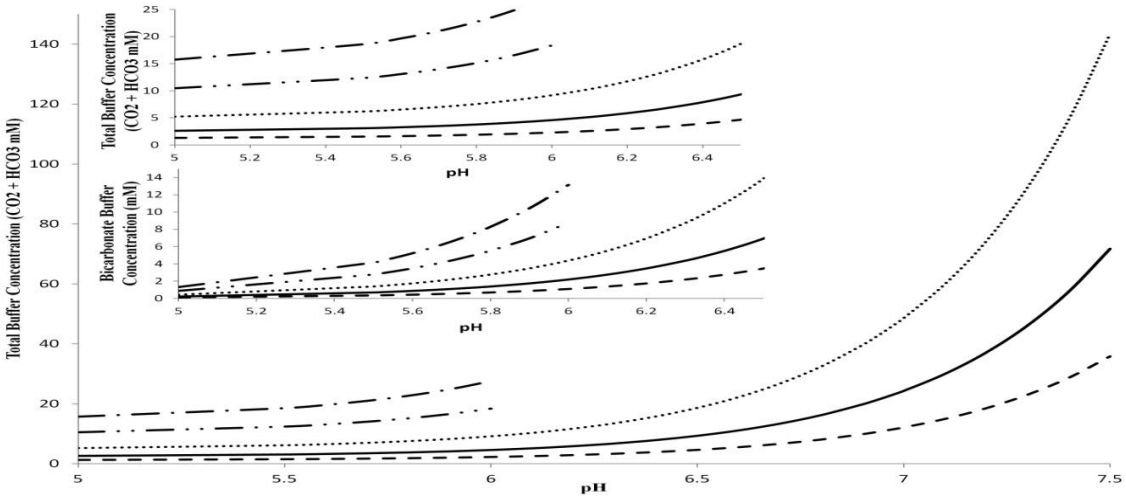

Figure 2. 1. Total buffer and Bicarbonate buffer concentrations (mM) at physiologically relevant pH values as function of %CO2 in the solution (100% = 1atm) at 37^{o} C. Key (– – –) 5% CO_2; (———) 10% CO_2; (·····) 20% CO_2; (— ·) 40% CO_2; (— · ·) 60% CO_2;

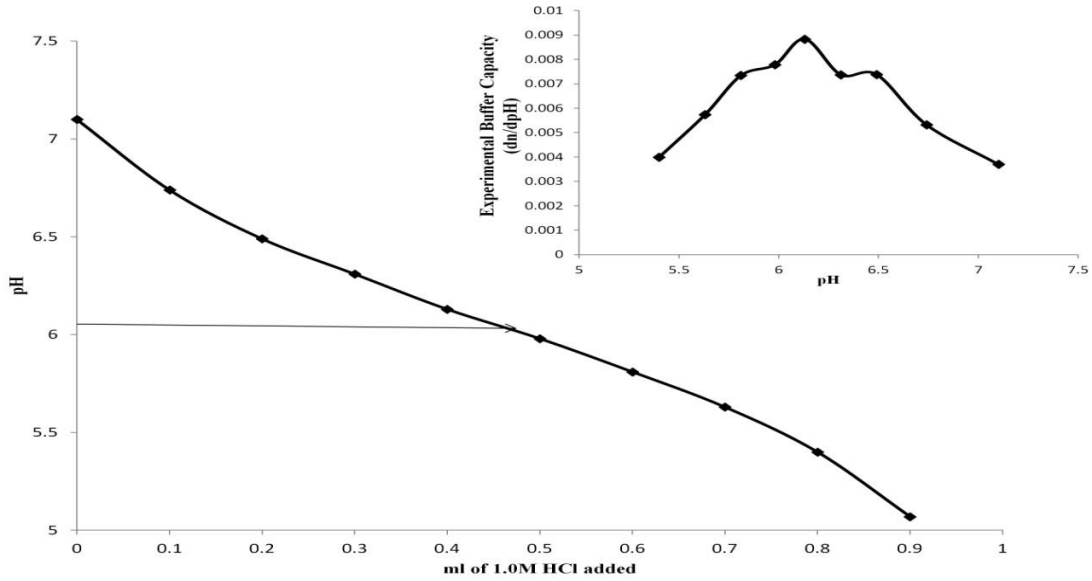

Figure 2. 2. Titration curve for a closed bicarbonate buffer system at 37^{o}C and isotonic ionic strength (0.154M).

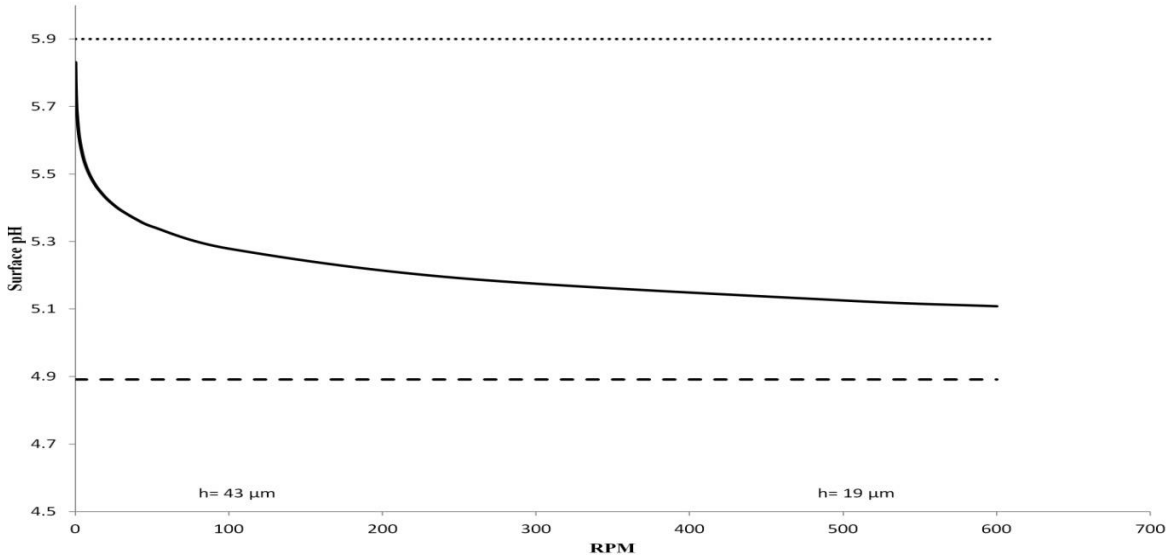

Figure 2. 3. The predicted surface pH of ibuprofen in 10mM bicarbonate buffer at pH 6.5 and different rotational speeds at 37^{o}C. Key (·····) BCE Model Predictions; (———) IRR Model Predictions; (– – –) CAI Model Predictions;

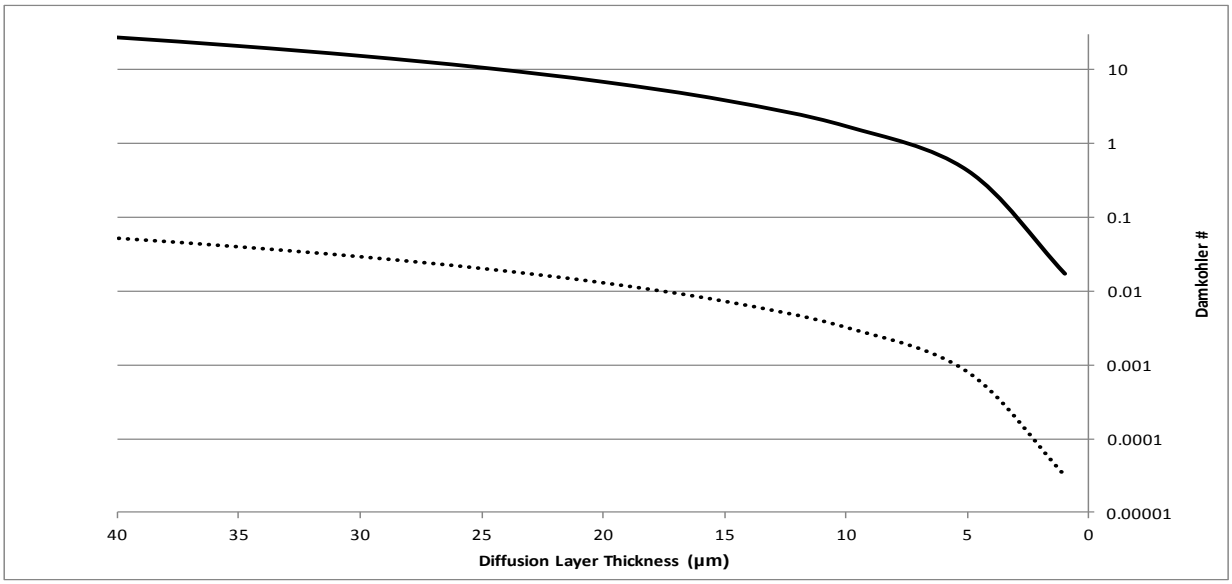

Figure 2. 4 The calculated Damkohler numbers for the hydration and dehydration reactions as a function of diffusion layer thickness. Key (———) Damkohler numbers for the dehydration reaction; (·····) Damkohler numbers for the hydration reaction;

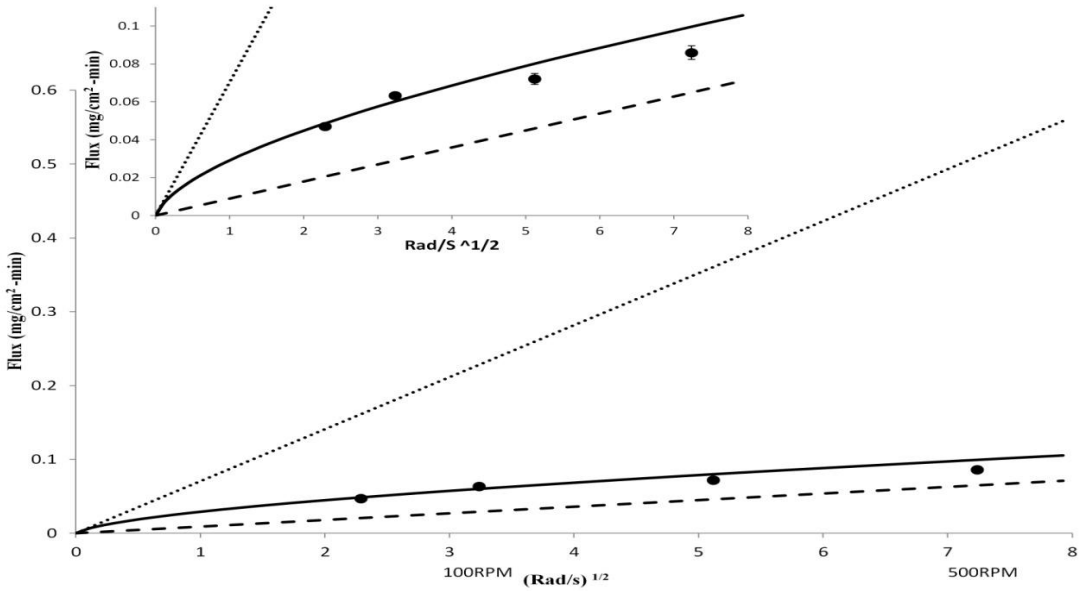

Figure 2. 5. The experimental (50, 100, 250, and 500 RPM) and predicted flux of ibuprofen in 10mM bicarbonate buffer at pH 6.5 and different rotational speeds at 37^{o}C. Key (•) Experimental Flux; (⋯⋯) BCE Model Flux Predictions; (——) IRR Model Flux Predictions; (– – –) CAI Model Flux Predictions;

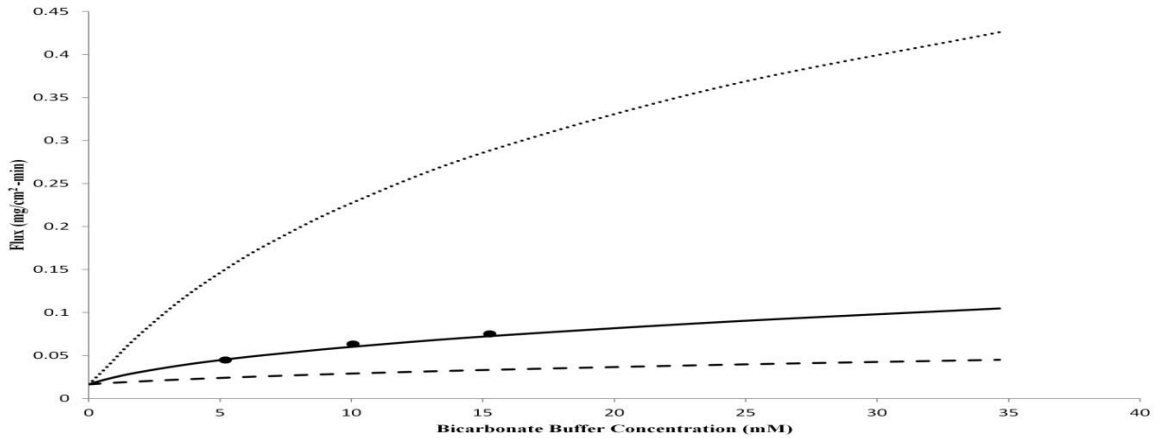

Figure 2. 6. The experimental and predicted flux of ibuprofen in bicarbonate buffer at multiple concentrations (at pH 6.5 and 37^{o}C). Key (•) Experimental Flux; (.....) BCE Model Flux Predictions; (——) IRR Model Flux Predictions; (– – –) CAI Model Flux Predictions;

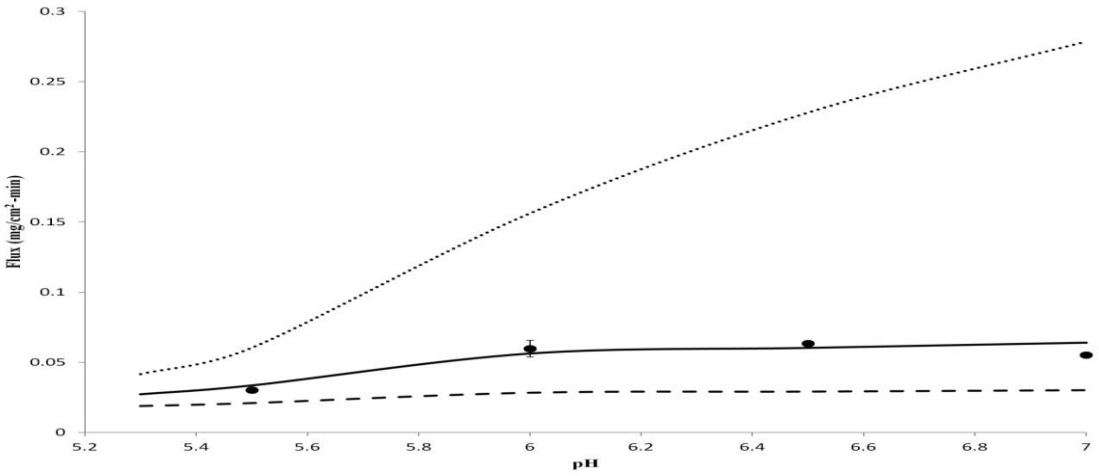

Figure 2. 7. The experimental and predicted flux of ibuprofen in 10 mM bicarbonate buffer at bulk pH values of 5.3(3.5mM HCO_3^-), 6, 6.5 and 7 at 37^oC. Key (•) Experimental Flux; (·····) BCE Model Flux Predictions; (——) IRR Model Flux Predictions; (– – –) CAI Model Flux Predictions;

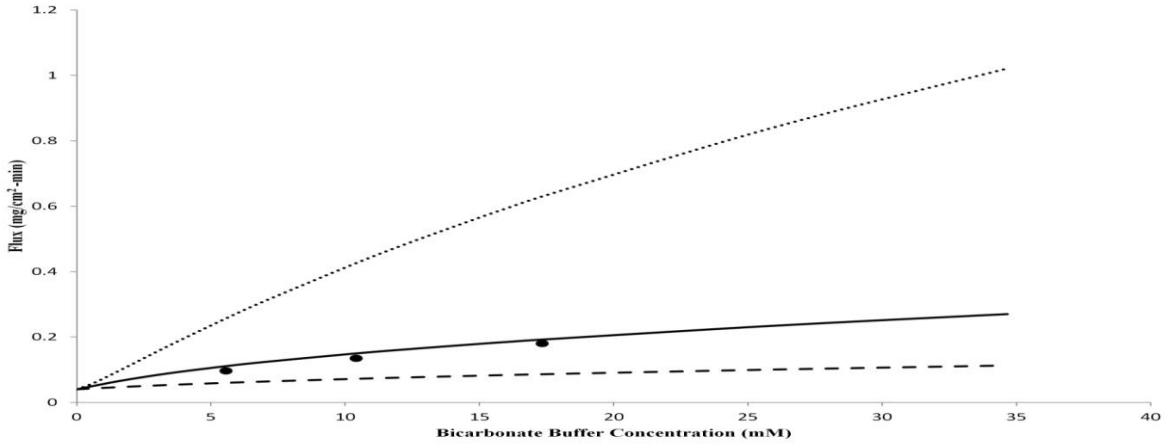

Figure 2. 8. The experimental and predicted flux of Ketoprofen in bicarbonate buffer at multiple concentrations (at pH 6.5 and 37^oC). Key (•) Experimental Flux; (·····) BCE Model Flux Predictions; (——) IRR Model Flux Predictions; (– – –) CAI Model Flux Predictions

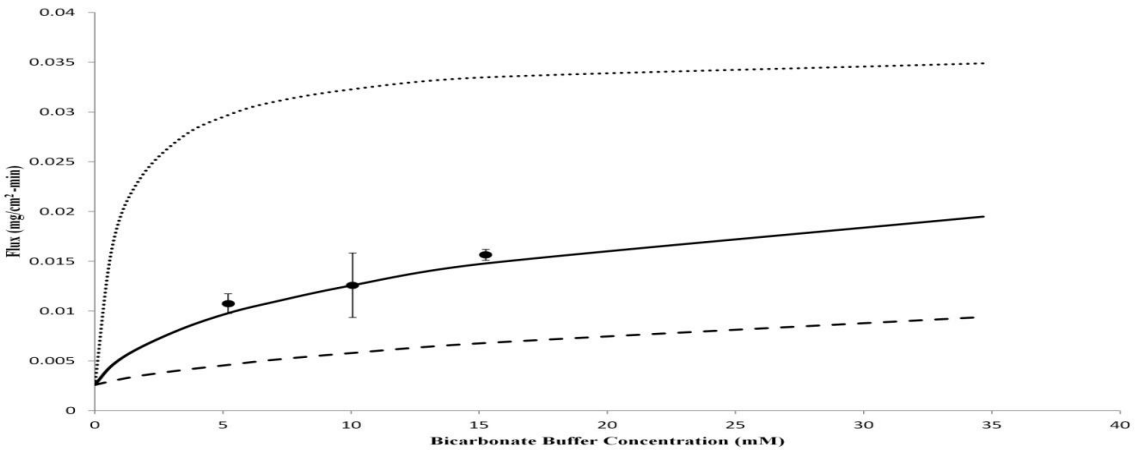

Figure 2. 9. The experimental and predicted flux of indomethacin in bicarbonate buffer at multiple concentrations (at pH 6.5 and 37^{o}C). Key (•) Experimental Flux; (·····) BCE Model Flux Predictions; (———) IRR Model Flux Predictions; (– – –) CAI Model Flux Predictions;

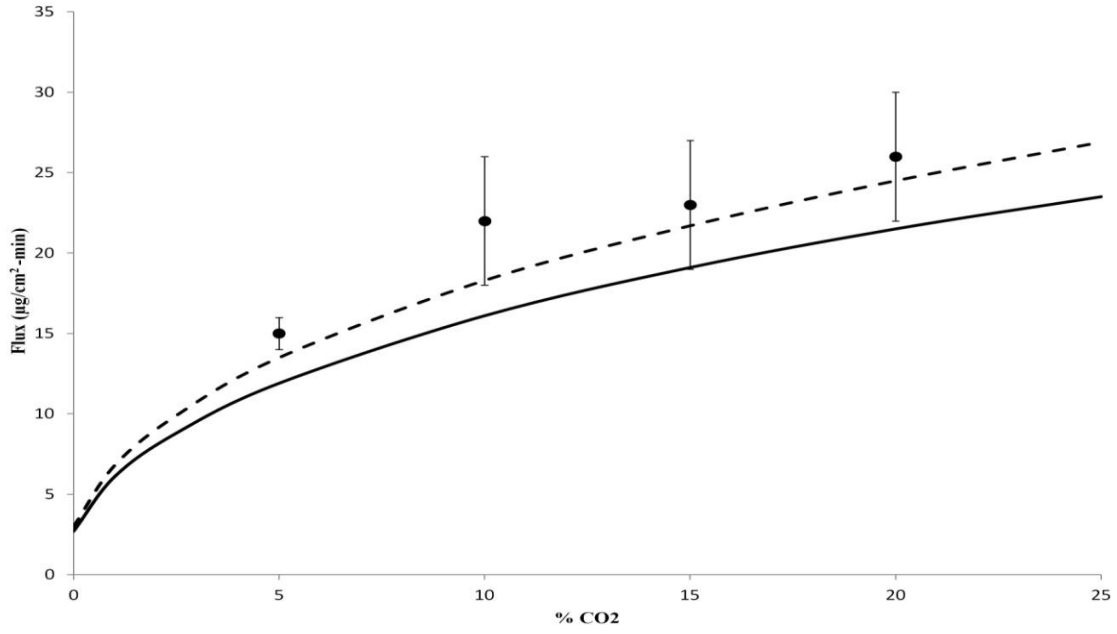

Figure 2. 10. The experimental (data interpolated from McNamara et al. 2003 figure 3) and predicted flux of indomethacin in bicarbonate buffer at multiple concentrations (at pH 6.8 and 37^{o}C). Key (•) Experimental Flux; (– – –) IRR Model Flux Predictions based on indomethacin pKa = 4.17; (———) IRR Model Flux Predictions based on indomethacin pKa = 4.27;

References

1. Mooney K, Mintun M, Himmelstein K, Stella V 1981. Dissolution kinetics of carboxylic acids II: Effect of buffers. J Pharm Sci 70(1):22-32.
2. Amidon GL, Lennernas H, Shah VP, Crison JR 1995. A theoretical basis for a biopharmaceutic drug classification: The correlation of in vitro drug product dissolution and in vivo bioavailability. Pharm Res 12(3):413-420.
3. Aunins JG, Southard MZ, Myers RA, Himmelstein KJ, Stella VJ 1985. Dissolution of Carboxylic Acids III. The Effect of Polyionizable Buffers. Journal of Pharmaceutical Sciences 74(12):1305 - 1316.
4. McNamara DP, Amidon GL 1988. Reaction plane approach for estimating the effects of buffers on the dissolution rate of acidic drugs. Journal of Pharmaceutical Sciences 77(6):511-517.
5. Sheng JJ, McNamara DP, Amidon GL 2009. Toward an In Vivo Dissolution Methodology: A Comparison of Phosphate and Bicarbonate Buffers. Molecular Pharmaceutics 6(1):29-39.
6. Neervannan S, Southard MZ, Stella VJ 2012. Dissolution of Weak Acids Under Laminar Flow and Rotating Disk Hydrodynamic Conditions: Application of a Comprehensive Convective-Diffusion-Migration-Reaction Transport Model. Journal of Pharmaceutical Sciences 101(9):3180-3189.
7. Jacobs MH, Stewart DR 1942. The Role of Carbonic Anhydrase in Certain Ionic Exchanges Involving the Erythrocyte. The Journal of General Physiology 13:539 - 552.
8. Kaunitz JD, Akiba Y 2006. Duodenal Carbonic Anhydrase: Mucosal Protection, Luminal Chemosensing, and Gastric Acid Disposal. The Keio Journal of Medicine 55(3):96 - 106.
9. Kaunitz JD, Akiba Y 2007. Review article: duodenal bicarbonate - mucosal protection, luminal chemosensing and acid-base balance. Alimentary Pharmacology & Therapeutics 24:169-176.
10. McNamara DP, Whitney KM, Goss SL 2003. Use of a physiologic bicarbonate buffer system for dissolution characterization of ionizable drugs. Pharmaceutical Research 20(10):1641-1646.
11. Hogan DL, Ainsworth MA, Isenberg JI 1994. Review Article: Gastroduodenal Bicarbonate Secretion. Aliment Pharmacol Ther 8:475-488.
12. Sjoblom M 2011. Duodenal epithelial sensing of luminal acid: role of carbonic anhydrases. Acta Physiologica 201:85-95.
13. Brinkman A, Glasbrenner B, Vlatten A, Eberhardt H, Geldner G, Radermacher p, Georgieff M, Weideck H 2001. Does Gastric Juice pH Influence Tonometric PCO_2 Measured by Automated Air Tonometry. Am J Respir Crit Care Med 163:1150-1152.
14. McGee LC, Hastings AB 1942. The carbon dioxide tension and acid-base balance of jejunal secretions in man. J Biol Chem 142:893-904.
15. Rune S 1972. Acid-base parameters of duodenal contents in man. Gastroenterology 62:533-539.
16. Kaunitz JD, Akiba Y 2006. Review article: duodenal bicarbonate - mucosal protection, luminal chemosensing and acid-base balance. Aliment Pharmacol Ther 24 Suppl 4:169-176.
17. Kivela A, Kivela J, Saarnio J, Parkkila S 2005. Carbonic anhydrase in normal gastrointestinal tract and gastrointestinal tract and gastrointestinal tumours. World Journal of Gastroenterology 11(2):155-163.
18. Neervannan S, Southard MZ, Stella VJ 2012. Dissolution of Weak Acids Under Laminar Flow and Rotating Disk Hydrodynamic Conditions: Application of a Comprehensive Convective-Diffusion-Migration-Reaction Trnasport Model. Journal of Pharmaceutical Sciences 101(9):3180-3189.

19. Boni JE, Brickl RS, Dressman J 2007. Is bicarbonate buffer suitable as a dissolution medium? Journal of Pharmacy and Pharmacology 59(10):1375-1382.
20. Fadda HM, Merchant HA, Arafat BT, Basit AW 2009. Physiological bicarbonate buffers: stabilisation and use as dissolution media for modified release systems. International Journal of Pharmaceutics 382(1-2):56-60.
21. Garbacz G, Kolodziej B, Koziolek M, Weitschies W, Klein S 2014. A dynamic system for the simulation of the fasting luminal pH-gradients using hydroden carbonate buffers for dissolution testing of ionisable compounds. European Journal of Pharmaceutical Sciences 51:224-231.
22. Wallin M, Bjerle I 1989. A Mass Transfer Model for Limestone Dissolution From a Rotating Cylinder. Chemical Engineering Science 44(1):61-67.
23. Dreybrodt W, Buhmann D 1991. A mass transfer model for dissolution and precipitation of calcite from solutions in turbulent motion. Chemical Geology 90:107-122.
24. Dreybrodt W, Lauckner J, Zaihua L, Svensson U, Buhmann D 1996. The kinetics of the reaction $CO_2 + H_2O \rightarrow H^+ HCO_3^-$ as one of the rate limiting steps for the dissolution of clacite in the system H_2O-CO_2-$CaCO_3$. Geochimica et Cosmochimica Acta 60(18):3375-3381.
25. Liu Z, Dreybrodt W 1997. Dissolution kinetics of calcium carbonate minerals in H_2O-CO_2 solutions in turbulent flow: The role of the diffusion boundary layer and the slow reaction $H_2O + CO_2 = H^+ + HCO_3^-$ Geochimica et Cosmochimica Acta 61(14):2879-2889.
26. Kaufmann G, Dreybrodt W 2007. Calcite dissolution kinetics in the system $CaCO_3$-H_2O-CO_2 at high undersaturation. Geochimica et Cosmochimica Acta 71(1398-1410).
27. Mooney KG, Mintun M, Himmelstein K, Stella V 1981. Dissolution kinetics of carboxylic acids I: Effect of pH under unbuffered conditions. J Pharm Sci 70(1):13-22.
28. Levich VG. 1962. Physicochemical Hydrodynamics. ed., New jersey: Prentice Hall.
29. Grijseels H, Crommelin DJA, Blaey CJD 1981. Hydrodynamic Approach to Dissolution Rate. Pharmaceutisch Weekblad - Scientific Edition 3:129 -144.
30. Mooney KG, Rodriguez-Gaxiola M, Mintun M, Himmelstein KJ, Stella VJ 1981. Dissolution Kinetics of Phenylbutazone Journal of Pharmaceutical Sciences 70(12):1358-1365.
31. Karl AL, Majella EL, Corrigan OI 2003. Effect of buffer media composition on the solubility and effective permeability coefficient of ibuprofen. International Journal of Pharmaceutics 253:49-59.
32. Guo D, Thee H, Silva Gd, Chen J, Fei W, Kentish S, Stevens GW 2011. Borate-Catalyzed Carbon Dioxide Hydration via the Carbonic Anhydrase Mechanism. Environmental Science & Technology 45:4802-4807.
33. Fagerberg J, Tsinman O, Sun N, Tsinman K, Avdeef A, Bergstrom C 2010. Dissolution Rate and Apparent Solubility of Poorly Soluble Drugs in Biorelevant Dissolution Media. Molecular Pharmaceutics 7(5):1419-1430.
34. Tsinman K, Avdeef A, Tsinman O, Voloboy D 2009. Powder Dissolution Method for Estimating Rotating Disk Intrinsic Dissolution Rates of Low Solubility Drugs. Pharmaceutical Research 26(9):2093-2100.
35. Amidon GL, Lennernas H, Shah VP, Crison JR 1995. A theoretical basis for a biopharmaceutic drug classification: the correlation of in vitro drug product dissolution and in vivo bioavailability. Pharm Res 12(3):413-420.
36. Avdeef A, Tsinman O 2008. Miniaturized Rotating Disk Intrinsic Dissolution Rate Measurement: Effects of Buffer Capacity in Comparisons to Traditional Wood's Apparatus. Pharmaceutical Research 25(11):2613-2627.
37. Zeebe RE 2011. On the molecular diffusion coefficients of dissolved CO_2, HCO_3^-, and CO_3^{2-} and their dependence on isotopic mass. Geochimica et Cosmochimica Acta 75:2483-2498.
38. Nassanen R 1947. Potentiometric Study on the First Ionization of Carbonic Acid in Aqueous Solutions of Sodium Chloride. Acta Chemica Scandinavica 1:204 - 209.

39. Frank MJW, Kuipers JAM, Swaaij WPMv 1996. Diffusion Coefficients and Viscosities of CO_2 + H_2O, CO_2 + CH_3OH, NH_3 + H_2O, and NH_3 + CH_3OH Liquid Mixtures. J Chem Eng Data 41:297-302.

Chapter 3

In Vivo Predictive Dissolution: Comparing the effect of bicarbonate and phosphate buffer on the dissolution of weak acids and weak bases

Abstract

Bicarbonate is the main buffer in the small intestine and it is well known that buffer properties such as pKa can affect the dissolution rate of ionizable drugs. However, bicarbonate buffer is complicated to work with experimentally. Finding a suitable substitute for bicarbonate buffer may provide a way to perform more physiologically relevant dissolution tests. The dissolution of weak acid and weak base drugs was conducted in bicarbonate and phosphate buffer using rotating disk dissolution methodology. Experimental results were compared to the predicted results using the film model approach of Mooney et al. based on equilibrium assumptions as well as a model accounting for the slow hydration reaction, $CO_2 + H_2O \rightarrow H_2CO_3$. Assuming carbonic acid is irreversible in the dehydration direction: $CO_2 + H_2O \leftarrow H_2CO_3$, the transport analysis can accurately predicted rotating disk dissolution of weak acid and weak base drugs in bicarbonate buffer. The predictions show that matching the dissolution of weak acid and weak base drugs in phosphate and bicarbonate buffer is possible. The phosphate buffer concentration necessary to match physiologically relevant bicarbonate buffer (eg: 10 mM $[HCO_3^-]$, pH=6.5) is typically in the range of <1-25mM and is very dependent upon drug solubility and pKa..

Introduction

Dissolution can be an important diagnostic tool for predicting the *in vivo* effects when a drug product administered orally. The identification of an *in vitro* dissolution test that accurately predicts *in vivo* dissolution is therefore essential. Bicarbonate (HCO_3^-) is secreted by the pancreas and epithelial cells in the small intestine to neutralize gastric acid emptied into the duodenum and buffer the intestinal fluid maintaining intestinal pH . Conducting dissolution experiments in bicarbonate buffer would be more physiologically realistic. However, the preparation of physiologically relevant bicarbonate buffer is more complex experimentally. CO_2 gas must be constantly added to water to obtain a constant bicarbonate buffer concentration. This is generally a slow process that can also affect the hydrodynamics and dissolution of drug product/particles due to the potential presence of gas bubbles at solid liquid interfaces. Therefore using a buffer solution that produces equivalent buffer effect on drug dissolution as bicarbonate buffer would be preferred.

Phosphate buffer is a logical buffer to consider matching the effects of bicarbonate buffer and creates a more physiologically relevant dissolution test. Phosphate buffer is commonly used in dissolution testing and is a buffer proposed in the guidance by the FDA to be used for *in vivo* biowaivers [1]. Additionally, phosphate has a pKa (6.8) that is within the pH range of the small intestine and the dissolution of weak acid drugs in phosphate buffer has been accurately predicted using the film model and reaction plane model [2-4].

Phosphate buffer is currently used today as the buffer component in USP simulated intestinal fluid (SIF), and in fasted state simulated intestinal fluid (FASSIF) with concentrations of 50mM and 29mM respectively[5,6]. However, the average bicarbonate buffer concentration in the small intestine is ~6-20mM [7]. The difference in physiological bicarbonate buffer

concentrations and typical phosphate buffer concentrations illustrates the variation between the dissolution media that is currently used versus the fluid present in the small intestine. These differences have been studied experimentally and significant differences in dissolution between physiologically relevant bicarbonate buffer and phosphate buffer have been observed[4,8-11]. In order to accurately predict this difference and an equivalent phosphate buffer, the physicochemical properties of the drug and buffer must be taken account. Additionally, Krieg and coworkers demonstrated the importance of reaction kinetics on the ability of bicarbonate to buffer the pH in the diffusion layer and at the surface of dissolving drug. This reaction component introduces an additional complexity for matching the buffer capacities of bicarbonate and phosphate in the diffusion layer and for predicting an equivalent phosphate buffer for dissolution testing. A further complication is changes in bulk pH with low buffer capacities and low physiological volumes during dissolution usually requiring a pH-Stat to maintain bulk pH.

This paper will experimentally examine the buffer effects of phosphate and bicarbonate using rotating disk dissolution of weak acid and weak base drugs. The experimental data will be compared to predictions of the film model and the IRR model outlined in Krieg et al. that predicts the dissolution of drugs in bicarbonate buffer by incorporating the dehydration reaction rate and assuming that H_2CO_3 undergoes an irreversible reaction to form CO_2 and H_2O. Results will show that the dissolution of both weak acid and weak base drugs can be accurately predicted in buffers with different physicochemical properties. These results may provide the basis for predicting phosphate buffer concentrations that are more indicative of the buffer present in the luminal fluid of the intestine and offer a more physiologically relevant dissolution buffer.

Applying a simultaneous diffusion and reaction model to phosphate buffer

Phosphate buffer is determined by the following ionization reactions:

$$H_3PO_4 \overset{K_{a1}}{\longrightarrow\!\!\!\!\longleftarrow} H_2PO_4^{-1} \qquad pKa_1 = 1.86\ ^{2} \quad \text{(Rxn. 3.1)}$$

$$H_2PO_4^{-1} \overset{K_{a2}}{\longrightarrow\!\!\!\!\longleftarrow} HPO_4^{-2} \qquad pKa_2 = 6.8\ ^{12} \quad \text{(Rxn. 3.2)}$$

$$HPO_4^{-2} \overset{K_{a3}}{\longrightarrow\!\!\!\!\longleftarrow} PO_4^{-3} \qquad pKa_3 = 11.5\ ^{2} \quad \text{(Rxn. 3.3)}$$

At physiologically relevant pH values of the small intestine, the only relevant pKa value is 6.8 (pKa_2) as demonstrated by Aunins et al. who incorporated buffers with multiple pKa's into the simultaneous diffusion and chemical reaction model [2]. The values for pKa_1 (1.86) and pKa_3 (11.5) are not in the range of the physiologically relevant intestinal pH and therefore have no significant buffer effect. Therefore, the only species of relevance are monobasic phosphate and dibasic phosphate (Rxn 3.2). The reaction rates for ionization are assumed to be occurring so fast that they occur instantaneously relative to diffusion and the film model accurately predicts the impact of phosphate buffer on the dissolution of weak acid drugs as described by Mooney et al. and Aunins[2,13].

The same film model procedure can be applied to weak base drugs. A weak base drug will protonate at pH values below its pKa and consequently produce OH^- in solution. As a result, the pH at the surface of a weak base drug will generally be higher than that of the bulk solution pH. The addition of a buffer will act to decrease the surface pH. Hence the chemical equilibrium reactions must take this into account when solving for the flux of weak base drugs. The equilibrium reactions are shown below.

$$H^+ + OH^- \overset{K_w}{\longrightarrow\!\!\!\!\longleftarrow} H_2O \qquad \text{(Rxn. 3.4)}$$

$$B^- + H_2O \overset{K_b^D}{\underset{\leftarrow}{\rightarrow}} BH + OH^- \qquad \text{(Rxn.3.5)}$$

$$B^- + H^+ \overset{K_1^*}{\underset{\leftarrow}{\rightarrow}} BH + H_2O \qquad \text{(Rxn.3.6)}$$

$$B^- + H_2PO_4^- \overset{K_2}{\underset{\leftarrow}{\rightarrow}} BH + HPO_4^{-2} \qquad \text{(Rxn.3.7)}$$

$$HPO_4^{-2} + H_2O \overset{K_b^B}{\underset{\leftarrow}{\rightarrow}} H_2PO_4^- + OH^- \qquad \text{(Rxn.3.8)}$$

Where B^- is deprotonated form of the weak base drug, BH is the protonated form of the weak base drug.

The assumptions made in the film model for weak acids are applied to weak bases with the chemical equilibrium adjusted accordingly. A cubic equation can be obtained for the OH^- concentration at the surface of the tablet which allows for the pH at the surface of the tablet to be calculated. This cubic equation is shown below.

$$p[OH^-]_0{}^3 + q[OH^-]_0{}^2 + r[OH^-]_0 + s = 0 \quad \text{(Eq. 3.1)}$$

$$p = D_{OH}D_{HPO_4^{-2}}$$

$$q = D_{OH}D_{H_2PO_4^-}K_b^B + D_{HPO_4^{-2}}D_H[H^+]_h + D_{HPO_4^{-2}}D_{H_2PO_4^-}[H_2PO_4^-]_h - D_{HPO_4^{-2}}D_{OH}[OH^-]_h$$

$$r = D_{H_2PO_4^-}D_HK_b^B[H^+]_h + D_{H_2PO_4^-}^2K_b^B[H_2PO_4^-]_h - D_{H_2PO_4^-}D_{OH}K_b^B[OH^-]_h - D_{H_2PO_4^-}^2K_b^B[H_2PO_4^-]_h - D_{H_2PO_4^-}D_{HPO_4^{-2}}K_b^B[HPO_4^{-2}]_h - D_{BH}D_{HPO_4^{-2}}K_b^D[B^-]_0 - D_HD_{HPO_4^{-2}}K_w$$

$$s = -D_{BH}D_{H_2PO_4^-}K_b^DK_b^B[B^-]_0 - D_HD_{H_2PO_4^-}K_wK_b^B$$

This same transport analysis that assumes instantaneous chemical equilibrium was applied to bicarbonate buffer through two different approaches. The BCE model (bulk chemical equilibrium) assumes that the hydration and dehydration reactions in the formation of

bicarbonate are fast enough to reach chemical equilibrium instantaneously (pKa =6.04). The CAI model (carbonic acid ionization) assumes that the hydration and dehydration reactions are too slow to occur at all in the diffusion layer (pKa = 3.55). A more thorough explanation of these models is given in Krieg et al[14].

Applying a simultaneous diffusion and reaction model to with an irreversible chemical reaction to weak base drugs

The same IRR model scheme from Krieg, et al. to model weak acid dissolution was used to model the impact of the slow hydration and dehydration reactions on bicarbonate buffer by assuming that H_2CO_3 undergoes an irreversible chemical reaction to form CO_2 and H_2O[14]. The chemical reactions that were considered for the analysis are shown below.

$$H^+ + OH^- \overset{K_w}{\underset{\longrightarrow}{\longleftarrow}} H_2O \qquad \text{(Rxn. 3.9)}$$

$$B^- + H_2O \overset{K_b^D}{\underset{\longrightarrow}{\longleftarrow}} BH + OH^- \qquad \text{(Rxn.3.10)}$$

$$B^- + H^+ \overset{K_1^*}{\underset{\longrightarrow}{\longleftarrow}} BH + H_2O \qquad \text{(Rxn.3.11)}$$

$$B^- + H_2CO_3 \overset{K_2}{\underset{\longrightarrow}{\longleftarrow}} BH + HCO_3^- \qquad \text{(Rxn. 3.12)}$$

$$HCO_3^- + H_2O \overset{K_b^B}{\underset{\longrightarrow}{\longleftarrow}} H_2CO_3 + OH^- \qquad \text{(Rxn.3.13)}$$

$$H_2CO_3 \overset{k_d}{\rightarrow} CO_2 + H_2O \qquad \text{(Rxn. 3.14)}$$

The role the dehydration reaction rate (k_d) plays in the calculation for the hydroxide ion concentration at the surface of the dissolving drug is evident when comparing equation 3.1 to equation 3.2 shown below.

$$p[OH^-]_0{}^3 + q[OH^-]_0{}^2 + r[OH^-]_0 + s = 0 \quad \text{(Eq. 3.2)}$$

$$p = -D_{HCO_3} D_{OH}$$

$$q = -D_{HCO_3} D_H [H^+]_h + D_{HCO_3} D_{OH} [OH^-]_h - \left(h\sqrt{D_{H_2CO_3} k_d}\right) K_b^B D_{OH} - \left(h\sqrt{D_{H_2CO_3} k_d}\right) D_{HCO_3} [H_2CO_3]_h$$

$$r = D_{HCO_3} D_{BH} K_b^D [B^-]_0 - \left(h\sqrt{D_{H_2CO_3} k_d}\right) K_b^B D_H [H^+]_h + D_{HCO_3} D_H K_W + \left(h\sqrt{D_{H_2CO_3} k_d}\right) K_b^B D_{OH} [OH^-]_h + \left(h\sqrt{D_{H_2CO_3} k_d}\right)^2 K_b^B [H_2CO_3]_h + \left(h\sqrt{D_{H_2CO_3} k_d}\right) D_{HCO_3} K_b^B [HCO_3^-]_h - \left(h\sqrt{D_{H_2CO_3} k_d}\right)^2 K_b^B [H_2CO_3]_h$$

$$s = \left(h\sqrt{D_{H_2CO_3} k_d}\right) D_{BH} K_b^D K_b^B [B^-]_0 + \left(h\sqrt{D_{H_2CO_3} k_d}\right) D_H K_w K_b^B$$

Materials and Methods

Benzoic acid (Sigma Aldrich - St. Louis, Missouri, USA; > 99.5%, Lot# MKBG2270V), ibuprofen (Albermarle – Baton Rouge, Louisiana, USA; Lot#11550-0005), indomethacin (Alexis Biochemicals – San Diego, California, USA; ≥ 98%, Lot# L25666), 2-napthoic acid (Sigma Aldrich- St. Louis, Missouri, USA; Lot #14709KHV), ketoprofen (Sigma Aldrich- St. Louis, Missouri, USA; Lot# 044K0790), and Haloperidol (TCI Portland, Oregon, USA; >98.0% Lot#D6C3D-R1) were used as received. All other chemicals used were of analytical grade. Distilled water was used for all experiments. All dissolution runs were performed in a jacketed beaker at 37°C. Two runs were done for each experimental condition described below. Samples were analyzed using a UV spectrophotometer (Agilent Technologies - Santa Clara, California, USA; Model# 61103A). The samples were obtained using a flow through system that recycled the analyzed solution back into the dissolution vessel. The standard curves were also made using the UV flow through system.

The solubility of 2-naphthoic acid was measured by agitating the suspension in 0.1N hydrochloric acid solution while being kept at 37°C. Samples were filtered before dilution in pH

6.5 50 mM phosphate buffer. The pKa and solubility of the other compounds studied are shown in Table 3.

Dissolution experiments using phosphate buffer were performed in duplicates at pH 6.5 at several different phosphate concentrations and medium volumes. The exact experimental parameters can be seen in tables 1 and 2. Solutions were made using sodium monobasic phosphate, sodium hydroxide, and sodium chloride to make it isotonic. A disc of compressed drug with a tablet diameter of 1cm was used for ibuprofen, indomethacin, ketoprofen, and haloperidol. A compressed disc with a tablet diameter of 0.472cm was used for benzoic acid and 2-naphthoic acid. Differences in volume and tablet diameter used for these experiments were made according to the solubility and predicted flux of each drug to achieve desirable experimental conditions (sink conditions and adequate sensitivity for UV analysis). All experiments were carried out at 100RPM.

For the rotating disk dissolution experiments in bicarbonate buffer, different bicarbonate buffer concentrations were prepared by continuously flowing quantities of 100% dry compressed air and 100% carbon dioxide in a 0.9%NaCl solution at appropriate ratios. The $\%CO_2$(aq) in solution was determined using a CO_2 monitor (YSI 8500 – Yellow Springs, Ohio, USA) and pH was monitored using a pH meter (Beckman Φ 40 – Brea, California, USA). Solid sodium hydroxide and 5N NaOH was added to adjust pH. The exact experimental parameters can be seen in tables 3.1 and 3.2. Note that the buffer concentration may be defined either as the bicarbonate concentration or the sum of bicarbonate and CO2 as shown in tables 3.1 and 3.2. The flux of the drugs was predicted by applying the mathematical models outlined in this paper and Krieg et al. and the parameters given in Table3.3 using MATLAB (Mathworks – Natick, Massachusetts, USA).

Results

Ibuprofen Results

Figure 3.1 shows the flux of ibuprofen in bicarbonate and phosphate buffer over a range of buffer concentrations along with theoretical predictions at pH 6.5. The data for the flux of ibuprofen, indomethacin, and ketoprofen in bicarbonate buffer was shown and explained in Krieg et al.[14]. The rotating disk flux of ibuprofen in phosphate buffer is accurately predicted by the simultaneous diffusion and chemical reaction model as expected. The predictions show that an increase in phosphate buffer concentration results in a significant increase in the flux but ibuprofen still serves as a self-buffer and influences surface pH under the conditions studied. The figure 1 plot shows that the phosphate buffer concentrations needed to match physiologically relevant bicarbonate buffer are 4-8mM.

Indomethacin Results

Figure 3.2 shows the flux of indomethacin in bicarbonate and phosphate buffer over a range of buffer concentrations along with theoretical predictions at pH 6.5. The simultaneous diffusion and chemical reaction model accurately predicts the experimental flux of indomethacin in phosphate buffer. The calculated pH at the surface of indomethacin approaches the bulk pH at low concentrations of phosphate buffer as expected due to the low intrinsic solubility of indomethacin which makes it a poor self-buffer. Bicarbonate is not able to buffer the surface pH of indomethacin as effectively as phosphate buffer. Therefore very low phosphate buffer concentrations (1-2mM) are needed to match physiologically relevant bicarbonate buffer. As was seen for ibuprofen, the slow hydration reaction rate has a significant impact on the buffer capacity of bicarbonate and only the IRR model can accurately predict the flux of indomethacin in bicarbonate buffer.

Ketoprofen Results

Figure 3.3 shows the flux of ketoprofen in bicarbonate and phosphate buffer over a range of buffer concentrations along with theoretical predictions at pH 6.5. The predictions show that an increase in buffer concentration results in a significant increase in the flux. The predicted flux matches the experimental flux in phosphate buffer. The experimental flux of ketoprofen in bicarbonate buffer is only accurately predicted when the dehydration reaction rate is incorporated by applying the IRR model. Figure 3shows phosphate buffer concentrations needed to match physiologically relevant bicarbonate buffer are ~5-12mM

2-Napthoic Acid Results

Figure 3.4 shows the flux of 2-Napthoic acid in bicarbonate and phosphate buffer over a range of buffer concentrations along with theoretical predictions at pH 6.5. The predictions show that an increase in buffer concentration results in a significant increase in the flux. The solubility of 2-naphthoic acid is similar to ibuprofen. Therefore 2-napthoic acid acts similarly as a self-buffer at the dissolving surface. The predicted flux matches the experimental flux in phosphate buffer. As was seen for all of the weak acids previously, the experimental flux of 2-naphthoic acid in bicarbonate buffer is not predicted accurately by the BCE and CAI models and is only accurately predicted when the dehydration reaction rate is incorporated by applying the IRR model. Figure 3.4 shows phosphate buffer concentrations needed to match physiologically relevant bicarbonate buffer are similar to ibuprofen (3-10mM).

Benzoic Acid Results

Figure 3.5 shows the flux of benzoic acid in bicarbonate and phosphate buffer over a range of buffer concentrations at pH 6.5. The flux of benzoic acid in phosphate buffer is accurately predicted by the simultaneous diffusion and chemical reaction model. The predictions

and results show that a large increase in buffer concentration does not cause a significant increase in the flux. This is due to the high solubility of benzoic acid which is apparent in the large flux value for benzoic acid at zero buffer concentration. A highly soluble weak acid drug will lead to a high concentration of drug at the surface and a high [H^+] that limits the pH change at the surface even in the presence of high buffer concentration. In effect, benzoic acid solubility very effectively serves as a self-buffer and controls surface pH under the conditions studied.

As observed with all of the weak acid drugs, the BCE and CAI models do not accurately predict the flux of benzoic acid in bicarbonate buffer. However unlike the other weak acid drugs the IRR model did not accurately predict the flux of benzoic acid in bicarbonate buffer. In the case of benzoic acid dissolution in bicarbonate buffer, it was observed throughout these experiments that gas bubbles continuously formed at the surface of the dissolving tablet. This likely affected the hydrodynamics and effective surface area of the dissolving drug available for dissolution. Therefore, the experimental flux would not be expected to match the predicted flux for the dissolution of benzoic acid in bicarbonate buffer for any of the models that were used. The gas bubbles at the dissolving surface were likely carbon dioxide. The concentration of CO_2 at the surface depends on the [H^+] concentration (Equation 3). When [H^+] is sufficiently high, the CO_2 (aq) concentration can exceed its solubility causing CO_2 to come out of solution.

$$[CO_2(aq)] = \frac{[H^+][HCO_3^-]}{K_{a1}} \qquad \text{(Eqn. 3.3)}$$

The IRR model does not calculate concentration of CO_2 (aq) at the surface of the tablet. However, the BCE model predicts similar surface pH values and enables the calculation of the concentration of carbon dioxide at the surface of the tablet. At the highest experimental CO_2 partial pressure (37% CO_2) the BCE model predicts a nearly saturated solution (98% saturated) of CO_2 at the surface of the tablet. The assumptions made in the IRR model are consistent with

the buildup of carbon dioxide in the diffusion layer even though the predictions were not accurate. The IRR model assumes that the concentration of carbon dioxide will only increase in the diffusion layer without an ability to be transformed into carbonic acid. Additionally, the high solubility of benzoic acid leads to a low pH in the diffusion layer that will generate more carbon dioxide and could cause the concentration of carbon dioxide to increase to a point where it comes out of solution. So, while not precisely quantitative, these predictions are very consistent with the hypothesis that the bubbles formed at the dissolving benzoic acid compact surface are due to saturated CO_2 conditions in the diffusion layer and at the dissolving surface.

Haloperidol Results

Figure 3.6 shows haloperidol flux, a weak base, in bicarbonate and phosphate buffer over a range of buffer concentrations at pH 6.5. The predictions show that an increase in buffer concentration results in a significant increase in the flux. The solubility of haloperidol is similar to indomethacin and, in the same way, the low solubility of the drug prevents it from effectively self-buffering the surface pH. As was seen with the weak acid drugs, rotating disk experimental flux in phosphate buffer is predicted accurately by the simultaneous diffusion and chemical reaction model. The predictions for bicarbonate buffer also match what was seen for the weak acid drugs. The experimental flux of haloperidol in bicarbonate buffer falls between predictions assuming instantaneous hydration/dehydration reactions (BCE model : pKa = 6.04) or no hydration/dehydration reactions (CAI model: pKa = 3.55). Experimental flux of haloperidol in bicarbonate buffer is only accurately predicted when the IRR model is used for the predictions. The experimental data and predictions in bicarbonate and phosphate buffer show that phosphate is much better at buffering the surface pH. Therefore very low concentrations of phosphate buffer would be needed to match bicarbonate (<1mM)

Figure 3.7 shows the experimental and predicted flux of haloperidol in 10mM bicarbonate buffer with bulk pH values of 6, 6.5, and 7. As the bulk pH decreases, the experimental and predicted flux in bicarbonate increases. This is due to an increase in H^+ in the solution and consequently a decrease the surface pH and an increase the ionized form of the drug in the diffusion layer, leading to an increase in the overall flux of the weak base drug. The BCE model overestimates and the CAI model underestimates the effect that changing the bulk pH will have on the surface pH and the flux of the drug. The IRR model accurately predicts experimental flux of haloperidol in bicarbonate buffer.

Discussion

The importance the reaction rates play in the buffering capacity of bicarbonate is apparent when comparing all of the experimental results in bicarbonate and phosphate buffer. The drug flux data further confirms the accuracy of the film model to predict the dissolution of weak acid drugs in phosphate buffer and it also shows that it can be successfully applied to weak base drugs. The IRR model accurately predicts the experimental flux of weak acid and weak base drugs in bicarbonate buffer. Furthermore, the experimental data for haloperidol and the data presented in Krieg, et al. demonstrates the ability of the IRR model to be used under various experimental conditions (eg: different bulk pH, drug solubilities, rotational speeds). The results also give good approximations of the phosphate buffer concentrations needed to match physiologically relevant bicarbonate buffer concentrations for rotating disk dissolution of drugs with varying physiochemical properties. For the drugs studied in this paper, the phosphate buffer concentrations needed to match physiologically relevant bicarbonate buffer were ~1-15mM based on the experimental data and the IRR model predictions.

The dynamic nature of bicarbonate buffer can be observed by comparing the IRR model predictions to the BCE model predictions. If the hydration and dehydration reactions were fast enough that chemical equilibrium was achieved instantaneously, as seen in the BCE model, bicarbonate would be a very good buffer in the diffusion layer. According to the BCE model, a 10mM bicarbonate buffer would provide the same buffering ability in the diffusion layer as ~50mM phosphate buffer at a bulk of pH 6.5. Therefore when the reaction time is unlimited (i.e. in the bulk solution) and the rates of the hydration and dehydration reactions do not play a limiting role in buffering capacity (i.e. the BCE model), bicarbonate acts as a strong buffer. However, when the reaction time is finite, (i.e. in the diffusion layer using the IRR model), the buffer capacity of bicarbonate is much lower but this lower buffer capacity is partially compensated for by the dehydration reaction of H2CO3.

Predicting Physiologically Relevant Phosphate Buffer Concentrations

While there have been recent advancements in preparing bicarbonate buffer and controlling buffer concentration[15] , the process of making bicarbonate buffer is not ideal for performing dissolution experiments. The experimental data in this paper and the data in Krieg et al. demonstrate that the IRR model can accurately predict the effect bicarbonate has on buffering surface pH of weak acid and weak base drugs under rotating disk dissolution conditions. This paper and previous work illustrates the ability to accurately predict rotating disk drug dissolution in phosphate buffer using the film model that assumes chemical equilibrium is achieved instantaneously [2,4]. Therefore applying each of these models to their respective buffer system will give accurate estimations for phosphate buffer concentrations that will simulate physiologically relevant bicarbonate buffer.

To estimate phosphate buffer concentrations that would match physiologically relevant bicarbonate buffer, the physicochemical properties of ibuprofen were used (see table 3.3) with the exception of drug pKa and solubility which were varied, and the IRR model was applied. For weak acids, the drug pKa was varied from 3-8 and for weak bases the drug pKa was varied from 5-10. The drug solubility was varied from 10^{-1} M to 10^{-6} M. The physiologically relevant bicarbonate buffer chosen for the predictions was 15% CO_2 (10.4 mM bicarbonate concentration) at pH 6.5 as representative of GI conditions[16]. The diffusion layer thickness for these predictions was chosen as 30μm based on the work of Hintz and Johnson[17].

The relationship between equivalent phosphate buffer concentration and the pKa of weak acid drugs, pKw-pKa for weak base drugs, and log(drug solubility) is shown in Figure 3.8. For weak acid drugs, when the pKa - log(drug solubility) is plotted versus the equivalent phosphate buffer concentration necessary to match physiologically relevant bicarbonate buffer a single curve is obtained as shown in Figure 3.8. The same is true for weak base drugs when the when (pKw-pKa- log(drug solubility) is plotted versus equivalent phosphate buffer as shown in Figure 3.8. This is due to the relationship between the weak acid drug Ka (for a weak base: Kw-Ka) and the solubility of the drug in the cubic equation of the film model. These two parameters only appear in the cubic equation as being multiplied together. Therefore if one parameter is decreased by an order of magnitude while the other is increased by an order of magnitude, this will result in the same solution for the cubic equation and pH at the surface of the drug.

Predictions at bulk pH of 6.0, 6.5 and 7.0 show that phosphate buffer concentrations needed to match physiologically relevant bicarbonate buffer are higher for both weak acid and weak base drugs at a pH of 6 and the lower at pH 7. This is due to the low pKa for the ionization reaction of carbonic acid (3.55) which is used in the IRR model. As the bulk pH is lowered, the

buffering capacity increases. This is evident in the case of weak acid drugs. There is a wide range of equivalent phosphate buffer concentrations needed to match weak acid drugs (~1 to 95mM) depending on the bulk pH and drug properties (ie: solubility and pKa). As the drug pKa increases and the drug solubility decreases for weak acid drugs, the phosphate buffer concentration needed to provide the same buffer effect decreases. However, a more representative BCS class 2a drug range would lead to the equivalent phosphate buffer concentration becoming much more condensed over the bulk pH's tested and results in equivalent phosphate concentrations of 1mM to 25mM range. For example, ibuprofen is predicted to require an equivalent phosphate buffer concentration of ~11mM at pH 6 and ~2mM at pH 7.

In the case of weak base drugs, the matching phosphate buffer concentration for physiologically relevant bicarbonate buffer is less than 2mM for all drug pKa values and solubilities evaluated. This is due to weak base drugs forming OH^- at the surface of the dissolving drug which increases the pH and makes the bicarbonate buffer relatively ineffective. The carbonic acid ionization reaction pKa is much lower than the pH at the surface so the irreversible reaction provides only a minor increase in buffer capacity and makes bicarbonate a very poor buffer for weak base drugs. Therefore very little phosphate buffer is needed to decrease the pH at the surface of the dissolving weak base drug to have the same effect as physiologically relevant bicarbonate buffer.

The predictions of phosphate buffer concentrations that match physiologically relevant bicarbonate buffer offer a dissolution medium that can better simulate the buffer capacity in the small intestine. However, there are additional considerations that must be taken into account when dealing with the dissolution of a dosage form. The first is that, as a weak acid or weak

base drug dissolves, the bulk pH may be changing which will cause the pH at the surface to change. This problem could be overcome by maintaining a relatively constant bulk pH through titration (eg: pH-Stat). Another consideration is that, as a drug particle is dissolving, the diffusion layer thickness of the particle may be considered to change[17-19]. The bicarbonate buffer model and the data for flux of ibuprofen at different rotational speeds (different diffusion layer thickness) in Krieg et al. shows that the predicted pH at the surface of the drug is dependent on the diffusion layer thickness. This aspect makes the selection of an appropriate diffusion layer thickness a significant parameter for particle dissolution in bicarbonate buffer. Of course, the dosage form and excipients could affect disintegration and dissolution which could have a significant impact on the phosphate buffer concentration that best simulates physiologically relevant bicarbonate buffer.

Conclusions

The experimental data obtained from rotating disk dissolution shows that the simultaneous diffusion and chemical reaction model accurately predicts drug flux where "instantaneous" chemical reactions occur as is the case for phosphate buffer. In the case of bicarbonate buffer, the predicted flux and experimental results show the importance of reaction kinetics in buffering the pH in the diffusion layer and at the surface of the dissolving drug. The results for the weak acids ibuprofen, indomethacin, 2-naphthoic acid, ketoprofen, and the weak base haloperidol dissolution demonstrates that the experimental flux in bicarbonate buffer cannot be predicted accurately by assuming that chemical equilibrium is instantly achieved and the reaction rates must be taken into account. Due to the slow reaction rate between CO_2 and H_2O, the BCE model overestimates and the CAI model underestimates the impact of bicarbonate buffer throughout the convective-diffusion layer and at the surface of the tablet. We show that

the slow hydration and dehydration reactions can be accounted for by assuming that CO_2 does not react with H_2O in the convective-diffusion layer while H_2CO_3 undergoes an irreversible chemical reaction forming CO_2 and H_2O in the convective-diffusion layer. This unique attribute of the bicarbonate buffer-diffusion-reaction system can accurately predict drug dissolution in bicarbonate buffer.

Matching the dissolution rate (flux) of weak acid and weak base drugs in phosphate and bicarbonate buffer systems is possible but it is a complex function of buffer pH and pKa, drug pKa and solubility, and diffusion layer thickness. The accuracy of the IRR model to predict rotating disk dissolution in bicarbonate buffer allowed for predictions of equivalent phosphate buffer concentrations that matched physiologically relevant bicarbonate buffer for both weak acid and weak base drugs. An important conclusion of this work is that, while it is possible to identify an equivalent phosphate buffer for a drug, a precise match for dosage form testing is difficult because of the complex nature mentioned above. A second important conclusion of this work is that low phosphate buffer concentrations (1-25mM) appear to be more physiologically relevant and may better simulate the impact of bicarbonate buffer on the dissolution of weak acid drugs. For weak base drugs, extremely low phosphate buffer concentrations (less than 2 mM) would be needed to match physiologically relevant bicarbonate buffer. These predicted equivalent phosphate buffer concentrations suggest that the current phosphate buffer concentrations used for dissolution testing (often 50 mM) likely do not accurately reflect the dissolution media and conditions that a drug will experience in the intestine.

Tables

Table 3. 1. Rotating disk dissolution experimental parameters applied to the weak acid drugs examined

Drug	Ibuprofen	Indomethacin	Ketoprofen	2-Naphthoic Acid	Benzoic Acid
Bulk pH	6.5	6.5	6.5	6.5	6.5
Percent CO2	7-8, 14-16, 21-22	7-8, 14-16, 21-22	7-8, 14-16, 24-26	7-8, 14-16, 22-25	13, 26, and 37
Total Buffer concentration $[CO_2(aq)]+[HCO3^-]$ (mM)	6.5-7.5, 13-15, 19.5-20.5	6.5-7.5, 13-15, 19.5-20.5	6.5-7.5, 13-15, 22-24	6.5-7.5, 13-15, 20.5-23.5	12.5, 21.5, 29.1
Bicarbonate Concentration $[HCO3^-]$ (mM)	5-5.5, 10-11, 14.5-15.5	5-5.5, 10-11, 14.5-15.5	5-5.5, 10-11, 16.5-18.0	5-5.5, 10-11, 15-17	9, 18, and 25.6
Phosphate Buffer Concentration $[H_2PO_4-+HPO4^{-2}]$ (mM)	3.5, 5.2, 6.95, 13, 25, and 43.5	2.5, 13, 25, and 43.5	10, 25, and 50	10, 25, and 50	13, 25, and 43.5
Volume of Dissolution Medium (ml)	150	100	300	200	300
RPM	100	100	100	100	100

Table 3. 2. Rotating disk dissolution experimental parameters applied to the weak base drug Haloperidol			
Drug	Haloperidol		
Bulk pH	6.0	6.5	7.0
Percent CO2	45	7-8, 14-16*, 22	5
Total Buffer concentration $[CO_2(aq)]+[HCO3^-]$ (mM)	20.7	6.5-7.5, 13-15*, 20.5	12.2
Bicarbonate Concentration [HCO3-] (mM)	9.9	5-5.5, 10-11*, 15	11
Phosphate Buffer Concentration $[H_2PO_4^-+HPO4^{-2}]$ (mM)	NA	2.5, 13, 25, and 43.5	NA
Volume of Dissolution Medium (ml)	75	75	75
RPM	100	100	100
* denotes the experimental parameters that were used for pH 6.5 in bicarbonate buffer in Figure 7			

Table 3. 3. Drug and buffer properties at 37°C that were applied to the simultaneous diffusion and reaction model			
Species	Solubility (M)	pKa	Diffusion Coefficient (cm^2/s)
Benzoic Acid	0.0334 [20]	4.19 [21]	12.0×10^{-6} [b]
Ibuprofen	3.30×10^{-4} [22]	4.43 [22]	7.93×10^{-6} [b]
Indomethacin	5.963×10^{-6} [c]	4.27 [23]	6.8×10^{-6} [24]
Ketoprofen	5.303×10^{-4} [c]	4.02 [25]	9.3×10^{-6} [2]
2-napthoic acid	3.044×10^{-4} [c]	4.22 [26]	9.86×10^{-6} [b]
Haloperidol	8.514×10^{-6} [24]	8.0 [27]	6.6×10^{-6} [24]
Phosphate		6.8 [12]	11.5×10^{-6} [2]
Bicarbonate		6.04 [c]	14.6×10^{-6} [28]
Carbonic Acid		3.55 [29]	14.6×10^{-6} [28]
Carbon Dioxide	0.02403	6.04 [c]	24.9×10^{-6} [30]
Values were taken from literature (2,31-38), estimated using the Wilke-Chang equation (b), or measured experimentally (c).			

Figures

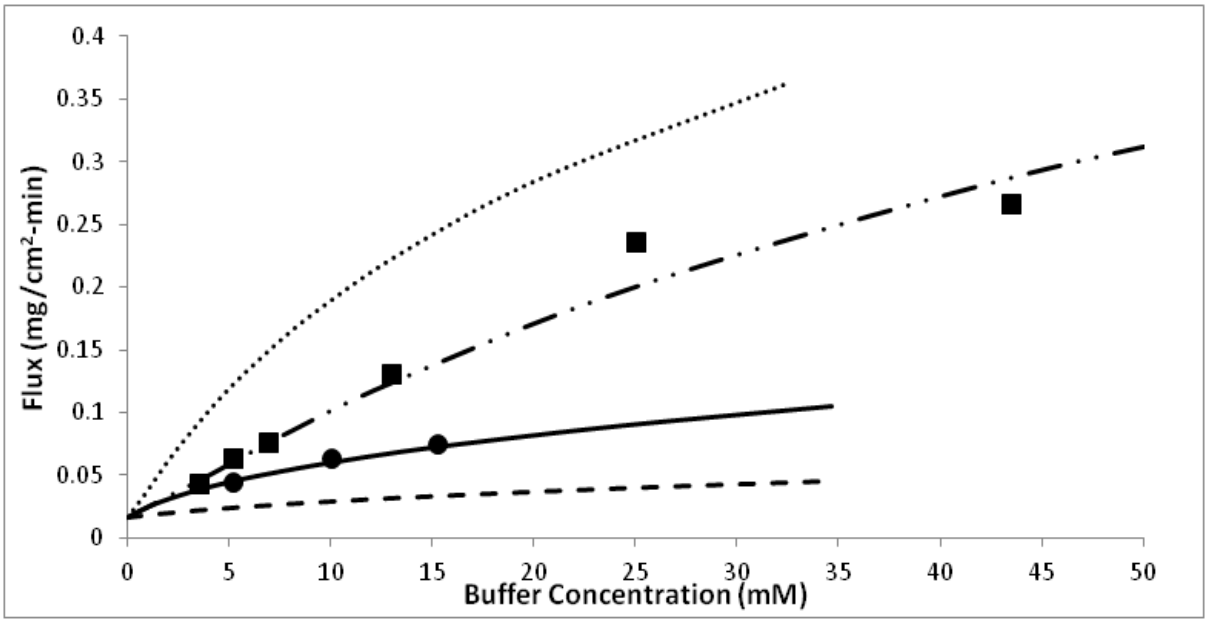

Figure 3. 1 The experimental and predicted flux of ibuprofen in bicarbonate and phosphate buffer at multiple concentrations (at pH 6.5 and 37°C). Key (■) Experimental Flux in Phosphate Buffer; (— · ·) Predicted Flux in Phosphate Buffer (BCE); (●) Experimental Flux in Bicarbonate Buffer; (·····) BCE Model Flux Predictions; (———) IRR Model Flux Predictions; (– – –) CAI Model Flux Predictions;

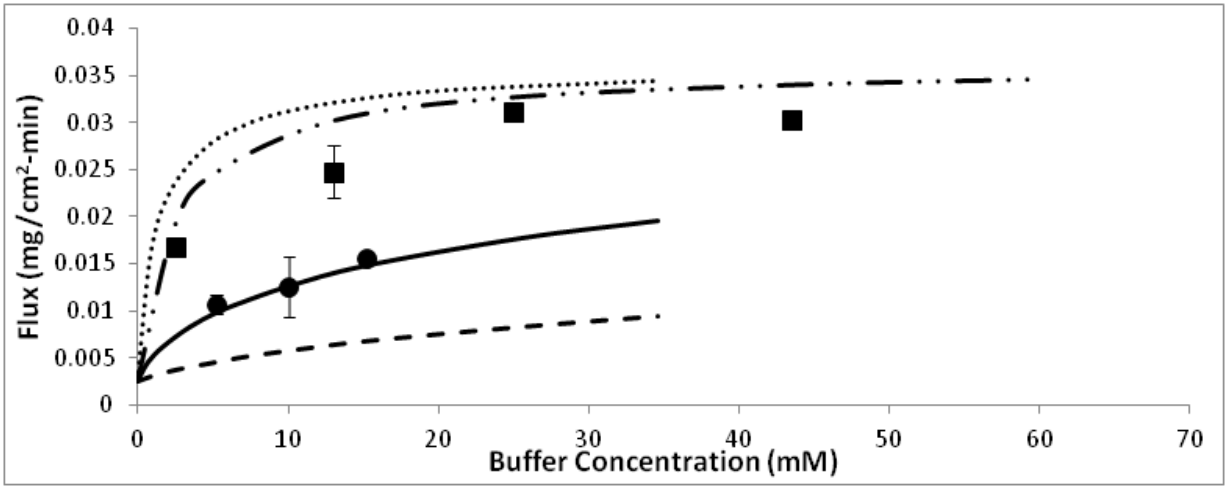

Figure 3. 2 The experimental and predicted flux of indomethacin in bicarbonate and phosphate buffer at multiple concentrations (at pH 6.5 and 37°C). Key (■) Experimental Flux in Phosphate Buffer; (— · ·) Predicted Flux in Phosphate Buffer (BCE); (●) Experimental Flux in Bicarbonate Buffer; (·····) BCE Model Flux Predictions; (———) IRR Model Flux Predictions; (– – –) CAI Model Flux Predictions;

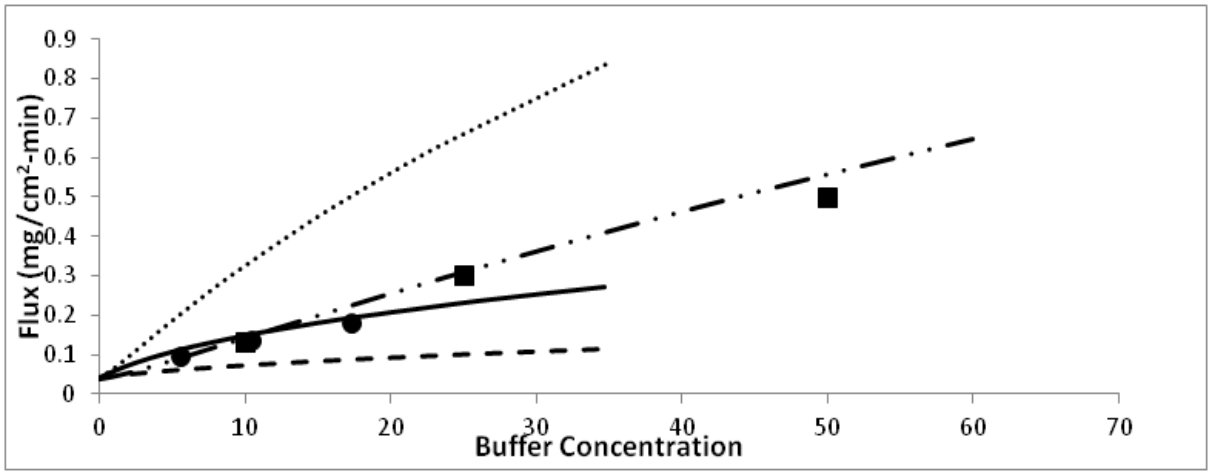

Figure 3. 3. The experimental and predicted flux of ketoprofen in bicarbonate and phosphate buffer at multiple concentrations (at pH 6.5 and 37°C). Key (■) Experimental Flux in Phosphate Buffer; (—・・) Predicted Flux in Phosphate Buffer (BCE); (●) Experimental Flux in Bicarbonate Buffer; (·····) BCE Model Flux Predictions; (———) IRR Model Flux Predictions; (– – –) CAI Model Flux Predictions;

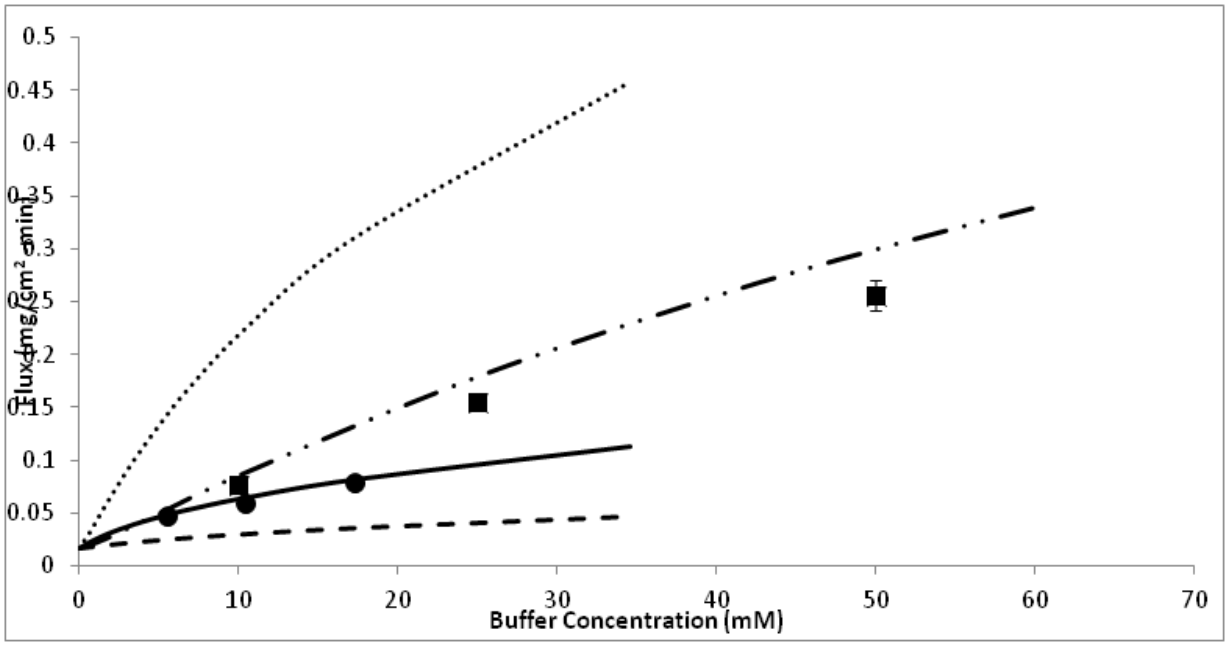

Figure 3. 4. The experimental and predicted flux of 2-napthpoic acidin bicarbonate and phosphate buffer at multiple concentrations (at pH 6.5 and 37°C). Key (■) Experimental Flux in Phosphate Buffer; (—・・) Predicted Flux in Phosphate Buffer (BCE); (●) Experimental Flux in Bicarbonate Buffer; (·····) BCE Model Flux Predictions; (———) IRR Model Flux Predictions; (– – –) CAI Model Flux Predictions;

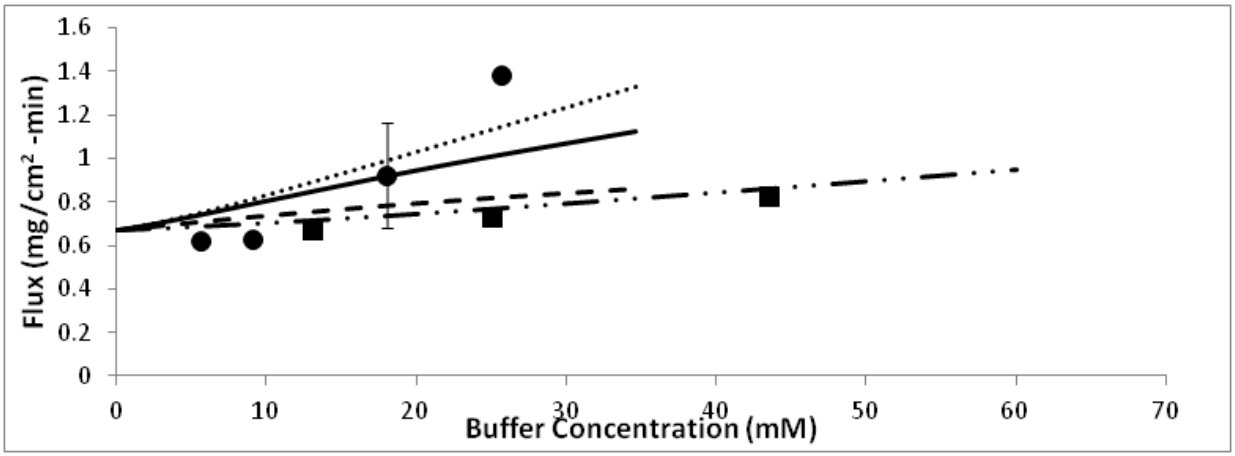

Figure 3. 5. The experimental and predicted flux of benzoic acid in bicarbonate and phosphate buffer at multiple concentrations (at pH 6.5 and 37°C). Key (■) Experimental Flux in Phosphate Buffer; (— · ·) Predicted Flux in Phosphate Buffer (BCE); (●) Experimental Flux in Bicarbonate Buffer; (·····) BCE Model Flux Predictions; (———) IRR Model Flux Predictions; (– – –) CAI Model Flux Predictions;

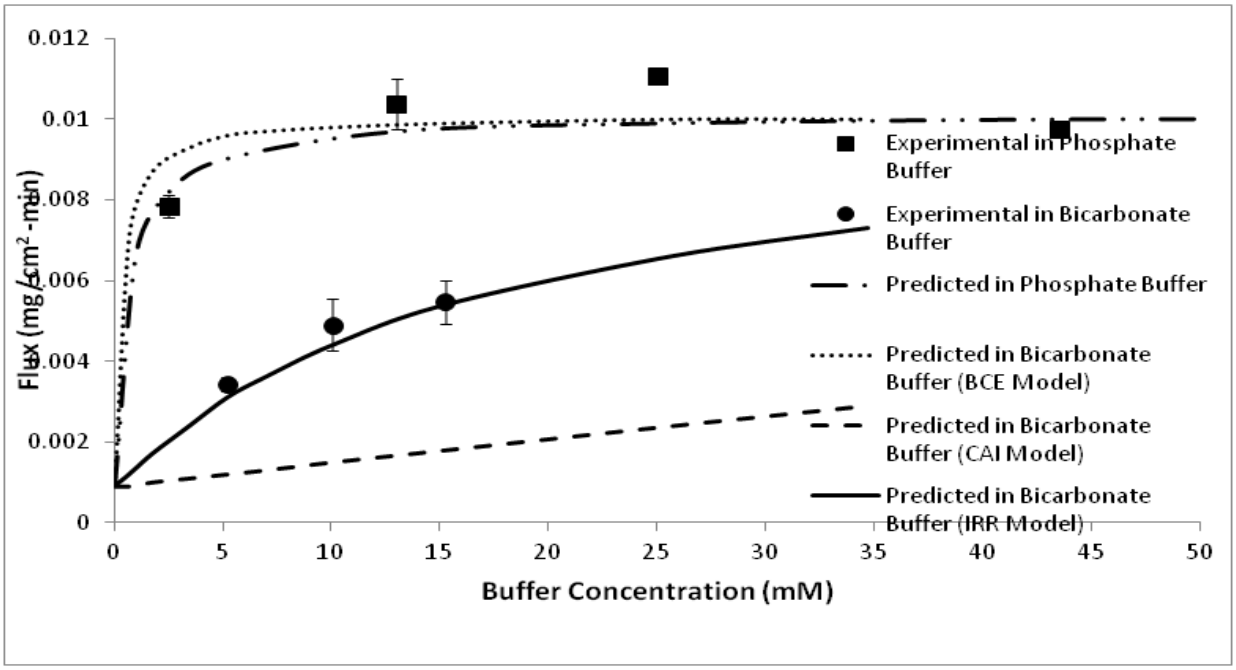

Figure 3. 6. The experimental and predicted flux of haloperidol in bicarbonate and phosphate buffer at multiple concentrations (at pH 6.5 and 37°C). Key (■) Experimental Flux in Phosphate Buffer; (— · ·) Predicted Flux in Phosphate Buffer (BCE); (●) Experimental Flux in Bicarbonate Buffer; (·····) BCE Model Flux Predictions; (———) IRR Model Flux Predictions; (– – –) CAI Model Flux Predictions;

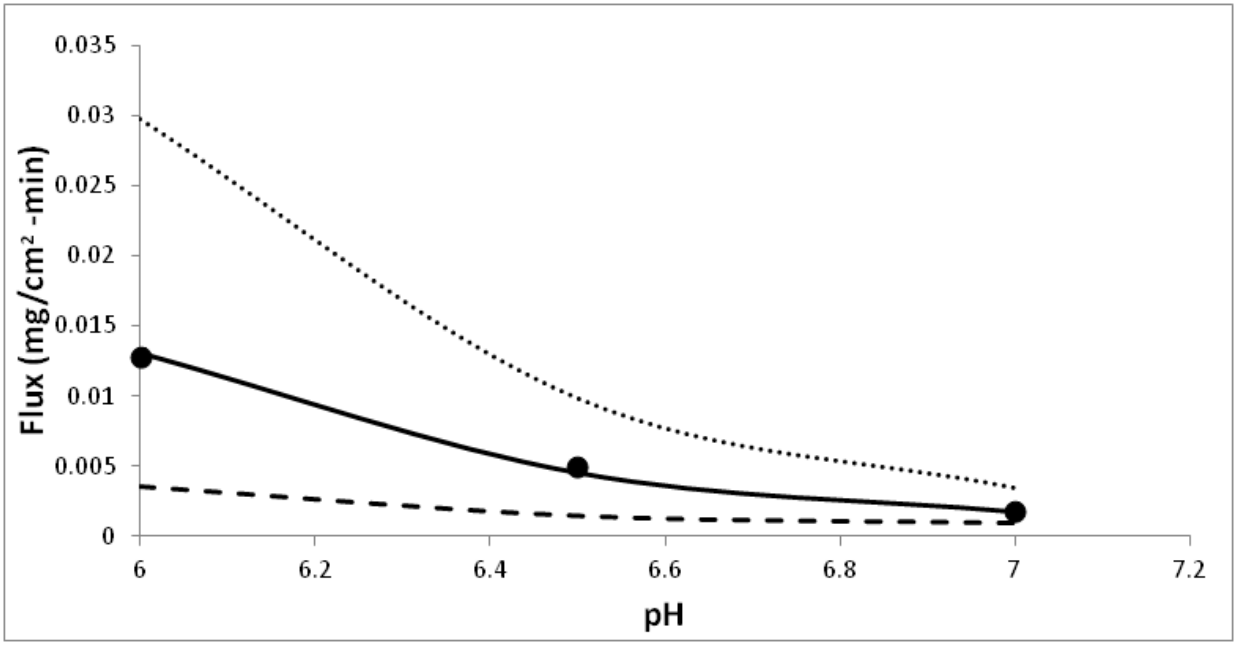

Figure 3. 7. The experimental and predicted flux of haloperidol in 10 mM bicarbonate buffer at bulk pH values 6, 6.5, and 7 at 37^{o}C. Key (•) Experimental Flux; (.....) BCE Model Flux Predictions; (——) IRR Model Flux Predictions; (– – –) CAI Model Flux Predictions;

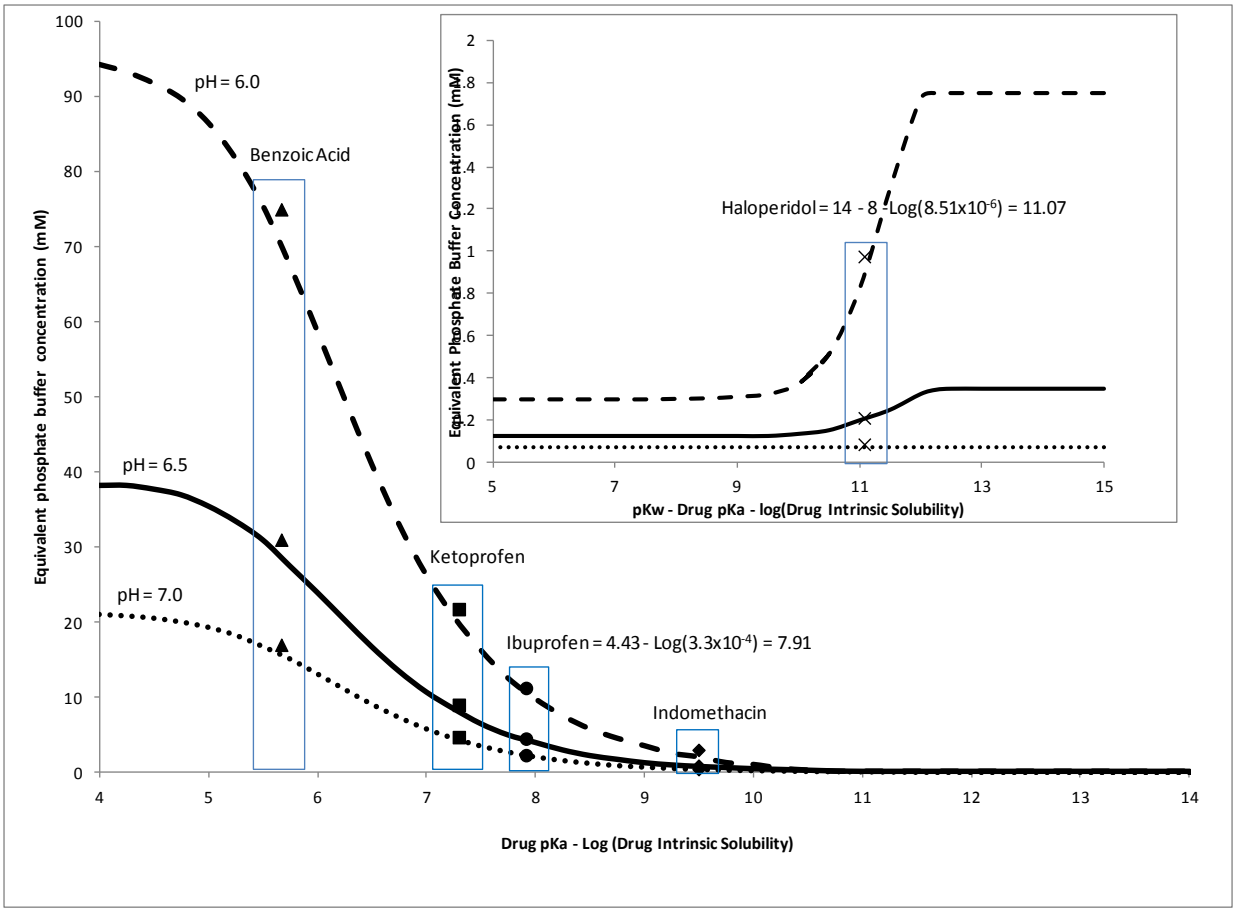

Figure 3. 8. The predicted equivalent phosphate buffer concentration needed to match 10.5mM bicarbonate buffer for weak acid drugs with drug pKa's of 3-8 and weak base drugs with pKa's of 5-10 and drug solubilities of 0.1M-10^{-6}M for both. Key: (– – –) Equivalent buffer predictions at pH 6 (h=30µm). (———) Equivalent buffer predictions at pH 6.5 (h=30µm); (·····) Equivalent buffer predictions at pH 7 (h=30µm); (▲) Equivalent buffer predictions for benzoic acid; (■) Equivalent buffer predictions for ketoprofen; (⬬) Equivalent buffer predictions for ibuprofen; (◆) Equivalent buffer predictions for indomethacin; (X) Equivalent buffer predictions for haloperidol

References

1. FDA. 2000. Guidance for industry. Waiver of the In Vivo Bioavailability and Bioequivalence Studies for Immediate-Release Solid Oral Dosage Forms Based on a Biopharmaceutics Classification System. ed., Washington, DC: U.S. Department of Health and Human, Food and Drug Administration (FDA), Center for Drug Evaluation and Research.

2. Aunins JG, Southard MZ, Myers RA, Himmelstein KJ, Stella VJ 1985. Dissolution of Carboxylic Acids III. The Effect of Polyionizable Buffers. Journal of Pharmaceutical Sciences 74(12):1305 - 1316.

3. McNamara DP, Amidon GL 1988. Reaction plane approach for estimating the effects of buffers on the dissolution rate of acidic drugs. Journal of Pharmaceutical Sciences 77(6):511-517.

4. Sheng JJ, McNamara DP, Amidon GL 2009. Toward an In Vivo Dissolution Methodology: A Comparison of Phosphate and Bicarbonate Buffers. Molecular Pharmaceutics 6(1):29-39.

5. USP. 2000. The United States Pharmacopeia USP 24, The National Formulary NF19. ed., Rockville, MD: United States Pharmacopeial Convention.

6. Galia E, Nicolaides E, Horter D, Lobenberg R, Dressman JB 1998. Evaluation of various dissolution media for predicting in vivo performance of class I and II drugs. Pharmaceutical research 15(May):698.

7. McGee LC, Hastings AB 1942. The carbon dioxide tension and acid-base balance of jejunal secretions in man. J Biol Chem 142:893-904.

8. McNamara DP, Whitney KM, Goss SL 2003. Use of a physiologic bicarbonate buffer system for dissolution characterization of ionizable drugs. Pharmaceutical Research 20(10):1641-1646.

9. Boni JE, Brickl RS, Dressman J 2007. Is bicarbonate buffer suitable as a dissolution medium? Journal of Pharmacy and Pharmacology 59(10):1375-1382.

10. Fadda HM, Merchant HA, Arafat BT, Basit AW 2009. Physiological bicarbonate buffers: stabilisation and use as dissolution media for modified release systems. International Journal of Pharmaceutics 382(1-2):56-60.

11. Liu F, Merchant HA, Kulkarni RP, Alkademi M, Basit AW 2011. Evolution of a Physiological pH 6.8 Bicarbonate Buffer System: Application to the Dissolution Testing of Enteric Coated Products. European Journal of Pharmaceutics & Biopharmaceutics 78:151-157.

12. Chuy S, Bell L 2006. Buffer pH and pKa values as affected by added glycerol and sucrose. Food Research International 39:342 - 348.

13. Mooney K, Mintun M, Himmelstein K, Stella V 1981. Dissolution kinetics of carboxylic acids II: Effect of buffers. J Pharm Sci 70(1):22-32.

14. Krieg BJ, Taghavi SM, Amidon GL, Amidon GE 2014. In Vivo Predictive Dissolution: Transport Analysis of the CO2, Bicarbonate In Vivo Buffer System. J Pharm Sci 103(11):3473-3490.

15. Garbacz G, Kolodziej B, Koziolek M, Weitschies W, Klein S 2014. A dynamic system for the simulation of the fasting luminal pH-gradients using hydroden carbonate buffers for dissolution testing of ionisable compounds. European Journal of Pharmaceutical Sciences 51:224-231.

16. Mudie DM, Amidon GL, Amidon GE 2010. Physiological Parameters for Oral Delivery and in Vitro Testing. Mol Pharmaceutics 7(5):1388-1405.

17. Hintz RJ, Johnson KC 1989. the effect of particle size distribution on dissolution rate and oral absorption. Int J Pharm 51:9-17.

18. Wang J, Flanagan DR 1999. General Solution for Diffusion-Controlled Dissolution of Spherical Particles 1. Theory. J Pharm Sci 88(7):731 - 738.
19. Sheng JJ, Sirois PJ, Dressman JB, Amidon GL 2008. Particle Diffusional Layer Thickness in a USP Dissolution Apparatus II: A Combined Function of Particle Size and Paddle Speed. Journal of Pharmaceutical Sciences 97(11):4815-4829.
20. French DL, Himmelstein KJ, Mauger JW 1995. Physicochemical Aspects of Controlled Release of Substituted Benzoic and Naphthoic Acids from Carbopol Gels. Journal of Controlled Release 37:281 - 289.
21. McMurry J. 2010. Organic Chemistry with Biological Applications 2e, ed., Belmont, Ca: Brooks/Cole. p 619.
22. Karl AL, Majella EL, Corrigan OI 2003. Effect of buffer media composition on the solubility and effective permeability coefficient of ibuprofen. International Journal of Pharmaceutics 253:49-59.
23. Fagerberg J, Tsinman O, Sun N, Tsinman K, Avdeef A, Bergstrom C 2010. Dissolution Rate and Apparent Solubility of Poorly Soluble Drugs in Biorelevant Dissolution Media. Molecular Pharmaceutics 7(5):1419-1430.
24. Tsinman K, Avdeef A, Tsinman O, Voloboy D 2009. Powder Dissolution Method for Estimating Rotating Disk Intrinsic Dissolution Rates of Low Solubility Drugs. Pharmaceutical Research 26(9):2093-2100.
25. Avdeef A, Tsinman O 2008. Miniaturized Rotating Disk Intrinsic Dissolution Rate Measurement: Effects of Buffer Capacity in Comparisons to Traditional Wood's Apparatus. Pharmaceutical Research 25(11):2613-2627.
26. Underberg WJM, Schulman SG 1979. Fluorimetric Determination of Acidity Constants of Naphthoic and Anthroic Acids. AnalChimActa 105:311-317.
27. Li S, Wong S, Sethia S, Almoazen H, Joshi YM, Serajuddin ATM 2005. Investigation of Solubility and Dissolution of a Free Base and Two Different Salt Forms as a Function of pH. Pharmaceutical Research 22(4):628-635.
28. Zeebe RE 2011. On the molecular diffusion coefficients of dissolved CO_2, HCO_3^-, and CO_3^{2-} and their dependence on isotopic mass. Geochimica et Cosmochimica Acta 75:2483-2498.
29. Nassanen R 1947. Potentiometric Study on the First Ionization of Carbonic Acid in Aqueous Solutions of Sodium Chloride. Acta Chemica Scandinavica 1:204 - 209.
30. Frank MJW, Kuipers JAM, Swaaij WPMv 1996. Diffusion Coefficients and Viscosities of CO_2 + H_2O, CO_2 + CH_3OH, NH_3 + H_2O, and NH_3 + CH_3OH Liquid Mixtures. J Chem Eng Data 41:297-302.

Chapter 4

Transport analysis to match Bicarbonate and Phosphate buffer for suspension and tablet dosage form dissolution

Abstract

Predicting and matching the dissolution of drugs in different buffer systems requires the evaluation of both drug and buffer properties that will impact dissolution. Chapters 2 and 3 have presented work using the rotating disk dissolution methodology to show that matching the buffer strengths of different buffer species is possible when applied to a well-defined hydrodynamic system and diffusion layer thickness. However, this analysis becomes more complicated when a suspension or tablet dosage form is introduced into the experimental study. Factors that can be neglected using the rotating disk methodology must be accounted for such as a change in particle size, change in bulk pH, and tablet disintegration.

All of the experimental work presented was done using ibuprofen and the USP 2 dissolution apparatus in 900ml of buffer solution with a paddle rotational speed of 50RPM. Initial experiments were performed on ibuprofen powder with a defined particle size to allow for the particle diffusion layer thickness parameter to be defined which would be the driving force for all of the surface pH predictions for bicarbonate buffer. It was assumed that matching surface pH values between bicarbonate and phosphate buffer would provide a matching dissolution profile. The experimental work shows that this assumption is correct if other factors such as disintegration or changing bulk pH are minimized.

Additionally an assessment of the added value of using both bicarbonate buffer and the predicted equivalent phosphate buffer were studied by evaluating the bioequivalence of 600mg ibuprofen reference and test tablets. These tablets were shown to not be bioequivalent based on *in vivo* results given by Alvarez et al. in 2011 [1]. However, Alvarez et al. also illustrated that *in vitro* dissolution studies in recommended dissolution media (pH 6.8 50mM phosphate buffer) could not discriminate between the dissolution rates to allow for the same conclusion. Therefore dissolution was performed in physiologically relevant bicarbonate buffer and the predicted equivalent phosphate buffer in this chapter to evaluate the ability of the buffers to provide *in vivo* predictive results. The dissolution data indicates that these buffers can provide meaningful information about dissolution rank order and statistically significant results to predict that the two formulations are not equivalent.

Introduction

Performing dissolution testing of oral dosage forms that are intended to be marketed or already on the market should provide the best determination of how that drug will dissolve in the gastro-intestinal tract when it is taken orally. Alvarez et al. showed the limitations of relying on the recommended WHO and USP monograph buffer systems for determining the bioequivalence of drug products [1]. Therefore making a dissolution test more predictive of *in vivo* results must emphasize the most important physiological parameters. For BCS class 2a (BCS Class 2 weak acid) drugs, the potential rate limiting factor after the drug has emptied into the intestine is dissolution [2]. Therefore an emphasis should be placed on BCS class 2a drugs using a dissolution medium that simulates the fluid of the intestines. A dissolution test that uses bicarbonate buffer or one that can replicate the same buffer effect as bicarbonate should provide more meaningful *in vivo* results.

As has been discussed, the preparation of physiologically relevant bicarbonate buffer is complicated and not an ideal process to perform on a large scale experimentally[3-6]. Using a phosphate buffer solution that dissolves drug particles and the active pharmaceutical ingredient (API) in a dosage form at the same rate as physiologically relevant bicarbonate buffer would be preferable. Phosphate buffer systems that match bicarbonate buffer and are easy to implement may be expected to offer a more *in vivo* predictive dissolution test for drugs in early development and can possibly be helpful in determining the bioequivalence of generic and reference drug products.

Rotating disk dissolution data has confirmed that transport analysis can accurately predict the flux of a drug in bicarbonate buffer (IRR model) and phosphate buffer (film model) under conditions of a constant well-defined diffusion layer thickness, constant drug surface area, and constant bulk pH[3,7,8]. When drug particles or dosage forms are being dissolved in a USP 2 apparatus, the diffusion layer thickness is not well defined, the surface area of the particle will decrease, and the bulk pH of the dissolution medium can either increase or decrease as the weak acid or weak base drug dissolves[9-11]. Therefore it is important to examine if the rotating disk dissolution transport analysis can be applied to suspension formulations (ie: drug particles) and tablet dosage forms in order to predict a phosphate buffer that matches bicarbonate buffer.

As previously shown, the diffusion layer thickness can have a significant impact on the pH at the surface of the drug when the drug is dissolved in bicarbonate buffer [3]. There have been numerous studies examining the diffusion layer thickness for particle dissolution in a USP 2 apparatus[9,11-14]. These models often use the concept of a critical diffusion layer thickness surrounding a dissolving spherical particle that represents the region adjacent to the dissolving surface where there is a large concentration gradient between the dissolving drug and the bulk

solution. This diffusion layer thickness is effectively constant at large particle sizes (ie: critical diffusion layer thickness) but once the particle is dissolved to the point of the critical radius, the diffusion layer thickness is equal to the particle size radius. These critical diffusion layer thickness values have varied in literature to be ~20-40µm in thickness. This variation in possible diffusion layer thickness values could have a significant impact on the predicted matching phosphate buffer. For example, the surface pH would vary in an 11mM bicarbonate buffer solution from a surface pH of 5.28 at a 40µm diffusion layer thickness to a surface pH of 5.15 at a 20µm diffusion layer thickness. This would decrease the solubility of ibuprofen from 0.549mg/ml to 0.425mg/ml, corresponding to a 23 percent decrease in solubility which could have a significant effect on the drug dissolution rate depending on the particle size of the drug.

This work will investigate the dissolution of ibuprofen particles and $Motrin_{IB}$ coated tablets in bicarbonate buffer in order to test if the CO_2-bicarbonate transport analysis (IRR model) can predict an equivalent phosphate buffer. The dissolution profiles will be compared to determine if the IRR model developed by Krieg et al. for rotating disk dissolution can be applied to drug particles and dosage forms that a person would take orally. Additionally bicarbonate and the equivalent phosphate buffer will be examined to determine whether a physiologically relevant buffer system will provide meaningful *in vitro* results that offer a more discriminating dissolution test for test and reference 600mg ibuprofen tablets. This evaluation of *in vitro* dissolution data will be used to assess the usefulness of physiologically relevant buffers as both a qualitative and quantitative tool to predict failures in bioequivalence.

Theoretical

The USP 2 apparatus particle dissolution data in bicarbonate buffer was used to estimate the correct diffusion layer thickness to apply to the IRR model to predict the correct surface pH

of the dissolving particles. This surface pH could then be matched by applying the film model of Mooney et al. to phosphate buffer to predict an equivalent phosphate buffer concentration to match the dissolution profile in bicarbonate buffer[7]. The pH at the surface was calculated for a range of diffusion layer thickness values as high as 40μm and as low as 15 μm. The surface pH at each diffusion layer thickness was used to calculate the solubility of the drug at the surface. The surface pH and solubility were assumed to be constant at the predicted surface pH for the initial diffusion layer thickness throughout the experiment even though the IRR model demonstrates that this is not the case. In the case of a 235um particle this is a safe assumption since the diffusion layer thickness changes very little before >90% of the particle has dissolved. The diffusion layer thickness used and corresponding solubility were applied to the Wang and Flanagan model for predicting particle dissolution shown in equation 4.1.

$$\frac{dm}{dt} = A\, D_{eff}\left(\frac{1}{h_{critical}} + \frac{1}{r_p}\right)\Delta C \qquad \text{Equation 4.1}$$

The diffusion layer thickness is a function of the radius of the dissolving particle (r_p) and a critical diffusion layer thickness ($h_{critical}$) values. To predict the dissolution profile for 235μm ibuprofen particles (assumed a monodisperse system) the best fit critical diffusion layer thickness and corresponding drug solubility was determined by calculating the residual sum of squares for the different predicted dissolution profiles compared to the experimental dissolution profile. This statistical analysis determined that a diffusion layer thickness that was equal to 18μm which would correspond to a surface pH calculation of 5.13 was the best fit dissolution profile.

$$\frac{dm}{dt} = A\, D_{eff}\left(\frac{1}{18\mu m} + \frac{1}{r_p}\right)\Delta C \qquad \text{Equation 4.2}$$

This critical diffusion layer thickness was used for all surface pH calculations which were used to predict the equivalent phosphate buffer concentration needed to match the same surface pH as bicarbonate buffer.

Materials and Methods:

All of the dissolution experiments were performed in single cell jacketed USP 2 apparatus in 900ml of dissolution media that was kept at 37^{o}C and the paddle was rotated at 50RPM. Ibuprofen was the API studied in all of the dissolution experiments. Ibuprofen dissolution was studied through the dissolution of ibuprofen particles (Albermarle – Baton Rouge, Louisiana, USA; Lot#11550-0005) which were placed directly into the USP 2 apparatus. The particle size was characterized by sieving and then using optical microscopy to determine the mean particle size. Dissolution was also performed on commercially available 200mg Motrin$_{IB}$ coated tablets (McNeil-PPC, INC – Fort Washington, PA, USA; NDC – 50580-110-07). The Motrin$_{IB}$ tablets were added as both intact tablets directly into the USP 2 apparatus and they were also predisintegrated in 20ml of 0.01N HCl solution. The entire suspension of the 20ml of 0.01N HCl solution and disintegrated tablet was added to the USP 2 apparatus to make 900ml of solution. The Motrin tablets did not easily disintegrate in the 0.01N HCl so a spatula was used to break the tablet into particles in the acid solution. All of the particle dissolution and Motrin$_{IB}$ tablet results reported were done in triplicate.

Dissolution was also performed on 600mg ibuprofen tablets utilized in the published research by Alvarez et al. The tablets studied were the Test 1 (batch S-10), Test 2 (batch V-1), Reference 1 (Abbot Laboratories, Madrid, Spain; Batch R-210) and the Reference 2 tablets (Abbot Laboratories, Madrid, Spain; Batch 134578D). All of the studies involving the 600mg tablets were done with the tablets pre-disintegrated. All of the test and reference dissolution results shown were done in duplicate.

For the dissolution experiments in bicarbonate buffer, the bicarbonate buffer was prepared by continuously flowing quantities of 100% dry compressed air and 100% carbon

dioxide in a 0.9%NaCl solution at appropriate ratios directly into the distilled water. The $\%CO_2(aq)$ in solution was determined using a CO_2 monitor (YSI 8500 – Yellow Springs, Ohio, USA) and pH was monitored using a pH meter (Beckman Φ 40 – Brea, California, USA). Solid sodium hydroxide and 5N NaOH was added to adjust pH. The exact experimental parameters can be seen in Table 4.1.

Dissolution experiments using phosphate buffer were made using sodium monobasic phosphate, sodium hydroxide, and sodium chloride to make the buffer solution isotonic. The exact experimental parameters can be seen in Table 4.1.

Samples for all of the dissolution studies were taken manually using a syringe and filtered (13mm Acrodisc 0.45μm filter). The samples were analyzed using a UV spectrophotometer (Agilent Technologies - Santa Clara, California, USA; Model# 61103A).

Results

Ibuprofen Particle Dissolution Results:

The analysis of particle dissolution in bicarbonate buffer was performed to estimate the size of the diffusion layer around the particle (ie: $h_{critical}$). This information allowed for calculation of the proper pH at the surface of the particle. This information was then used to predict the corresponding equivalent phosphate buffer concentration. This was achieved by performing dissolution experiments on 200mg of 235μm ibuprofen particles. In the case of the particle dissolution data this equivalent phosphate buffer concentration was predicted to be 3.5mM. The data shown in figure 4.1 shows that the predicted equivalent phosphate buffer (3.5mM) matches the dissolution data in bicarbonate buffer very well. However, the bulk pH must be kept constant throughout the experiment by titrating in 5N NaOH solution for this to occur. When no base is titrated into the bulk solution, the dissolution of the ibuprofen particles

in the predicted equivalent phosphate buffer is slower than the dissolution in bicarbonate buffer. This is due to the bulk pH changing to a much greater extent in the 3.5mM phosphate buffer solution than the bicarbonate buffer solution. The pH in the bicarbonate buffer solution never varied more than ±0.03 pH units during the dissolution experiments. However, if the equivalent phosphate buffer solution was not titrated, the pH would decrease almost 0.5 pH units over the course of the experiments. This is a significant drop in pH and would cause the predicted surface pH to decrease from 5.13 to 4.83 over the course of the experiment. Therefore this dictated the procedure of titrating 5N NaOH for all other experiments that involved the equivalent phosphate buffer.

Ibuprofen Tablet Dissolution Results:

Based on the accurate results for predicting an equivalent phosphate buffer for the dissolution of ibuprofen particles, the same dissolution procedure for dissolution of $Motrin_{IB}$ tablets in bicarbonate buffer and equivalent phosphate buffer was used. The results in Figure 4.2 show that a dosage form that must disintegrate before the dissolution can occur makes predicting an equivalent phosphate buffer a more challenging procedure. The coated $Motrin_{IB}$ tablet appeared to disintegrate faster in bicarbonate buffer which led to a faster dissolution rate than when the tablet was dissolved in the equivalent phosphate buffer. The hypothesis of disintegration being a rate-limiting factor was tested by pre-disintegrating the $Motrin_{IB}$ tablet in 0.01N HCl to eliminate the disintegration step but preventing the drug particles from dissolving to a significant extent. This data is shown for bicarbonate buffer and phosphate buffer in figure 4.3. When the coated $Motrin_{IB}$ tablet is pre-disintegrated in 0.01N HCl before being introduced into the USP 2 apparatus, the dissolution profiles are very similar. The equivalent phosphate buffer actually dissolves the pre-disintegrated $Motrin_{IB}$ tablet slightly faster than bicarbonate

buffer. This increase in dissolution rate is minimal but becomes more apparent after 50% percent of the drug has dissolved.

Bioequivalence Dissolution Study Results:

Preliminary results for the dissolution of the 600mg ibuprofen tablets in bicarbonate buffer showed that disintegration was a factor in the dissolution rate. Therefore the tablets were pre-disintegrated in 0.01NHCl before being added to the USP 2 dissolution apparatus to assess only the dissolution rate of the tablets and studies were performed on the pre-disintegrated tablets following the USP monograph dissolution protocol (900ml, 50RPM, pH 6.8 50mM phosphate buffer) to verify that disintegration was not the only factor in the *in vitro* dissolution outcome under these conditions. These studies showed that the pre-disintegrated tablets in pH 6.8 50mM buffer dissolved completely in 5 minutes. This illustrated that a high concentration of phosphate buffer can be a very non-discriminating buffer and led to a focus on the effect bicarbonate and the equivalent phosphate buffer have on dissolution.

Figures 4.4-4.7 show that the pre-disintegrated reference products dissolved faster in both the bicarbonate buffer and the equivalent phosphate buffer than the pre-disintgrated test products. These results followed the correct rank order based on the in vivo results from the Alvarez et al. study that showed a higher Cmax and lower Tmax for the reference products compared to the corresponding test products. Additionally, an f2 analysis of the dissolution results in bicarbonate buffer (figures 4.4 and 4.5) was performed and in each case the dissolution profiles through the first 30 minutes (where 85% of the dissolution occurred) gave f2 value that were <50. This analysis supports the conclusion that these two drug products are not equivalent.

The bicarbonate concentration was higher in these experiments (11.5mM) so a higher predicted phosphate buffer concentration (4mM) was predicted to match the dissolution in

bicarbonate buffer. The dissolution results in phosphate buffer (Figures 4.6 and 4.7) were similar to the dissolution results in bicarbonate buffer. However, they also followed the same trend as the pre-disintegrated $Motrin_{IB}$ tablets and the equivalent phosphate buffer had a faster dissolution rate that became much more noticeable after 50% of the ibuprofen had dissolved. In the case of the equivalent phosphate buffer, the correct rank order of the test and reference compounds was observed. However, the f2 value was only less than 50 (20.1) when comparing the dissolution profiles for the Reference 1 and Test 1 products (figure 4.6). The f2 value for the Reference 2 and Test 2 dissolution profile comparison (figure 4.7) was 51.3 with an average difference in percent dissolved at each time point of 9.4%. Therefore the percent difference is very close to the cutoff point for the two products to be considered not equivalent (10% difference at each time point). In each case it should be noted that two dissolution runs were performed at each experimental condition. Therefore if additional dissolution runs had been performed, a more meaningful f2 statistical comparison would likely have been achieved.

Discussion

The particle and drug product dissolution results show both the advantages and disadvantages to using a predicted equivalent phosphate buffer to match the dissolution in bicarbonate buffer. When the drug product has no effect on the dissolution of the particles, the dissolution in bicarbonate can be matched by applying the IRR transport model. However, in many cases the excipients of the dosage form can impact the product performance (e.g. $Motrin_{IB}$ and disintegration). The effect of the excipients on dissolution is a very important parameter that the IRR model does not take into account as it is constructed currently.

The bioequivalence dissolution studies show that dissolution cannot be the only consideration when comparing dosage forms to determine whether they are bioequivalent. The

dissolution data in bicarbonate buffer and the equivalent phosphate buffer indicates that the tablets are disintegrating in the stomach *in vivo*. The drug particles are then emptied into the intestine where they undergo dissolution and the reference product drug particles will dissolve faster in the intestine. In order to distinguish between the dissolution rates of the test and reference compounds *in vitro*, a buffer that provides a slower dissolution rate must be used. A 50mM phosphate buffer at pH 6.8 will dissolve the disintegrated ibuprofen tablets so fast that a noticeable difference in dissolution profiles would be difficult to distinguish. Therefore bicarbonate and the equivalent phosphate buffers would provide dissolution results that are more discriminating. However, the results in the bicarbonate and phosphate buffers in the USP 2 apparatus with 900ml of buffer at pH 6.5 still only offer the opportunity for a qualitative assessment for bioequivalence at this point. The experimental dissolution profiles in these buffer systems do not offer a quantitative assessment of the in vivo parameters. More physiological parameters must be considered before the quantitative assessment can be expected.

The faster dissolution rate that was noticeable in the equivalent phosphate buffer dissolution for the pre-disintegrated $\text{Motrin}_{\text{IB}}$ tablets and the 600mg ibuprofen tablets compared to the dissolution in bicarbonate can be attributed to two possibilities. The first possibility is that the bulk pH decreased to a greater extent in bicarbonate buffer because of the addition of 20ml of 0.01N HCl and the high dose of ibuprofen. When the 600mg pre-disintegrated tablet was being dissolved, the bulk pH in bicarbonate buffer decreased to ~6.35 and stayed constant at that pH throughout the dissolution experiment. The bulk pH during the dissolution in the equivalent phosphate buffer was kept at a constant pH of 6.5 throughout the experiments with titration. The other possibility for the dissolution in the equivalent phosphate buffer being faster is the changing diffusion layer thickness as the particle dissolved and its effect on the surface pH using

bicarbonate buffer. As the diffusion layer thickness decreases when the particle radius becomes ≤ 18μm , then the pH at the surface will also decrease which will cause the dissolution in bicarbonate buffer to slow down. Phosphate reaches a chemical equilibrium instantaneously so this phenomenon is only occurring with bicarbonate buffer.

Conclusion

The data shows that the IRR model can be accurately applied to the dissolution of particles or drug suspensions. However, the pH must be controlled in the equivalent phosphate buffer solution as the drug is being dissolved especially in the case of a large dose of a weak acid drug. A key component that seems to impact the use of the IRR model for tablets is the rate of disintegration. In the case of the $Motrin_{IB}$ coated tablets that were used, the tablet took some time to disintegrate and this lag time affected the dissolution rate which made the equivalent buffer predictions not applicable.

When the ibuprofen was introduced as particles or the dosage form as a suspension, then the model accurately predicts the same dissolution profiles for bicarbonate and phosphate. This would also presumably be the case if the tablet were a very fast disintegrating tablet. However, more work would need to be done to determine the accuracy of this assumption. Based on the dosage form restrictions and the limitations that come with using low buffer concentrations, performing dissolution in bicarbonate buffer would provide the best guidance for how an ionizable drug would dissolve *in vivo*. However, the equivalent phosphate buffer concentration can still be useful and provide a better substitute to the high phosphate concentration buffers that are currently used for dissolution testing.

The data suggests that using bicarbonate buffer and the equivalent phosphate offers a more discriminating dissolution test than the current dissolution testing protocols. These buffer

systems provide an opportunity to make accurate qualitative assessments to evaluate bioequivalence. However, more physiologic parameters need to be incorporated before an accurate quantitative assessment of bioequivalence can be made. This could possibly be done by incorporating more complex dissolution systems. One example would be using a multi-compartment dissolution system. In the case of acidic drugs, a compartment that mimics the stomach media and hydrodynamics could disintegrate the tablet allowing for dissolution of drug particles to occur in the intestinal compartment at physiologically relevant volumes. The predicted equivalent phosphate buffer could be used in the intestinal compartment to match bicarbonate buffer and provide a more in vivo predictive dissolution test. However, more work needs to be done to assess the viability of these more complex systems.

Tables

Table 4. 1. USP 2 apparatus experimental parameters applied to the different ibuprofen dosage forms

Drug	Ibuprofen 235µm Particles	200mg Motrin IB Coated Tablet	600mg Ibuprofen Test and Reference Products
Bulk pH	6.5	6.5	6.5
Percent CO2	15-16.5	15-16.5	16-17.5
Total Buffer concentration $[CO_2(aq)]+[HCO3^-]$ (mM)	10.5-11.5	10.5-11.5	11-12
Bicarbonate Concentration $[HCO3^-]$ (mM)	14-15.5	14-15.5	14.5-16
Phosphate Buffer Concentration $[H_2PO_4^- + HPO4^{-2}]$ (mM)	3.5	3.5	4
Volume of Dissolution Medium (ml)	900	900	900
RPM	50	50	50

Figures:

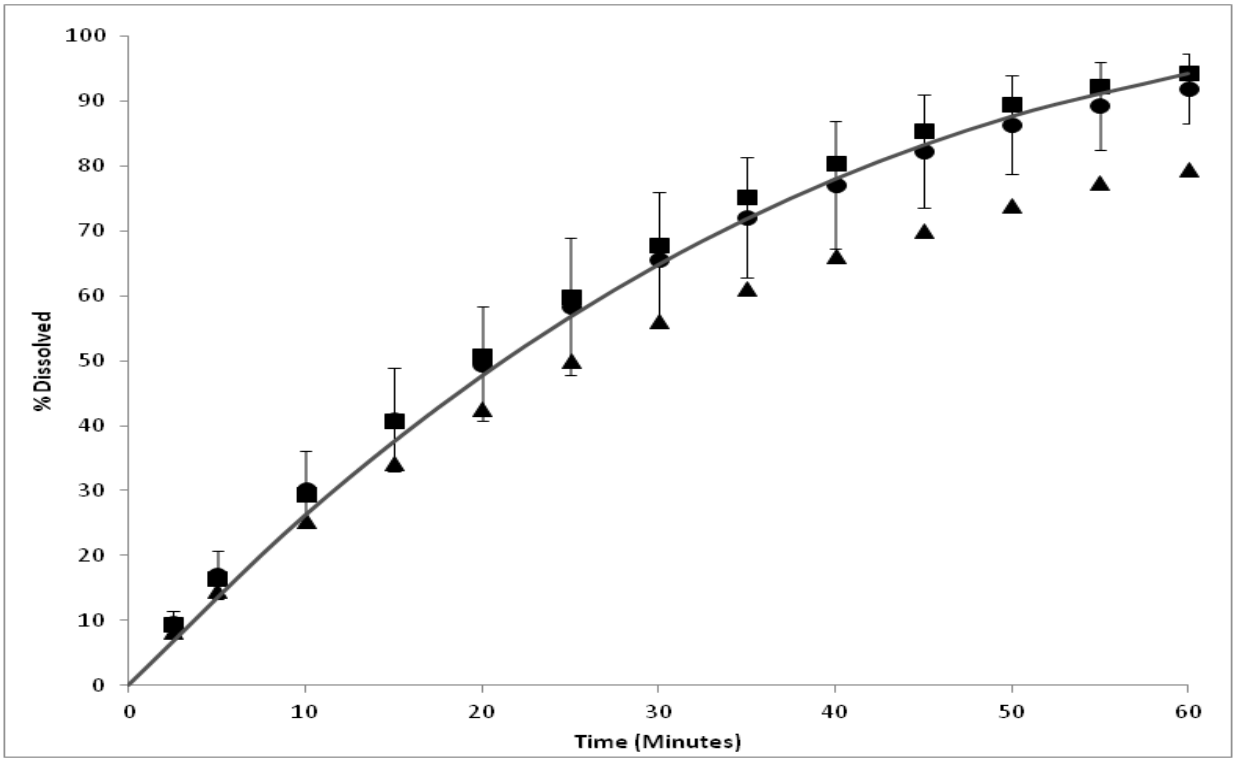

Figure 4. 1. USP 2 apparatus dissolution results of 235µm ibuprofen particles in 11mM bicarbonate buffer and 3.5mM phosphate buffer at pH 6.5 and at 37^{o}C. Key (●) Dissolution in bicarbonate buffer; (■) Dissolution in phosphate buffer bulk pH kept constant; (▲) Dissolution in phosphate buffer bulk pH not kept constant; (——) predictions in bicarbonate buffer based on h = 18µm which gives a surface pH of 5.13;

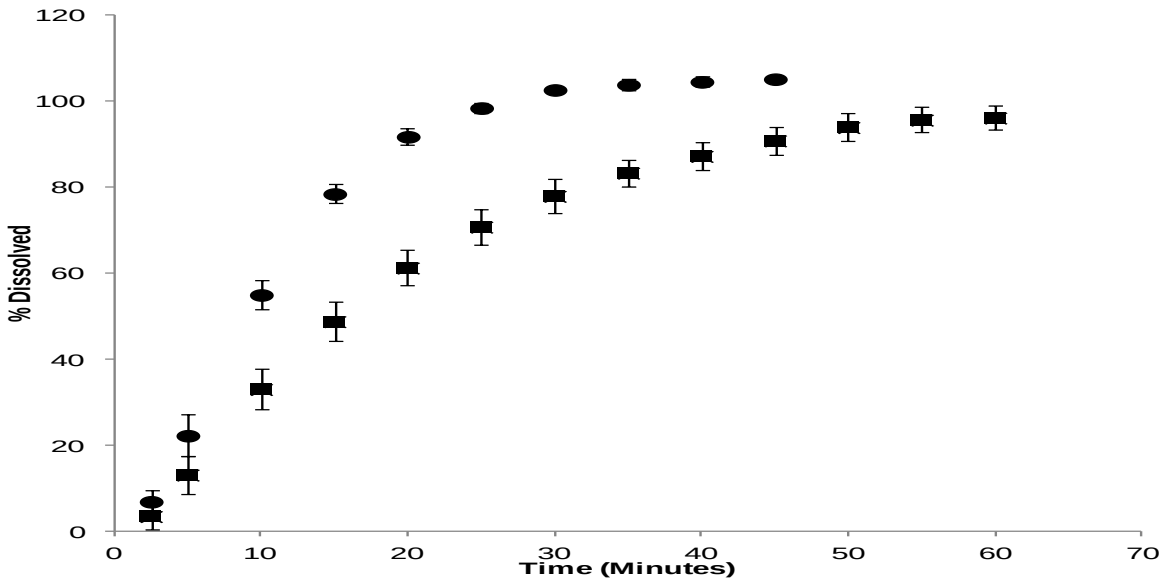

Figure 4. 2. USP 2 apparatus dissolution results of 200mg Motrin IB intact tablets in 11mM bicarbonate buffer and 3.5mM phosphate buffer at pH 6.5 and at 37^{o}C. Key (●) Dissolution in bicarbonate buffer; (■) Dissolution in phosphate buffer bulk pH kept constant.

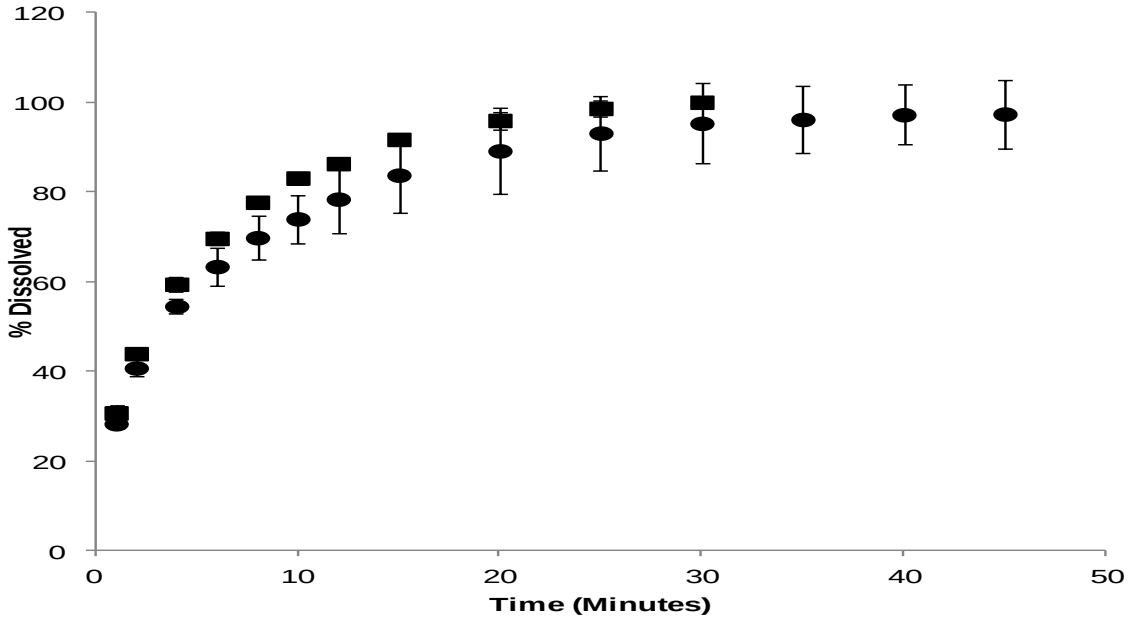

Figure 4. 3. USP 2 apparatus dissolution results of 200mg Motrin IB pre-disintegrated tablets in 11mM bicarbonate buffer and 3.5mM phosphate buffer at pH 6.5 and at 37^{o}C. Key (●) Dissolution in bicarbonate buffer; (■) Dissolution in phosphate buffer bulk pH kept constant.

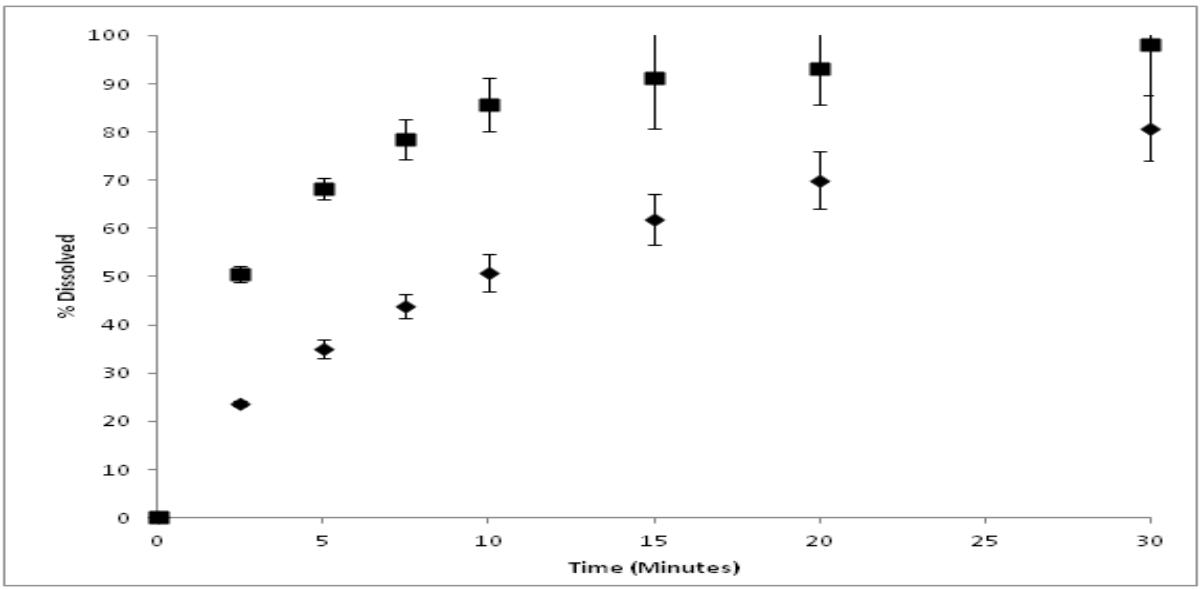

Figure 4. 4. USP 2 apparatus dissolution results of 600mg ibuprofen pre-disintegrated tablets test 1 and reference 1 drug products in 11.5 mM bicarbonate buffer at pH 6.5 and at 37^{o}C. Key (■) Dissolution results of the reference 1 drug product; (♦) Dissolution results of the test 1 drug product;

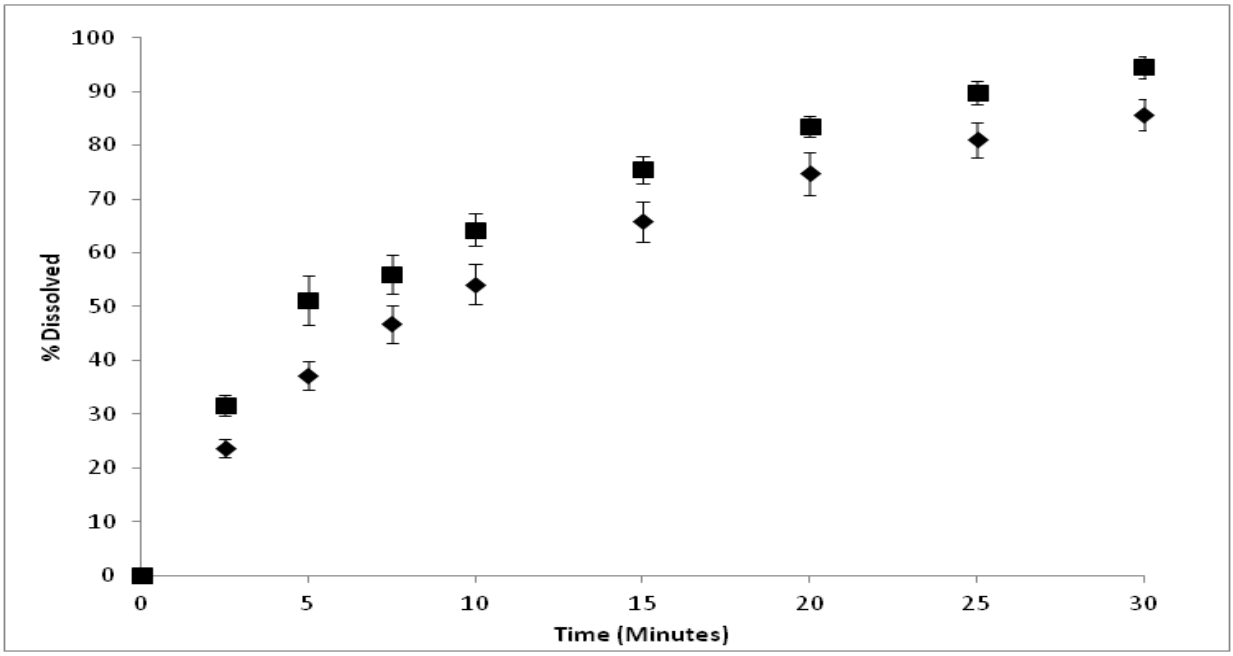

Figure 4. 5. USP 2 apparatus dissolution results of 600mg ibuprofen pre-disintegrated tablets test 2 and reference 2 drug products in 11.5 mM bicarbonate buffer at pH 6.5 and at 37^{o}C. Key (■) Dissolution results of the reference 2 drug product; (♦) Dissolution results of the test 2 drug product;

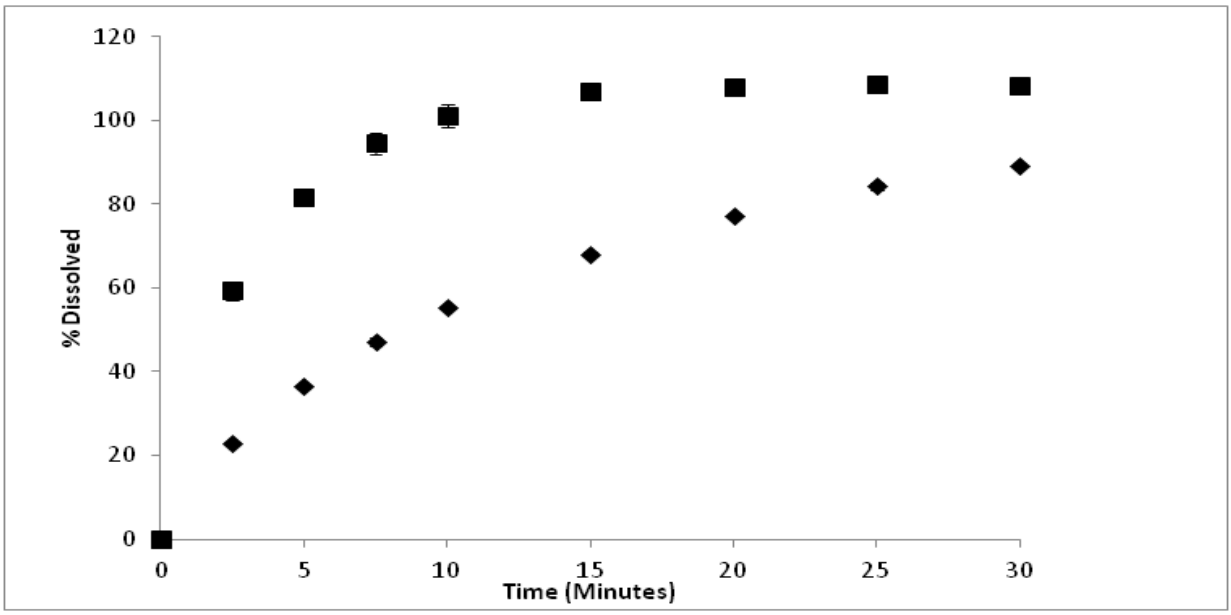

Figure 4. 6. USP 2 apparatus dissolution results of 600mg ibuprofen pre-disintegrated tablets test 1 and reference 1 drug products in 4 mM bicarbonate buffer at a bulk pH kept constant at 6.5 and at 37^{o}C. Key (■) Dissolution results of the reference 1 drug product; (♦) Dissolution results of the test 1 drug product;

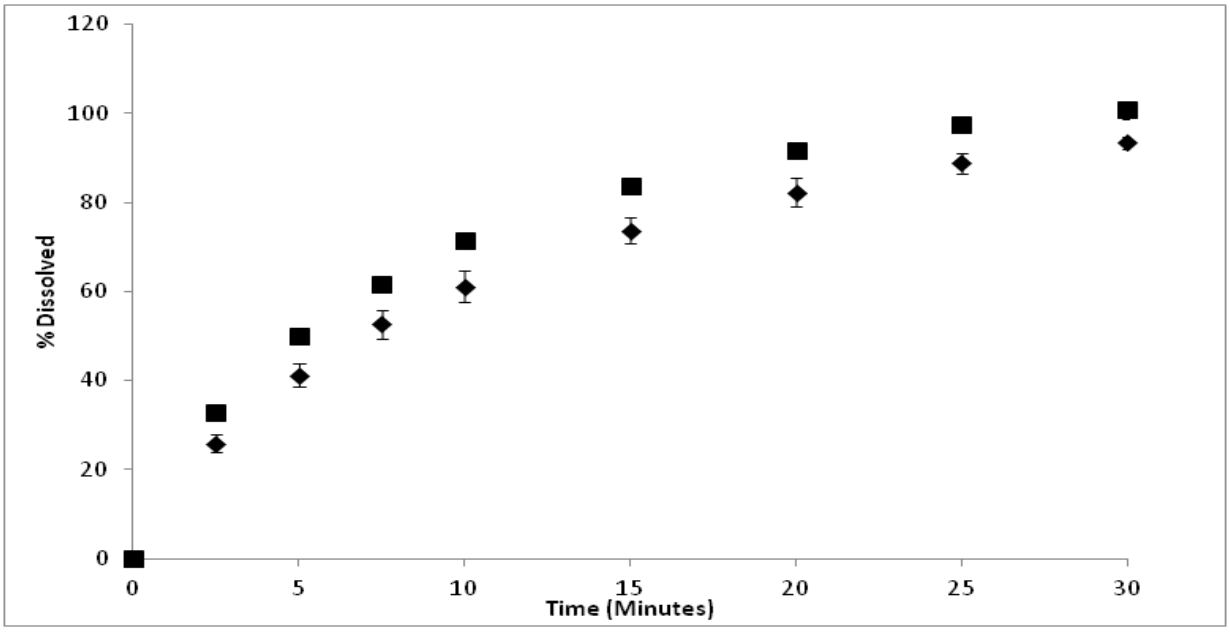

Figure 4. 7. USP 2 apparatus dissolution results of 600mg ibuprofen pre-disintegrated tablets test 2 and reference 2 drug products in 4 mM bicarbonate buffer at a bulk pH kept constant at 6.5 and at 37^{o}C. Key (■) Dissolution results of the reference 2 drug product; (♦) Dissolution results of the test 2 drug product;

References

1. Álvarez C, Núñez I, Torrado JJ, Gordon J, Potthast H, García-Arieta A 2011. Investigation on the possibility of biowaivers for ibuprofen. Journal of Pharmaceutical Sciences 100(6):2343-2349.
2. Tsume Y, Mudie DM, Langguth P, E AG, Amidon GL 2014. The Biopharmaceutics Classification System: Subclasses for in vivo predictive dissolution (IPD) methodology and IVIVC. European Journal of Pharmaceutical Sciences 57:152-163.
3. Krieg BJ, Taghavi SM, Amidon GL, Amidon GE 2014. In Vivo Predictive Dissolution: Transport Analysis of the CO2, Bicarbonate In Vivo Buffer System. J Pharm Sci 103(11):3473-3490.
4. Sheng JJ, McNamara DP, Amidon GL 2009. Toward an In Vivo Dissolution Methodology: A Comparison of Phosphate and Bicarbonate Buffers. Molecular Pharmaceutics 6(1):29-39.
5. Boni JE, Brickl RS, Dressman J 2007. Is bicarbonate buffer suitable as a dissolution medium? Journal of Pharmacy and Pharmacology 59(10):1375-1382.
6. Garbacz G, Kolodziej B, Koziolek M, Weitschies W, Klein S 2014. A dynamic system for the simulation of the fasting luminal pH-gradients using hydroden carbonate buffers for dissolution testing of ionisable compounds. European Journal of Pharmaceutical Sciences 51:224-231.
7. Mooney K, Mintun M, Himmelstein K, Stella V 1981. Dissolution kinetics of carboxylic acids II: Effect of buffers. J Pharm Sci 70(1):22-32.
8. Aunins JG, Southard MZ, Myers RA, Himmelstein KJ, Stella VJ 1985. Dissolution of Carboxylic Acids III. The Effect of Polyionizable Buffers. Journal of Pharmaceutical Sciences 74(12):1305 - 1316.
9. Wang J, Flanagan DR 1999. General Solution for Diffusion-Controlled Dissolution of Spherical Particles 1. Theory. J Pharm Sci 88(7):731 - 738.
10. Hintz RJ, Johnson KC 1989. the effect of particle size distribution on dissolution rate and oral absorption. Int J Pharm 51:9-17.
11. Sheng JJ, Sirois PJ, Dressman JB, Amidon GL 2008. Particle Diffusional Layer Thickness in a USP Dissolution Apparatus II: A Combined Function of Particle Size and Paddle Speed. Journal of Pharmaceutical Sciences 97(11):4815-4829.
12. Hintz RJ, Johnson KC 1989. The effect of particle size distribution on dissolution rate and oral absorption. International Journal of Pharmaceutics 51:9-17.
13. Sugano K 2008. Theoretical comparison of hydrodynamic diffusion layer models used for dissolution simulation in drug discovery and development. International Journal of Pharmaceutics 363(1-2):73-77.
14. Wang J, Flanagan DR 2002. General Solution for Diffusion-Controlled Dissolution of Spherical Particles. 2. Evaluation of Experimental Data. Journal of Pharmaceutical Sciences 91(2):534-542.

Chapter 5

USP 4 Particle Dissolution: The impact of fluid velocity on the dissolution of drug particles using dimensionless numbers

Abstract:

Dissolution testing is typically done in the USP 2 apparatus which has a broad velocity and hydrodynamic profile that is typically not in the range of that which a drug particle would encounter as it is being dissolved in the gastrointestinal tract. Therefore making predictions in the USP 2 apparatus for the hydrodynamic impact on dissolution is difficult and it may not be a meaningful tool to assess the impact of hydrodynamics *in vivo*. However, the USP 4 apparatus has a more well-defined velocity profile that can be adjusted to be kept in a physiologically relevant range by altering the flow rate of the fluid in the apparatus. This allows for the capability of modeling the impact of fluid velocity on particle dissolution using dimensionless numbers such as the Reynolds (Re), Schmidt (Sc), and the Sherwood (Sh) number.

Experimental work was performed in the USP 4 apparatus for three different particle size sieve factions of ibuprofen. These sieve fractions were analyzed using optical microscopy to characterize the particle size and obtain a mean particle diameter for each sieve cut. The dissolution of each ibuprofen sieve cut was evaluated at various flow rates (6, 11 and 25ml/min) to evaluate the impact of velocity and Re number on the dissolution of the particles.
This data was used to determine a mass transfer relationship that would provide the best explanation for defining the Sh number that could be used to predict particle dissolution at lower and more narrow Re number range ($0.06<Re<2$). This approach was accomplished by

successfully applying the mass transfer model of Nelson and Galloway with the Rowe modification[1,2]. The model was able to accurately predict the impact of velocity on particle dissolution for the different particle sizes and fluid velocities when the void fraction in the area around the particles could be estimated. However, there was a significant variation in the USP 4 dissolution data which was typically seen at the lower flow rates possibly due to particle agglomeration or packed bed formation.

Lastly the USP 4 data was compared to dissolution of the same sieve cuts in the USP 2 apparatus. The comparison of dissolution profiles showed much less experimental variation in the USP 2 apparatus and the average results for all of the sieve cuts were very similar to the USP 4 experimental data at 11ml/min. Therefore the USP 4 apparatus presents the opportunity to model the impact of velocity but the USP 2 apparatus provides a robust dissolution test that offers a hydrodynamic environment similar to the environment the particles would see at low flow rates and at *in vivo* relevant velocities.

Introduction

Dissolution in all of the USP apparatuses has shown that varying the hydrodynamics can impact the rate at which a drug dissolves and this is particularly true for the most commonly used USP 2 apparatus[3-7]. One of the main hydrodynamic components that can be elucidated from *in vivo* data is the flow rate and velocity in the gastrointestinal tract (GI). One of the disadvantages of the USP 2 apparatus, which is the most commonly used dissolution methodology, is the wide variation in velocities observed throughout the apparatus[8-11]. Also, the peak and bulk velocities (10-20cm/s) in the USP 2 apparatus are much larger than those seen in the intestinal tract (0.02-1cm/s)[8,12-14]. A dissolution test that can reduce the magnitude and variation in velocities would be preferred to understand the impact of hydrodynamics on particle dissolution and could offer a

more *in vivo* predictive dissolution test. For example, Katori et al. showed that very low rotational speeds in the USP 2 apparatus and low flow rates in the USP 4 apparatus can provide a IVIVC for controlled release tablets[15].

The USP 4 apparatus allows for a predictable and uniform fluid velocity profile throughout the cell[16-19]. The flow rates can be made to be very low in the USP 4 apparatus (i.e. 4ml/min) which would equate to an average fluid velocity of 0.06cm/s in the 12mm powder cell USP 4 apparatus. These low velocities are good approximations of intestinal velocities which would help to create a more meaningful hydrodynamic dissolution test experimentally. However, these low velocities may not be efficient at dispersing the particles which can cause the particles to agglomerate and form larger particles that will take longer to dissolve[20].

The ability to control the velocity that a particle experiences during the dissolution process allows for a better understanding of the impact of hydrodynamics on particle dissolution. Previous work has shown that changing the hydrodynamics in the different USP dissolution apparatuses can have a significant impact on both tablet and particle dissolution[4,21-24]. Being able to predict the impact that changing the velocity will have on particle dissolution would provide a significant benefit when trying to predict how the different flows in the GI tract will impact dissolution. Also, having a known velocity using the USP 4 apparatus creates the opportunity to expand on the particle dissolution models which rely on a diffusion layer thickness based on assumptions of the diffusion layer thickness being equal to the particle radius or a critical diffusion layer thickness [24-29]. The USP 4 apparatus can provide an experimental fluid velocity (particle velocity = ((flow rate/area for flow) + settling velocity)/2) that can be incorporated into the predictions for dissolution through non-dimensional numbers (eg: Sherwood number).

Dimensionless Number Analysis of Dissolution Results

The particle dissolution was predicted by using the Sherwood number (Sh #) which is a dimensionless number used to describe mass transfer. The Sh # is a parameter in the mass transfer coefficient for dissolution of a particle. It plays a role in defining the diffusion layer thickness (h_{eff}) of a dissolving particle [30].

$$\frac{dm}{dt} = A\ \frac{D_{eff}}{h_{eff}}\Delta C\ ; \qquad Equation\ 5.1$$

$$h_{eff} = \frac{d_p}{Sh} \qquad Equation\ 5.2$$

$$\frac{dm}{dt} = A\ \frac{D_{eff}\ Sh}{d_p}\Delta C \qquad Equation\ 5.3$$

The dimensionless number approach to quantify dissolution using the USP 4 apparatus is not a novel idea. This approach has been previously applied to both tablet and particle dissolution[20,22,31]. However, the definition for the Sh number for these dissolution studies has generally been based on the Ranz and Marshal model which will be discussed below. The Sh # is typically defined by the Reynolds number (Re #), and the Schmidt number (Sc #). Additionally there is usually a diffusion component that is a constant and set to equal = 2.The basic format of the Sh # for single particle solutions assuming infinite dilution is shown in equation 5.8.

$$Re = \frac{d_p \Delta U}{v};\quad Equation\ 5.4$$

$$\Delta U = \frac{fluid\ velocity + settling\ velocity}{2} \quad Equation\ 5.5$$

$$settling\ velocity = \frac{g(\rho_p - \rho_f)d_p}{18\mu} \quad Equation\ 5.6$$

$$Sc = \frac{v}{D_{eff}} \qquad Equation\ 5.7$$

$$Sh = 2 + \alpha Re^{x} Sc^{1/3} \qquad Equation\ 5.8$$

The ΔU term is the velocity that the drug particles are assumed to be experiencing as they are dissolving. The α and x terms in the Sh # vary in the literature with the experimental systems and conditions[32-38]. However, the Sh # that is most identifiable is the one proposed by Frossling and experimentally verified through the work of Ranz and Marshall who define it as $Sh=2+0.6Re^{0.5}Sc^{1/3}$ [32,39]. However, this work dealt with the evaporation of a single sphere of liquid into air and does not necessarily translate to many drug particles that could be interacting with each other as they are dissolving in liquid. This was specifically examined by D'arcy and Persoons who defined the diffusion layer thickness through the Ranz and Marshall model for their particle dissolution work. Their approach assumed that the dissolution would be not be affected by increasing the flow rate in a USP 4 apparatus. This assumption applied to the Ranz and Marshall Model did not accurately account for the dissolution data they observed at different flow rates. However, including the increasing fluid velocities they applied experimentally to the Ranz and Marshall approach does allow for more accurate predictions of dissolution (according to our calculations).

Therefore the Ranz and Marshall theory was first applied to the particle dissolution data in the USP 4 apparatus to test the accuracy for our dissolution system. However, this approach and several other Sh # variations in the literature did not accurately account for the experimental results in our system[33-36]. Much of the past experimental work of mass transfer focused on either ideal systems with a single particle or solid pellet or the focus was also on modeling a large variation in Re numbers where Re # <1 to Re # >1,000 [33-36,40]. These situations are quite different from those that a dissolving drug tablet or particle would typically experience in the intestinal tract or USP 4 apparatus (Re < 30)[41]. Therefore other work was evaluated to analyze

models studying the mass transfer of solid into liquids at low Sh # and Re #[1,2,40,42-45]. Many of these models differ from one another but there was a unifying trend in much of the mass transfer work modeling fluidized beds. The work by Nelson and Galloway offered an approach to calculate the Sh # when dealing with a packed or fluidized bed at low Re #'s. This approach is given in Equation 5.9-5.10.

$$Sh = \frac{2\zeta + \left\{ \frac{2\zeta^2(1-\epsilon)^{\frac{1}{3}}}{\left[1-(1-\epsilon)^{\frac{1}{3}}\right]^2} - 2 \right\} tanh\zeta}{\frac{\zeta}{1-(1-\epsilon)^{\frac{1}{3}}} - tanh\zeta} \qquad Equation\ 5.9$$

$$\zeta = \left(\frac{1}{(1-\epsilon)^{\frac{1}{3}}} - 1 \right) \frac{\alpha}{2} Re^{1/2}\, Sc^{1/3} \qquad Equation\ 5.10$$

The solution derived by Nelson and Galloway provides two rate limiting cases. The first limiting case is when the system has a void fraction of 1 (ie. single particle – infinite dilution) where the derivation reverts to the Ranz and Marshal model. The second limiting case is where the Sh # goes to zero as the Re # goes to zero in the presence of a packed or fluidized bed. This is shown in equation 5.11.

$$Sh = \frac{1}{(1-\epsilon)^{\frac{1}{3}}} \left(\frac{1}{(1-\epsilon)^{\frac{1}{3}}} - 1 \right) + \frac{\alpha^2}{2} ReSc^{2/3} \qquad Equation\ 5.11$$

However, this approach did not adequately account for mass transfer at higher Re numbers that may be seen in fluidized beds. Therefore Rowe proposed a modification to the Nelson and Galloway approach (shown in equation 5.12) to accurately describe mass transfer when dealing with higher Re # that exceeds the mass transfer predictions using the Ranz and Marshall theory.

$$Sh = \frac{2\frac{\zeta}{\epsilon} + \left\{ \frac{2\frac{\zeta^2}{\epsilon}(1-\epsilon)^{\frac{1}{3}}}{\left[1-(1-\epsilon)^{\frac{1}{3}}\right]^2} - 2 \right\} tanh\zeta}{\frac{\epsilon}{1-(1-\epsilon)^{\frac{1}{3}}} - tanh\zeta} \qquad Equation\ 5.12$$

The ϵ symbol is the void fraction in the system. The definition for $\zeta$is the same as it appears in Equation 5.10 and the α term is still hypothesized to be equal to 0.6 just as it is in the Ranz and Marshall model. A plot using the approach applied in equation 12 is shown in figure 5.2 with the experimental data. This figure supports the use of the Rowe modification for fitting the USP 4 particle dissolution data. However, one of the unknown parameters in applying the Nelson and Galloway approach with the Rowe modification to the USP 4 system is quantifying the void fraction without understanding the conditions the particles are experiencing while they are being dissolved.

Additionally, the Re # for the particles was assumed to be equal to the fluid velocity during the flow portion of the pumping pulse and equal to the particle settling velocity during the no flow portion of the pulse. Therefore the velocity is dependent on particle size and density. The equation for settling velocity shows that this dependence is at its greatest for large particle sizes and at low flow rates. However, as the particle dissolves, the particle velocity becomes more dependent on the fluid flow rate. This can be observed in figure 5.1which shows the velocity profiles for the particles sizes and flow rates used for the experiments.

The main goal of this chapter was to use the USP 4 apparatus to accurately determine the impact that fluid velocity has on the dissolution of drug particles under physiologically relevant velocities as well as compare the dissolution in the USP 4 apparatus to dissolution in the USP 2 apparatus. This work has shown that the dissolution of different particle sizes at different flow rates can be predicted accurately with the Nelson and Galloway approach that was modified by

Rowe as long as the void fraction is known or can be estimated. Additionally this work evaluated the viability of using the USP 4 apparatus to obtain meaningful hydrodynamic results in comparison to the USP 2 apparatus.

Materials and Methods:

The dissolution of 10mg of ibuprofen (Albermarle – Baton Rouge, Louisiana, USA; Lot#11550-0005) particles was studied using the Sotax CE-7 USP apparatus 4 with the 12mm powder cells. Three different sieve cuts of ibuprofen were analyzed through optical microscopy to determine the particle size. The mean particle diameter of the three different sieve cuts were 45µm, 111µm, and 235µm. The true density of the ibuprofen particles was measured to be 1.118mg/ml. Each of the sieve cuts was studied at flow rates of 11 and 25ml/min. Additionally, the 45µm and 111µm sieve cuts were also studied at 6ml/min. Ten milligrams of the ibuprofen particles were introduced into the USP 4 Cells as part of a suspension composed of 50mM Acetate buffer ~pH4.00 and composed of Avicel RC-591microcrystalline cellulose powder (FMC BioPolymer – Philadelphia, Pennsylvania, USA; Lot#13825182) and sodium dodecyl sulfate (Fisher Scientific – Fair Lawn, New Jersey, USA; Lot # 125937) 20mg/ml ibuprofen/1.5% Avicel/0.75mM sodium dodecyl sulfate (SDS) suspension. The dissolution medium for the USP 4 dissolution tests consisted of 550ml of 0.75mM SDS, pH 4.5, 50mM acetate buffer (ibuprofen solubility =0.15mg/ml). A closed system was used for the USP 4 set up so the fluid was continually recycled from the USP 4 cells to the 550ml of bulk fluid. Each cell had its own 550ml of bulk fluid. The samples were taken using a peristaltic pump to pull 2ml from the bulk solution of all the samples individually and all at the same time.

Additionally dissolution of the 45, 111, and 235µm diameter ibuprofen particle sieve cuts was performed in the USP 2 apparatus. The same suspensions were used for each but 20mg of

ibuprofen was added for each dissolution test. The dissolution medium composition was that was used for the USP4 but the volume used in the USP 2 apparatus was 900ml. The paddle was rotated at 50 RPM. The 3ml samples were pulled manually using a syringe and filtered using a 0.45µm acrodisc syringe filter.

All of the dissolution samples were analyzed using a UV spectrophotometer (Agilent Technologies, Model# 61103A).

MATLAB was used for dissolution simulations. The ibuprofen particles sieve cuts were assumed to be monodisperse for all of the dissolution simulations and equal to the mean particle size that was measured.

Results

Figure 5.2 shows the calculations for $Sh/Sc^{1/3}$ based on the results for each experimental condition as well as the theoretical values based on the Rowe Modification to the Nelson and Galloway approach for Sh #'s at different Re #'s assuming varying void fractions. The experimental results were evaluated from zero to 50% dissolved to calculate the experimental $Sh/Sc^{1/3}$. The experimental $Sh/Sc^{1/3}$ values are consistent with the Rowe modification to the Nelson and Galloway approach for low Re numbers in packed or fluidized bed situations [1,2,45]. The experimental data is in good agreement with the assumption that there is a void fraction of 0.25 applying the Rowe approach. Therefore all of the experimental dissolution profiles were predicted utilizing the Rowe modification while assuming a void fraction of 0.25.

Figure 5.3 shows how the Sh # changes with particle size and flow rate based on the Rowe approach assuming a void fraction of 0.25. A large particle at a high flow rate will have a large Sh # due to a large Re #. When assuming the presence of a void fraction due to a packed or fluidized bed, the Rowe model calculates a Sh number that goes to zero as the particle size and

fluid flow go to zero (Re goes to 0). This is different than the Ranz and Marshall model which states that the Sh number will become a constant equal to two when the Re number equals zero. The reason for the difference in these models is that the Ranz and Marshall model assumes the spherical particle is undergoing mass transfer in an infinite stagnant fluid which leads to a steady state solution that equals two when the Re # is equal to zero. However, the Nelson and Galloway model which was modified by Rowe assumes that the drug particle is a part of a collection of particles that no longer conform to a non-zero steady state solution and therefore the Sh # goes to zero as the Re # goes to zero.

Figure 5.4 shows the impact of velocity and particle size on the diffusion layer thickness when applying the Rowe modification to the Nelson and Galloway approach while assuming a void fraction of 0.25. Increasing the velocity decreases the size of the diffusion layer. However, as the particle radius goes to zero, so too does the Sh # as shown in figure 5.3. This leads to the diffusion layer thickness either staying relatively constant throughout the dissolution process as seen in the predictions at a 25ml/min flow rate or the diffusion layer thickness increasing as the particle is dissolving at flow rates of 6ml/min and 11ml/min flow rates. This is due to the relationship of diffusion layer thickness, Sh #, and particle size given in equation 2. At flow rates of 6ml/min and 11ml/min the Sh # is decreasing faster than the particle size because of the lower Re numbers which leads the diffusion layer thickness to increase as the particle is dissolving. However, for a the faster flow rate (larger Re number) of 25ml/min the particle size and Sh # are decreasing at similar rates which is why there is a fairly constant diffusion layer thickness.

Figure 5.4 also displays the initial diffusion layer thickness necessary to fit the data using an assumption of a critical diffusion layer thickness when applied to the experimental data.

These values were calculated for each dissolution experiment for the different particle sizes and flow rates used. The calculations followed the Wang and Flanagan approach which assumes the diffusion layer thickness is a function of a critical diffusion layer thickness value and the radius of the particle $\frac{1}{h_{eff}} = (\frac{1}{h_{critical}} + \frac{1}{r_p})$. These calculated values for diffusion layer thickness depended on the particle size and the fluid flow rate. The values are in good agreement with the calculations using dimensionless numbers while assuming a void fraction of 0.25. Therefore if an accurate characterization of the particle's velocity and void fraction are known, then the dimensionless numbers approach will provide accurate predictions for the dissolution of drug particles based on physical properties of the dissolution system. However, if these properties of the system are unknown, then there is no benefit to using the dimensionless number approach. In cases with limited knowledge of the system, an average critical diffusion layer thickness approach may be a more practical way to predict particle dissolution.

Figure 5.5 shows the experimental and predicted results for the dissolution of 45µm ibuprofen particles in the USP 4 apparatus at flow rates of 6ml/min, 11ml/min, and 25ml/min. The experimental and predicted results show that as the flow rate is increased, the dissolution rate of the particles increases as well. The experimental data shows a large variation in the results. The predictions do a fairly good job at predicting the data at all of the flow rates. The large variation in the percent dissolved at the low flow rate could be due to the particles not being dispersed well enough which could lead to the particles agglomerating and forming larger particles which take longer to dissolve. The data and predictions correspond well with the Rowe modification to the Nelson and Galloway model assuming a void fraction of 0.25.

Figure 5.6 shows the experimental and predicted results for the dissolution of 111µm ibuprofen particles in the USP 4 apparatus at flow rates of 6ml/min, 11ml/min, and 25ml/min.

The predictions using the Rowe approach do a good job of accurately predicting the dissolution of the particles at all of the flow rates. The 6ml/min flow rate data displays a lot of variation similar to the 45um data and again this could be caused by particles agglomerating which is likely more prevalent at lower flow rates.

Figure 5.7 shows the experimental and predicted results for the dissolution of 235µm ibuprofen particles in the USP 4 apparatus at flow rates of 11ml/min and 25ml/min. The experimental results show a large amount of variation. This could be due to particle agglomeration but also a packing of particles at the top of the cell which corresponds well with the assumption that there is a void fraction of 0.25. The Avicel was insoluble and would accumulate at the top of the cell which made it necessary to incorporate glass wool at the top of the cell before the filter in order to prevent the flow from being disrupted by catching the particles. Therefore the glass wool and the suspension particles could be two sources of the low void fraction that is being seen.

Figures 5.8-5.10 show the dissolution results of the three different sieve cuts in the USP 2 apparatus in the same dissolution medium composition as the USP 4 apparatus dissolution work but in 900ml of fluid. The paddle was stirred at a rate of 50RPM. The dissolution results show very little variation between dissolution runs unlike the USP 4 apparatus dissolution work. Also the results are compared to the dissolution data in the USP 4 apparatus at 11ml/min and the dissolution profiles are very similar for each of the three different sieve cuts.

Discussion

The USP 4 data shows that particle dissolution is a function of particle size and fluid velocity. This relationship can be accurately approximated using dimensionless numbers but it does not conform to an infinite dilution approach of Ranz and Marshall. This leads to the

application of the Rowe modification to the Nelson and Galloway model which applies to particles in packed or fluidized beds. When it was assumed that there was a void fraction of 0.25, the predictions were able to accurately account for the experimental data. The presence of a void fraction is most likely due the particles being localized to a small area in the USP 4 cells, the presence of glass wool, and the large number of Avicel particles that are insoluble in the dissolution media.

This adjusted equation to calculate the experimental Sh # is consistent with other mass transfer data at low Re #'s in a packed bed and it does a accurate job of fitting all of the USP 4 dissolution data presented [1,2,45]. However, applying this approach a priori adds the complexity of estimating the void fraction to solve for the dissolution of particles in the USP 4 apparatus. This approach cannot be accurately applied to the USP 4 apparatus without being able to estimate or calculate the void fraction that the particles are encountering in the USP 4 system before the experiment is undertaken. Therefore this is not an ideal experimental system and would require more experimental work to determine an approach to quantify the fluid velocity and void fraction. This approach could be applied to more data with glass wool to evaluate its robustness. Also, studies could be done on a low dose suspension without insoluble excipients to determine if the results conform to the Ranz and Marshall approach for predicting the mass transfer of drug particles.

When comparing dissolution in the USP 2 apparatus at 50 RPM to dissolution in the USP 4 apparatus at an 11ml/min flow rate with a low void fraction, there is little difference observed in the dissolution profiles. The particles in the USP 2 apparatus settled to the bottom of the vessel, where there is limited fluid flow, for the majority of the dissolution runs. Therefore the hydrodynamics experienced by the ibuprofen particles in the USP 4 apparatus experiments and at

the bottom of the USP 2 apparatus are similar. This suggests that there may be little benefit to using the USP 4 apparatus when there is a large dose of drug or large amount of insoluble excipient in an effort to obtain a better simulation of in vivo fluid velocities. However, this would depend on the density of the drug and the dosage form used. If the drug particles stay suspended in the bulk solution and do not settle to the bottom of the apparatus, the dissolution would be expected to occur much quicker in the USP 2 apparatus. Also, if a low dose suspension was formed that only contained well dispersed solid drug particles, the dissolution in the USP 4 apparatus should conform to the Ranz and Marshall model. This would predict slower dissolution than the model proposed in this chapter and the dissolution would likely be slower than the dissolution of the particles that settled to the bottom of the USP 2 apparatus (see figure 5.2).

Conclusions

The USP 4 apparatus offers a more well-defined fluid velocity profile that is in the range of what is physiologically relevant and allows for accurate predictions to be made. However, there is significant experimental variation caused by possible particle agglomeration or particles forming a packed or fluidized bed at the top of the cell. Additionally for accurate predictions to be made, an accurate estimate for void fraction in the USP 4 cell must be made because of the large impact it can have on the dissolution data. The Avicel particles in the suspension were insoluble in the dissolution media and therefore were present in the USP 4 cells throughout the dissolution runs. The drug and Avicel particles were pushed by the fluid flow to the top of the cell where glass wool was placed to prevent the particles from impeding flow. These two factors and the dissolution data suggest that there was a significant decrease in the porosity around the

solid particles which leads to a low void fraction of 0.25 being an accurate assessment of the experimental conditions.

The experimental and predicted data shows that fluid velocity has a signficant impact on dissolution (and diffusion layer thickness). However, more work is needed to assess how effectively this model can be applied to other dosage forms and particles with different densities and solubilities. The major problem with using the dimensionless number approach for predicting dissolution in the USP 4 apparatus is the presence of too many unknown experimental variables in the USP 4 cells to accurately describe the conditions the drug particles are experiencing as they dissolve. Depending on the dosage form and location of the particles in the USP 4 cells, it is difficult to accurately assess the void fraction in the apparatus and how the particle surface area and velocity is being affected. The dimensionless number approach a priori will not be accurate unless these parameters are known with relative accuracy before the dissolution test is performed.

The dissolution profiles in the USP 2 apparatus were very similar to the dissolution profiles in the USP 4 apparatus at an 11ml/min flow rate and the results were much less variable. This illustrates that although the fluid velocity can be much greater and highly variable in the bulk fluid of the USP 2 apparatus, the actual velocities that the drug particle experiences when it is dissolving is not much different than that seen in the USP 4 apparatus in conditions of packed or fluidized beds. This is likely due to the particles settling at the bottom of the USP 2 apparatus shortly after being introduced into the system. Bai et al. showed that computational fluid dynamic (CFD) predictions of velocity at the bottom of the USP 2 vessel are < 1cm/s which is much less than what the particles would experience in the bulk solution. Therefore if the particles settle to the bottom of the vessel fast enough, the velocities they will experience during

dissolution are similar to what a particle may experience in the USP 4 apparatus when the particles encounter conditions of packed or fluidized beds.

Figures

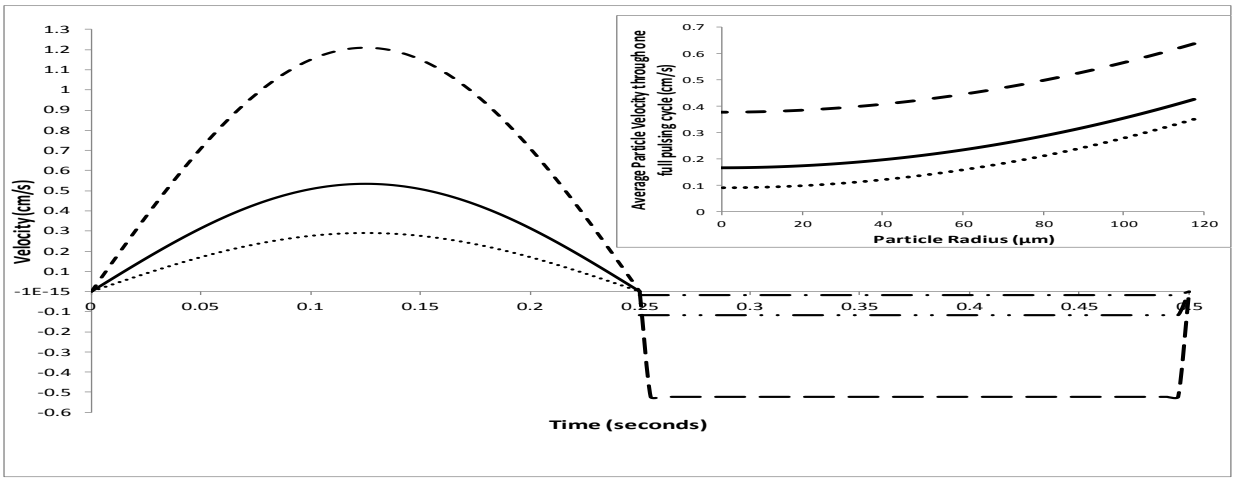

Figure 5. 1. The calculated velocity profiles for the different experimental flow rates and pparticle sizes. Key (⋯⋯) Calculated velocity profile for a flow rate of 6ml/min; (——) Calculated velocity profile for a flow rate of 11ml/min; (– –) Calculated velocity prfile for a flow rate of 25 ml/min; (— —) Calculated settling velocity for a 235μm particle; (— · ·) Calculated settling velocity for a 111μm particle; (— ·) Calculated settling velocity for a 45μm particle;

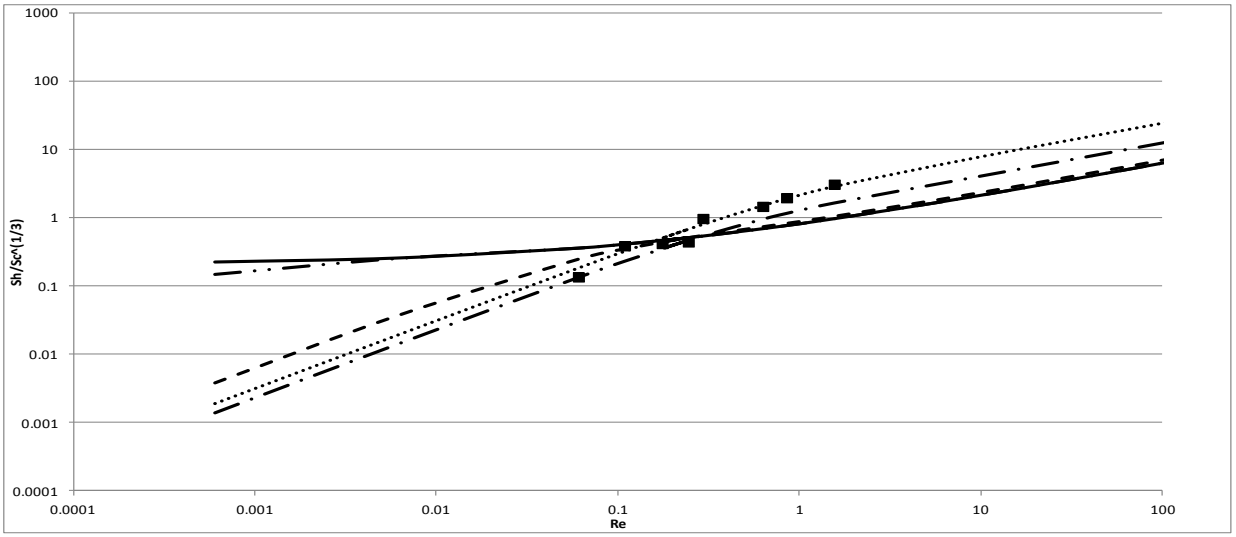

Figure 5. 2. Calculated $Sh/Sc^{1/3}$ based on the Nelson and Galloway approach with the Rowe modification at different void fractions and the experimental $Sh/Sc^{1/3}$ and as a function of Re #. Key (——) Calculated Sh #'s based on the Ranz and Marshall ; (— · ·) Calculated Sh #'s with void fraction = 0.999 ; (– –) Calculated Sh #'s void fraction = 0.90; (— ·) Calculated Sh #'s void fraction = 0.50; (⋯⋯) Calculated Sh #'s void fraction = 0.25;

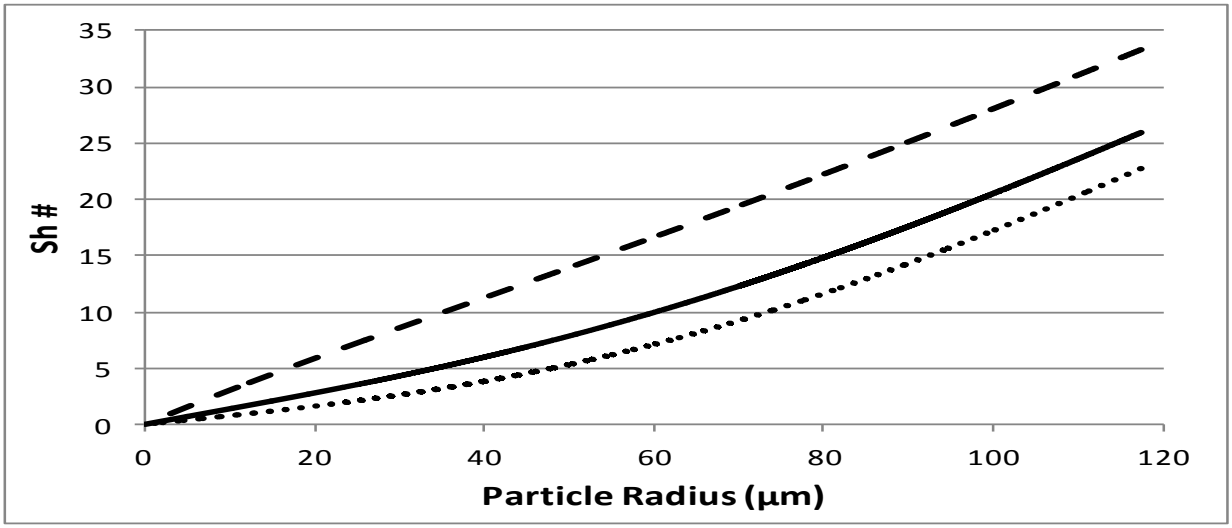

Figure 5. 3. Calculated Sh #'s based on the best fit data and as a function of particle size and flow rate. Key (·····) Calculated Sh #'s for a flow rate of 6ml/min; (——) Calculated Sh #'s for a flow rate of 11ml/min; (– –) Calculated Sh #'s for a flow rate of 25 ml/min;

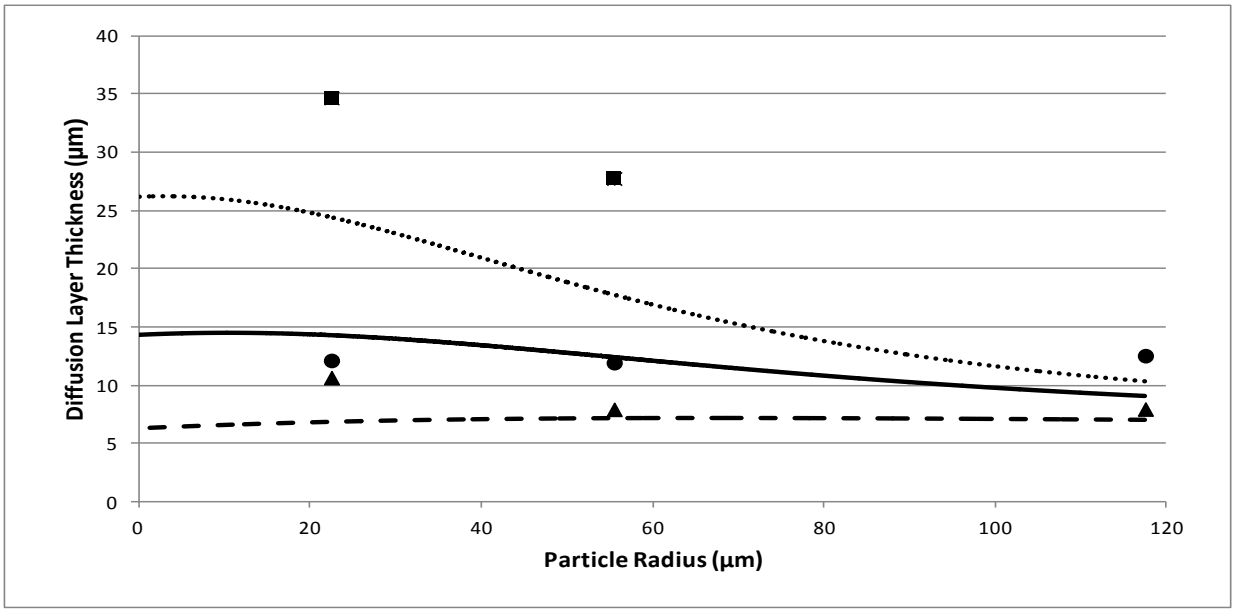

Figure 5. 4. Predictions for diffusion layer thickness using the best fit Sh# based on the dissolution data. Key (·····) predictions for diffusion layer thickness at flow rate of 6ml/min; (——) predictions for diffusion layer thickness at flow rate of 11ml/min; (– –) predictions for diffusion layer thickness at flow rate of 25ml/min; (■) calculated diffusion layer for the particle sizes tested at a flow rate of 6 ml/min; (●) calculated diffusion layer for particle sizes tested at a flow rate of 11 ml/min; (▲) calculated diffusion layer for particle sizes tested at a flow rate of 25 ml/min;

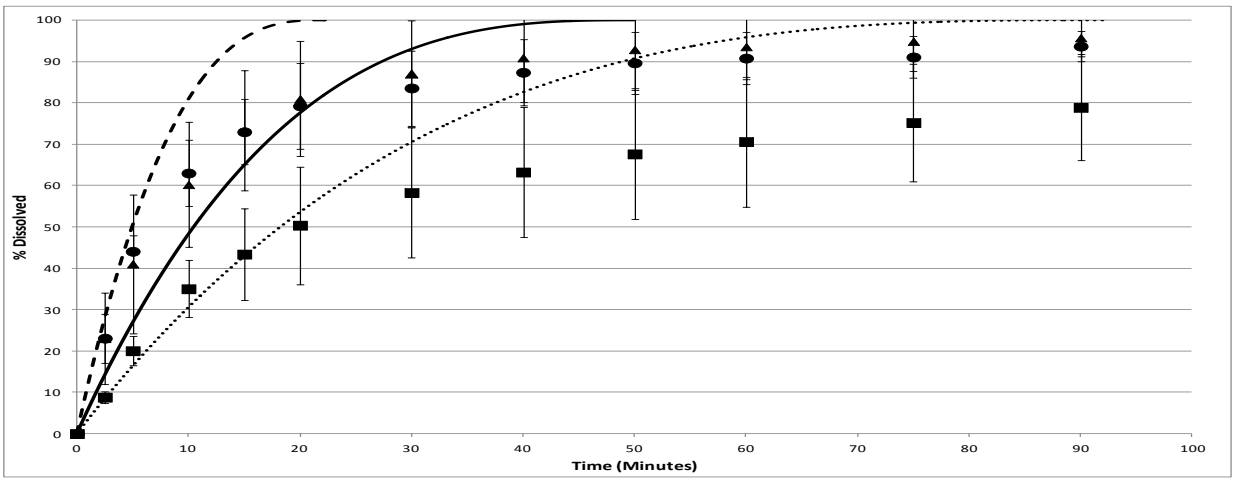

Figure 5. 5. USP 4 dissolution results of 45µm ibuprofen particles in 50mM Acetate buffer at pH 4.5 and at 37°C. Key (■) experimental dissolution at a flow rate of 6ml/min; (●) experimental dissolution at a flow rate of 11ml/min; (▲) experimental dissolution at a flow rate of 25ml/min; (·····) predicted dissolution at 6ml/min; (——) predicted dissolution at 11ml/min; (– –) predicted dissolution at 25ml/min;

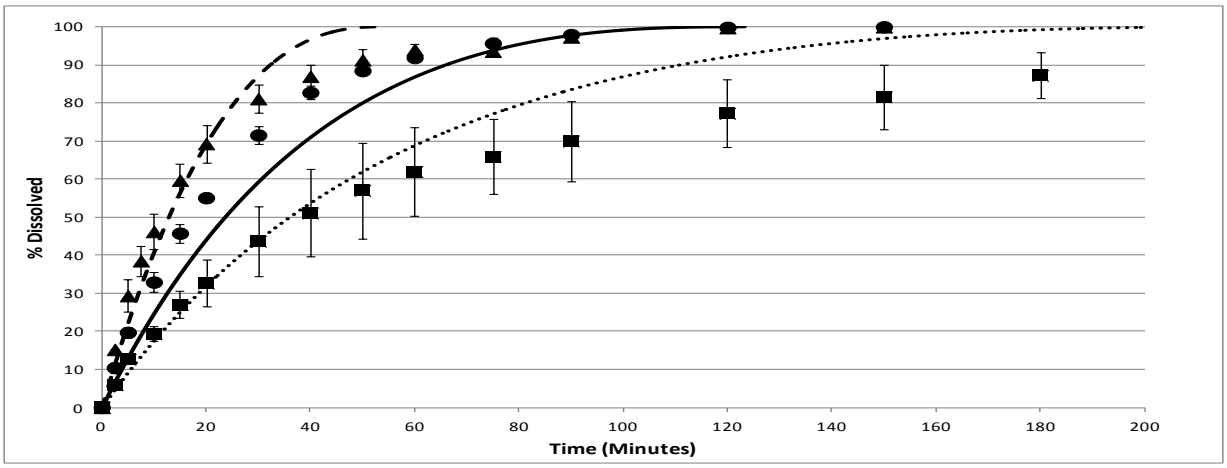

Figure 5. 6. USP 4 dissolution results of 111µm ibuprofen particles in 50mM Acetate buffer at pH 4.5 and at 37°C. Key (■) experimental dissolution at a flow rate of 6ml/min; (●) experimental dissolution at a flow rate of 11ml/min; (▲) experimental dissolution at a flow rate of 25ml/min; (·····) predicted dissolution at 6ml/min; (——) predicted dissolution at 11ml/min; (– –) predicted dissolution at 25ml/min;

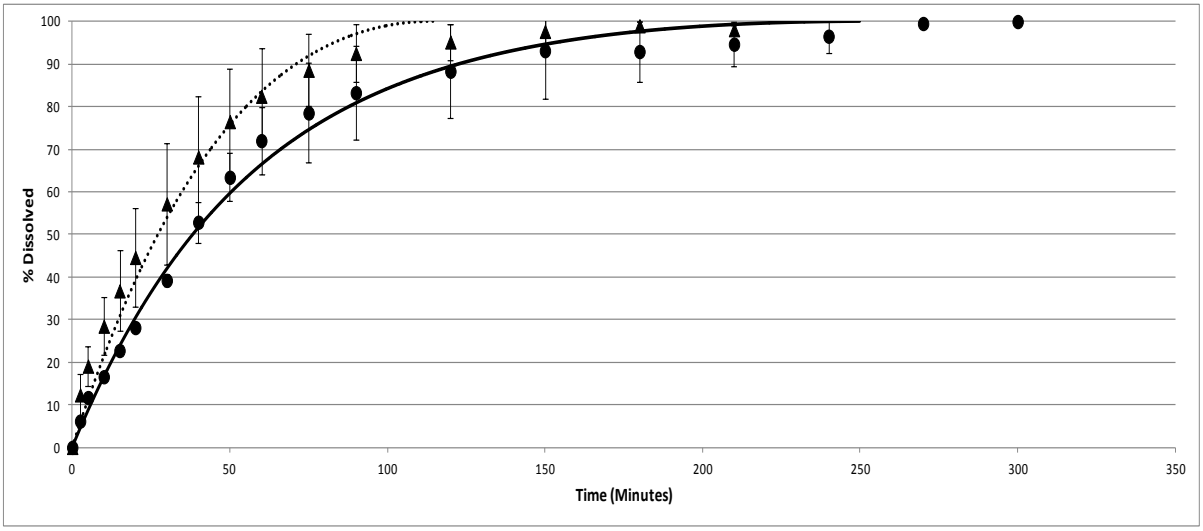

Figure 5. 7. USP 4 dissolution results of 235µm ibuprofen particles in 50mM Acetate buffer at pH 4.5 and at 37°C. Key (■) experimental dissolution at a flow rate of 6ml/min; (●) experimental dissolution at a flow rate of 11ml/min; (▲) experimental dissolution at a flow rate of 25ml/min; (·····) predicted dissolution at 6ml/min; (——) predicted dissolution at 11ml/min; (– –) predicted dissolution at 25ml/min;

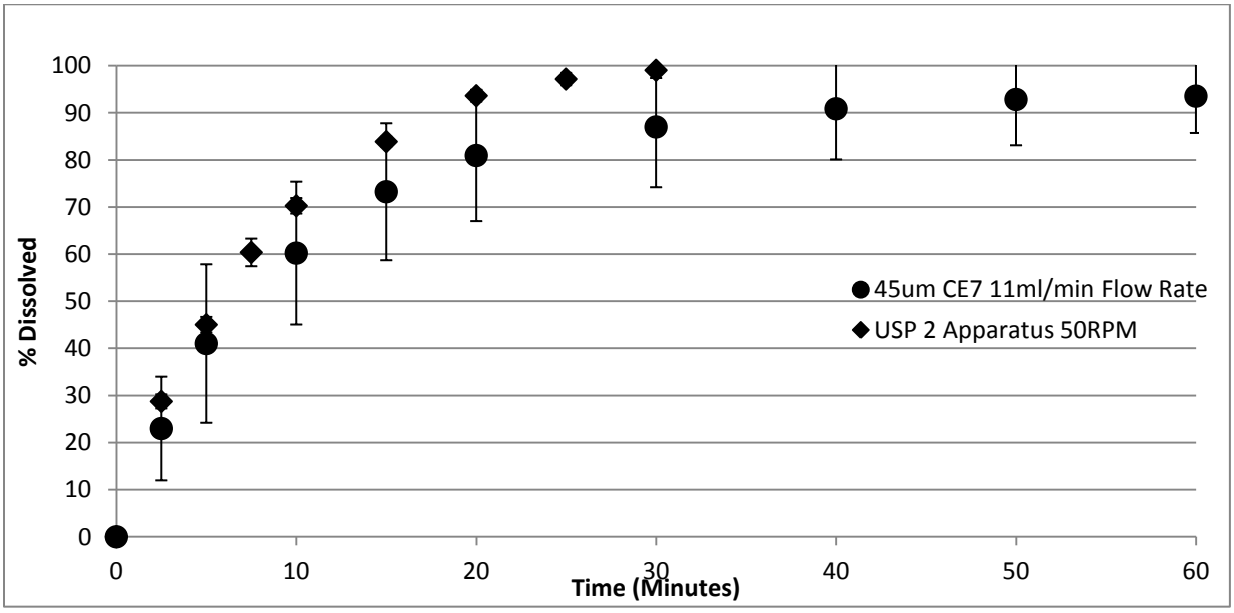

Figure 5. 8. USP 4 and USP2 dissolution results of 45µm ibuprofen particles in 50mM Acetate buffer at pH 4.5 and at 37°C. Key (●) experimental dissolution in the USP 4 apparatus at a flow rate of 11ml/min; (◆) experimental dissolution in the USP 2 apparatus

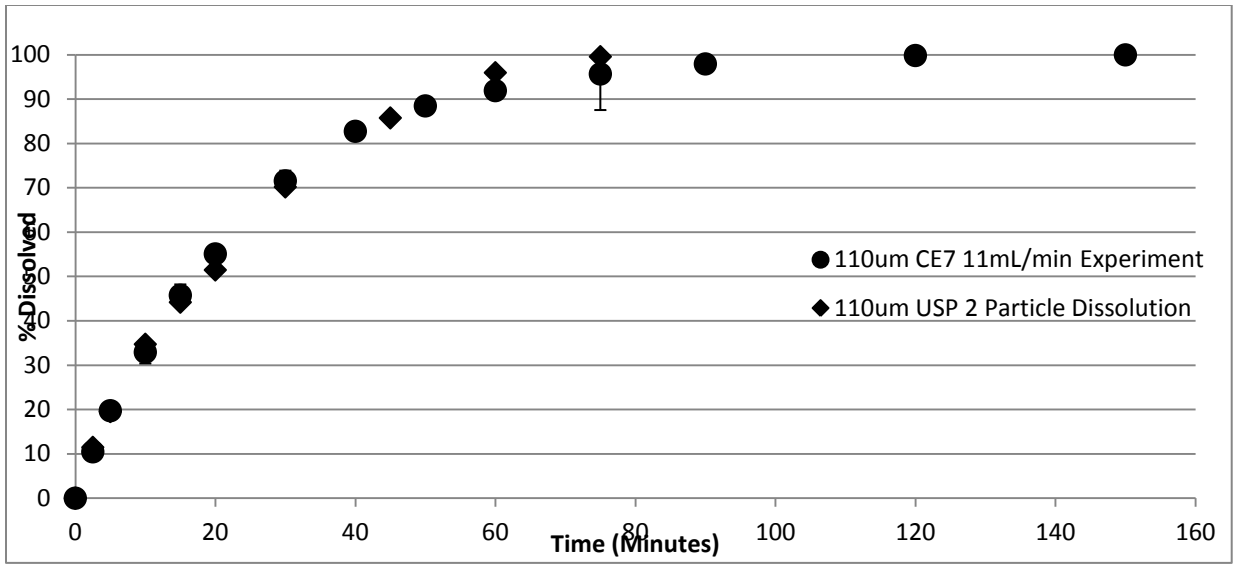

Figure 5. 9. USP 4 and USP2 dissolution results of 111µm ibuprofen particles in 50mM Acetate buffer at pH 4.5 and at 37°C. Key (●) experimental dissolution in the USP 4 apparatus at a flow rate of 11ml/min; (◆) experimental dissolution in the USP 2 apparatus.

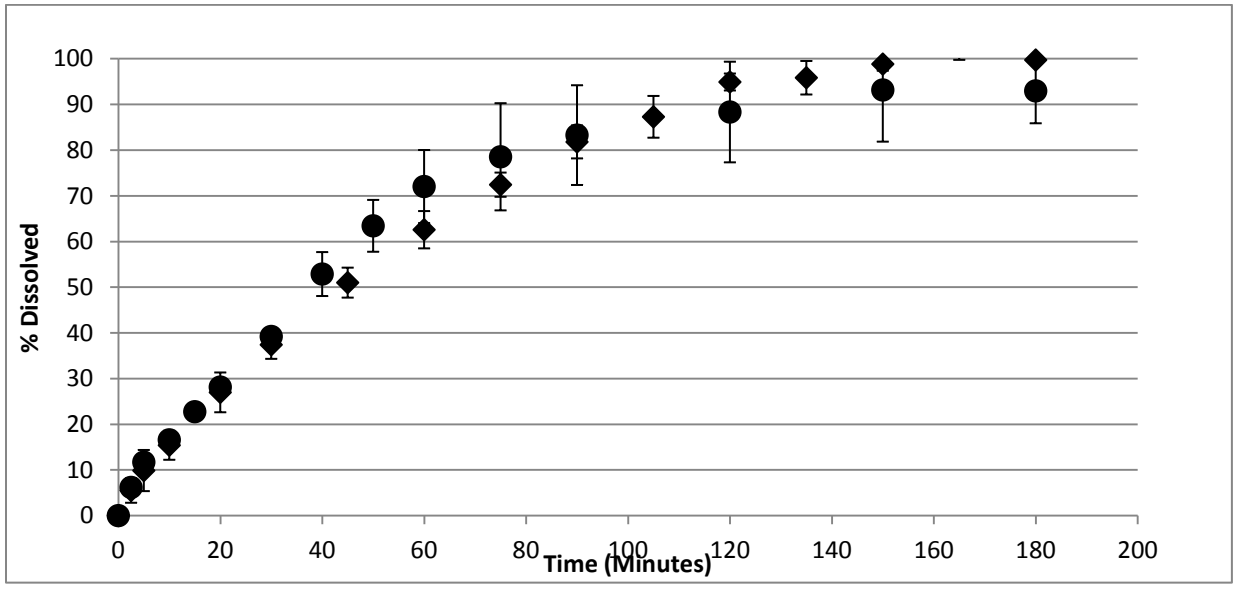

Figure 5. 10. USP 4 and USP2 dissolution results of 235µm ibuprofen particles in 50mM Acetate buffer at pH 4.5 and at 37°C. Key (●) experimental dissolution in the USP 4 apparatus at a flow rate of 11ml/min; (◆) experimental dissolution in the USP 2 apparatus

References

1. A NP, R GT 1975. Particle-To-Fluid Heat and Mass Transfer in Dense Systems of Fine Particles. Chemical Engineering Science 30:1-6.
2. Rowe PN 1975. Particle-To-Liquid Mass Transfer in Fluidised Beds. Chemical Engineering Sciences 30:7-9.
3. Wu Y, Ghaly ES 2006. Effect of Hydrodynamic Environment on Tablet Dissolution Using the Flow-Through Dissolution Apparatus. Pharmacology 25(1):75-83.
4. Carstensen JT, Lai Yu-Fun T, Prasad VK 1978. USP Dissolution IV: Comparison of Methods. Journal of Pharmaceutical Sciences 67(9):1303-1307.
5. Brown W 2005. Apparatus 4 Flow Through Cell: Some Thoughts on Operational Characteristics. Dissolution Technologies:28-30.
6. Yu LX, Wang JT, Hussain AS 2002. Evaluation of USP Apparatus 3 for Dissolution Testing of Immediate-Release Products. Aaps Pharmsci 4(1):1-5.
7. D'Arcy DM, Corrigan OI, Healy AM 2006. Evaluation of Hydrodynamics in the Basket Dissolution Apparatus Using Computational Fluid Dynamics-Dissolution Rate Implications. European Journal of Pharmaceutical Sciences 27:259-267.
8. Bai G, Wang Y, Armenante PM 2011. Velocity Profiles and Shear Strain Rate Variability in the USP Dissolution Testing Apparatus 2 at Different Impeller Agitation Speeds. International Journal of Pharmaceutics 403:1-14.
9. Kukura J, Baxter JL, Muzzio FJ 2004. Shear distribution and variability in the USP Apparatus 2 under turbulent conditions. International Journal of Pharmaceutics 279(1-2):9-17.
10. Ameur H, M B 2013. 3D hydrodynamics and shear rates' variability in the United States Pharmacopeia Paddle Dissolution Apparatus. International Journal of Pharmaceutics 452:42-51.
11. McCarthy LG, Kosiol C, Healy AM, Bradley G, Sexton JC, Corrigan OI 2003. Simulating the Hydrodynamic Conditions in the United States Pharmacopeia Paddle Dissolution Apparatus. AAPS PharmSciTech 4(22):1-16.
12. Pal A, Indireshkumar K, Schwizer W, Abrahamsson B, Fried M, Brasseur JG 2004. Gastric flow and mixing studied using computer simulation. Proceedings of the Royal Society B: Biological Sciences 271(1557):2587-2594.
13. Gutzeit A, Patak MA, Weymarn Cv, Graf N, Doert A, Willemse E, Binkert CA, Froehlich JM 2010. Feasibility of Small Bowel Flow Rate Measurement With MRI. Journal of Magnetic Resonance Imaging 32:345-351.
14. Diebold SM. 2005. Chapter 6. Physiological Parameters Relevant to Dissolution Testing: Hydrodynamic Considerations. Pharmaceutical Dissolution Testing, ed.
15. Katori N, Aoyagi N, Terao T 1995. Estimation of agitation intensity in the GI tract in humands and dogs based on in vitro/in vivo correlation. Pharm Res 12(2):237.
16. D'Arcy DM, Liu B, Bradley G, Healy AM, Corrigan OI 2010. Hydrodynamic and Species Transfer Simulations in the USP 4 Dissolution Apparatus: Considerations for Dissolution in a Low Velocity Pulsing Flow. Pharmaceutical Research 27(2):246-258.
17. Shiko G, Gladden LF, Sederman AJ, Connolly PC, Butler JM 2011. MRI Studies of the Hydrodynamics in a USP 4 Dissolution Testing Cell. Journal of Pharmaceutical Sciences 100(3):976-991.

18. D'Arcy DM, Liu B, Corrigan OI 2011. Investigating the effect of solubility and density gradients on local hydrodynamics and drug dissolution in the USP 4 dissolution apparatus. International Journal of Pharmaceutics 419:175-185.
19. Kakhi M 2009. Mathematical modeling of the fluid dynamics in the flow-through cell. International Journal of Pharmaceutics 376(1-2):22-40.
20. D'Arcy DM, Persoons T 2010. Mechanistic Modelling and Mechanistic Monitoring: Simulation and Shadowgraph Imaging of Particulate Dissolution in the Flow-Through Apparatus. Journal of Pharmaceutical Sciences 100(3):1102-1115.
21. Mirza T, Joshi Y, Liu Q, Vivilecchia R 2005. Evaluation of Dissolution Hydrodynamics in the USP, Peak™ and Flat-Bottom Vessels Using Different Solubility Drugs. Dissolution Technologies:11-16.
22. Cammarn SR, Sakr A 2000. Predicting dissolution via hydrodynamics: salicylic acid tablets in flow-through cell dissolution. International Journal of pharmaceutics 201:199-209.
23. Morihara M, Aoyagi N, Kaniwa N, Katori N, Kojim S 2002. Hydrodynamic Flows Around Tablets in Different Pharmacopeial Dissolution Tests. Drug Development & Industrial Pharmacy 28(6):665-662.
24. Sheng JJ, Sirois PJ, Dressman JB, Amidon GL 2008. Particle Diffusional Layer Thickness in a USP Dissolution Apparatus II: A Combined Function of Particle Size and Paddle Speed. Journal of Pharmaceutical Sciences 97(11):4815-4829.
25. Higuchi WI, Hiestand EN 1963. Dissolution rates of finely divided drug powders I. Effect of a distribution of particle sizes in a diffusion-controlled process. J Pharm Sci 52:67-71.
26. Hintz RJ, Johnson KC 1989. The effect of particle size distribution on dissolution rate and oral absorption. International Journal of Pharmaceutics 51:9-17.
27. Wang J, Flanagan DR 1999. General Solution for Diffusion-Controlled Dissolution of Spherical Particles 1. Theory. J Pharm Sci 88(7):731 - 738.
28. Niebergall PJ, Milosovich G, Goyan JE 1963. Dissolution Rate Studies II: Dissolution of Particles Under Conditions of Rapid Agitation. J Pharm Sci 52(3):236 - 241.
29. Lu ATK, Frisella ME, Johnson KC 1993. Dissolution Modeling: Factors Affecting the Dissolution Rates of Polydisperse Powders. Pharmaceutical Research 10(9):1308-1314.
30. Sugano K 2008. Theoretical comparison of hydrodynamic diffusion layer models used for dissolution simulation in drug discovery and development. International Journal of Pharmaceutics 363(1-2):73-77.
31. D'Arcy DM, Liu B, Persoons T, Corrigan OI 2011. Hydrodynamic Complexity Induced by the Pulsing Flow Field in USP Dissolution Apparatus 4. Dissolution Technologies:6-13.
32. Ranz WE, Marshall WR 1952. Evaporation From Drops: Part II. Chemical Engineering Progress 48(4):173 - 180.
33. Garner FH, Grafton RW 1954. Mass Transfer in Fluid Flow from a Solid Sphere. Proceedings of the Royal Society of London Series A, mathematical and Physical Sciences 224(1156):64-82.
34. Garner FH, Keey RB 1958. Mass-Transfer from Single Solid Spheres-1 Transfer at Low Reynolds Numbers. Chemical Engineering Science 9:119-129.
35. Garner FH, Suckling RD 1958. Mass Transfer from a Soluble Solid Sphere. AIChE Journal 4(1):114-124.
36. Steinberger RL, Treybal RE 1960. Mass Transfer From a Solid Soluble Sphere to a Flowing Liquid Stream. AIChE Journal 6(2):227-232.
37. Harriot P 1962. Mass Transfer to Particles: Part 1. Suspended in Agitated Tanks. AIChE Journal 8(1):93-101.
38. Linton M, Sutherland KL 1960. Transfer from a sphere into a fluid in laminar flow. Chemical engineering Science 12:214-229.
39. Frossling N 1938. The Evaporation of falling drops. Gerlands Beitrage zur Geophysik 52:213-220.

40. Kumar S, Upadhyay SN, Mathur VK 1977. Low Reynolds Number Mass Transfer in Packed Beds of Cylindrical Particles. Ind Eng Chem, Process Des Dev 16(1-8).
41. Abrahamsson B, Pal A, Sjoeberg M, Carlsson M, Brasseur JG 2005. A novel in vitro and numerical analysis of shear-induced drug release from extended-release tablets in the fed stomach. Pharmaceutical research 22(8):1215.
42. Brian PLT, Hales HB 1969. Effects of Transpiration and Changing Diameter on Heat and Mass Transfer to Spheres. AlChE 15(3):419-425.
43. Rexwinkle G, Heesink ABM, Van Swaaij WPM 1997. Mass Transfer in packed beds at low Peclet number - wrong experiments or wrong interpretations? Chemical Engineering Science 52(21 22):3995-4003.
44. Derksen JJ 2014. Simulations of Solid-Liquid Scalar Transfer for a Spherical Particle in Laminar and Turbulent Flow. AlChE 60(3):1202-1215.
45. Koloini T, Sopcic M, Zumer M 1977. Mass Transfer in Liquid-Fluidized Beds at Low Reynolds Numbers. Chemical Engineering Science 32:637-641.

Chapter 6

The Impact of *In Vivo* Relevant Fluid Velocity on *In vitro* HPMC Tablet Erosion and *In Vitro – In Vivo* Correlation

Abstract

The hydrodynamics and fluid velocity experienced by an eroding hydroxypropyl methylcellulose (HPMC) extended release tablet can have a significant effect on the rate at which the tablet erodes. An *in vitro* test that accurately simulates the *in vivo* environment should be a better predictor of *in vivo* erosion rate and drug release. The USP 4 apparatus was chosen to evaluate the impact of using an *in vivo* relevant velocity on tablet erosion and to assess its effectiveness in developing an *in vitro/in vivo* correlation. In this work the tablet erosion rates were measured in the USP 4 apparatus and were compared to the erosion rates of the same HPMC tablet formulations that were determined by Jain et al. in humans and using the USP 2 apparatus[1].

The tablet erosion studies done in the USP 4 apparatus utilized the 22.6mm flow through cell at a 25ml/min flow rate (0.1 cm/s velocity). The *in vivo* erosion rate measured in humans by Jain et al. was significantly greater compared to the *in vitro* erosion rate using the USP 4 apparatus. The erosion rate of the tablets in the USP 4 apparatus was also significantly less than the erosion rates observed using the USP 2 apparatus (50RPM ~ 10cm/s velocity).

The erosion rate data in the USP 2 apparatus provided a better correlation for the erosion rate data *in vivo*. Therefore, it appears that, while the USP 4 apparatus does provide a more well-defined erosion environment, it may not incorporate all of the physiological parameters that may

impact tablet erosion to provide a good IVIVC. To develop an *in vitro* erosion test that can provide meaningful insight into the *in vivo* erosion process, additional physiological parameters that impact erosion may need to be considered.

Introduction

Hydroxypropyl methylcellulose (HPMC) formulations have been widely studied to observe their controlled release behavior and to understand how the different formulations erode under different hydrodynamic conditions, in different dissolution apparatus, and in different media[2-7]. All of these parameters can contribute significantly to the erosion rate of the HPMC tablet formulation. Additionally, the formulation of HPMC and the excipients chosen can have a large impact on tablet erosion[7,8].

The erosion medium will not be a major focus in this study but the composition of the medium can have an impact on the erosion rate but this is a function of the HMPC form being studied[2,4,6]. The ionic strength and the concentration of surfactants are the two erosion medium parameters that have the most significant impact on HPMC tablet erosion[2,4,6,9]. However, the pH of the solution can also have an effect if there are wide variations in pH being studied. This would be most noticeable when analyzing erosion in simulated gastric fluid compared to simulated intestinal fluid [4-6].

The main focus of this study will be the *in vitro* hydrodynamic impact on the erosion of HPMC tablets and if making the conditions more *in vivo* relevant in terms of fluid velocity will offer a better *in vitro/in vivo* correlation. Adjusting the agitation rate or the RPM of the different dissolution apparatus can have a large effect on tablet erosion. Increasing the agitation rate will increase the erosion rate for HPMC tablets[10-12]. Also, the hydrodynamics of different dissolution methods have been shown to have a significant impact on the erosion process and the erosion

rate[10-15]. Therefore employing different dissolution methodologies that apply different hydrodynamic stresses on the tablet can lead to a wide variation in tablet erosion results. This makes it necessary to have all of the experimental parameters be relevant based on *in vivo* conditions when performing an erosion study on tablets made with different HPMC formulations to provide a meaningful IVIVC.

In vitro erosion studies have been done to develop an IVIVC using both the USP 2 and the USP 3 apparatus[1,3,12,16,17]. This has typically been done by examining the *in vitro* percent drug dissolved and the *in vivo* plasma concentration[12,16,17]. These correlations between the *in vitro* and *in vivo* parameters were typically done by using a Levy plot to display how the *in vitro* percent dissolved correlates to the fraction of the drug absorbed *in vivo*[12,17]. However, work has also been done to specifically correlate the *in vitro* and *in vivo* erosion rates [1,3]. This *in vitro* work typically involves the USP 2 apparatus and a marker (charcoal or magnetic moment) whose change is correlated to the *in vitro* erosion and this change in the marker is measured *in vivo*. The correlations between *in vitro* and *in vivo* tablet erosion following this method are the best when the polymer concentration is above the percolation threshold. However, these studies gave no consideration to the hydrodynamics and fluid velocity in the *in vitro* studies to correlate with the same parameters *in vivo*.

The goal of this study was to measure the erosion rate of the HPMC controlled release tablets using the USP 4 apparatus at an average velocity of 0.1cm/s in the USP 4 cell. This fluid velocity is what the tablets would likely encounter throughout the erosion process in the small intestine[18,19]. These *in vitro* erosion rates would then be compared to the *in vivo* small intestine erosion rates in humans that were observed for the same formulations by Jain et al. Additionally the erosion rate using the USP 4 apparatus was compared to the erosion rate using the USP 2

apparatus based on the work of Jain et al. The impact velocity has on the erosion of different HMPC tablet formulations and how much it contributes to the *in vivo* erosion rate will be presented and discussed. This study will help to assess the use of the USP 4 apparatus as an evaluation tool for *in vivo* erosion rates in humans.

Materials and Methods

HPMC Tablets were made using four different formulations that were used as supplied from AstraZeneca. The components for the four different formulations and their %w/w are given in table 6.1 which was reproduced from Jain et al. 2014.

The tablets were made by weighing 350mg of the powder for each of the different formulations and using direct compression via a carver tablet press and a 1cm diameter convex punch and die. A compression pressure of 170 MPa was applied for 30 seconds and then the pressure was slowly released over 30 seconds. The tablet thickness and weight was recorded. The tablet thickness ranged from 3.65mm to 3.90mm which is similar to the tablet thickness of 3.7mm measured by Jain et al for the same tablet formulations.

To ensure that the tablets were similar to those made by Jain et al., the tablet hardness was measured for each formulation. This was done by placing the tablets in a tablet hardness tester (Schleunger Tablet Tester 6D)to measure the breaking force of the tablets. The tablet hardness ranged from 61Nto107N and is in the range of reported values by Jain et al.

The tablet erosion study was performed using the Sotax CE7 USP 4 dissolution apparatus. The 22.6 mm cells were used with the 5mm red bead at the bottom of cell and filled with 1mm glass beads to have laminar flow throughout the cell. The tablets were placed with the long axis horizontally on the tablet holder. The erosion medium used was 500ml of pH 6.8 50mM phosphate buffer that was made isotonic with NaCl. A closed system was used so the

erosion medium was pumped into the cells and pumped back into the same bulk solution. Each USP 4 cell had its own bulk solution that was pumped into the cell and recycled back. The flow rate used for the experiments was 25ml/min. Experiments were done in duplicate for each tablet formulation at each time point.

The tablets were taken out at a specific time point and placed in a 9 well glass pyrex dish which was then placed in an oven (VWR BIO model) at 85^{o}C for at least 48 hours. The dried tablets were then weighed to calculate the percent weight loss that occurred. Whole tablets of each formulation that were not eroded were dried in the same way to determine the percent water that was contained in each formulation to account for the percentage of water in the tablet.

Results

Figure 6.1 shows the erosion data in the USP 4 apparatus. The data displays the same rank order erosion that was observed in the *in vitro* USP 2 study and the *in vivo* study by Jain et al. This also correlates well with past work based on the percent of the HPMC's in each of the formulations. Figure 6.1 also shows that the USP 4 erosion results display a linear increase over the duration of the study which was similar to the USP 2 erosion data by Jain et al. There was only minor variation in the percent erosion between each of the tablets at each time point.
The erosion rates throughout the duration of the experiment are shown in figure 6.2. Figure 6.2 also shows there was minor variation in the erosion rate over the entire timeframe of the experiment. Therefore even as the tablet swells in the USP 4 apparatus, which would cause a change in the velocity profile around the tablet due to the area available for fluid flow, there is little impact on the erosion rate for the tablet.

Figure 6.3 shows the impact of *in vitro* hydrodynamics by comparing the erosion rate data from the USP 4 apparatus to the USP 2 apparatus. The same buffer concentration and pH

was used for each erosion study. However, the ionic strength was made to be isotonic in the USP 4 test while the USP 2 erosion tests were done at an ionic strength that was based exclusively on 50mM phosphate buffer at pH 6.8. This difference could impact the data by slightly increasing the USP 4 erosion rates based on past work that examined the impact of ionic strength on tablet erosion[4,6]. This was also confirmed by preliminary work that replicated the USP 2 erosion work of Jain et al. that compared erosion in both isotonic and non-isotonic 50Mm phosphate buffer at pH 6.8. However, the major difference in these studies was the hydrodynamics in the USP 2 apparatus and the USP 4 apparatus. Comparing the erosion rates in the USP 4 apparatus to the erosion rates the in the USP 2 apparatus shows the erosion rate is around 3.5-4.5 times greater in the USP 2 apparatus than in the USP 4 apparatus. The greatest difference in erosion rates was seen for formulation 1 which contains the largest amount of methocel K4M. The smallest difference was seen for formulation 4 which contains the smallest percentage of HPMC and the faster eroding HPMC form K100LV.

Figure 6.4 compares the *in vitro* erosion rate using a physiologically relevant velocity in the USP 4 apparatus to the *in vivo* erosion rate data in the small intestine of humans. The erosion rate was much more variable in vivo but the mean erosion rate values were significantly higher than the USP 4 *in vitro* erosion rate. The *in vivo* erosion rates were 2-4.5 times greater than the *in vitro* erosion rates in the USP 4 apparatus. Again, formulation 1 showed the largest difference in erosion rates and formulation 4 showed the smallest difference.

Discussion

The impact of hydrodynamics on extended release polymer tablet erosion is significant when comparing the erosion data in the USP 4 apparatus to that of the USP 2 apparatus. Thus identifying the correct hydrodynamic environment an extended release tablet would see *in vivo* is

a key component for developing an accurate IVIVC for tablet erosion. The experimental data suggests that this is more significant in the case of slower eroding HPMC forms such as methocel K4M. The velocity chosen for the USP 4 experiment was 0.1 cm/s which is in the range of what the extended release tablet could expect to encounter in the small intestine of humans. However, the *in vivo* erosion was much faster than the *in vitro* erosion in the USP 4 apparatus. Therefore even though the velocity the tablet experiences is an important component of hydrodynamics it is not the only one that is involved in the tablet erosion *in vivo*. The shear rate is a very important hydrodynamic component that is not likely to be similar to in vivo conditions. The tablet is held in place by a tablet holder throughout the duration of the experiment and this setup would likely not account for the differences in shear the tablet would experience as it is traveling through the intestinal tract.

In addition to the hydrodynamics of the in vitro study not characterizing the *in vivo* environment, there are other factors that could limit the IVIVC based on the methods used. One of these factors could be the erosion medium used during the in vitro test. The erosion rate could be significantly increased in the USP 4 apparatus by adding more salt to the buffer solution or bile acids. However, this would still have to be done within the limits of physiologically relevant *in vivo* fluid of the gastrointestinal tract. Another possible parameter that cannot be taken into account in the USP 4 experiment is the sloughing off of the wetted tablet as it is traveling through the gastrointestinal tract and coming into contact with the wall of the intestine. Once the polymer tablet begins to swell in the erosion medium, it is easy for the outer portion of the tablet to rub off when it comes into contact with another object. This mechanism for release could possibly be observed using the USP 3 apparatus since the tablet would continually be coming into contact with the top and bottom mesh of the apparatus.

Conclusion:

The data shows that matching the *in vitro* velocities to the *in vivo* velocities in the intestinal tract is not enough to accurately correlate the *in vitro* erosion rate data to the *in vivo* erosion rate data in humans. This is likely due to the many other factors than can impact tablet erosion that were not simulated in the USP 4 *in vitro* study. The *in vitro* study did not account for parameter such as *in vivo* relevant media, *in vivo* shear rates, and the rubbing off of the tablet against the intestinal wall.

The bulk velocity (~10cm/s) the tablets saw in the USP 2 apparatus in the study by Jain et al. is a great deal larger than what is seen in the in the GI tract. However, the results in the USP 2 apparatus are a much better predictor of the *in vivo* erosion rates than the results in the USP 4 apparatus. This was not true however for formulation 4 and there is no physiological basis for performing *in vitro* erosion studies under the hydrodynamic conditions of the USP 2 apparatus with the tablet in a stationary basket. Therefore the USP 2 apparatus is not an ideal erosion methodology for developing an *in vitro* extended release polymer tablet erosion study that can better predict *in vivo* results. The next step in developing a better IVIVC methodology for eroding tablets would be to include physiologically relevant parameters that impact the erosion of the polymer tablets. This could be done by incorporating the parameters into either the USP 4 apparatus or a novel apparatus to better simulate the conditions the tablets would be seeing *in vivo*.

Tables

Table 6. 1. HPMC powder components for each tablet formulation

Component		Tablet Formulation			
		#1	#2	#3	#4
Methocel K4M	% (w/w)	23.0	10.0	-	-
Methocel K100LV	% (w/w)	17.0	30.0	40.0	20.0
DI-TAB	% (w/w)	57.6	57.6	57.6	77.6
Sicovit	% (w/w)	1.4	1.4	1.4	1.4
Pruv	% (w/w)	1.0	1.0	1.0	1.0

Figures

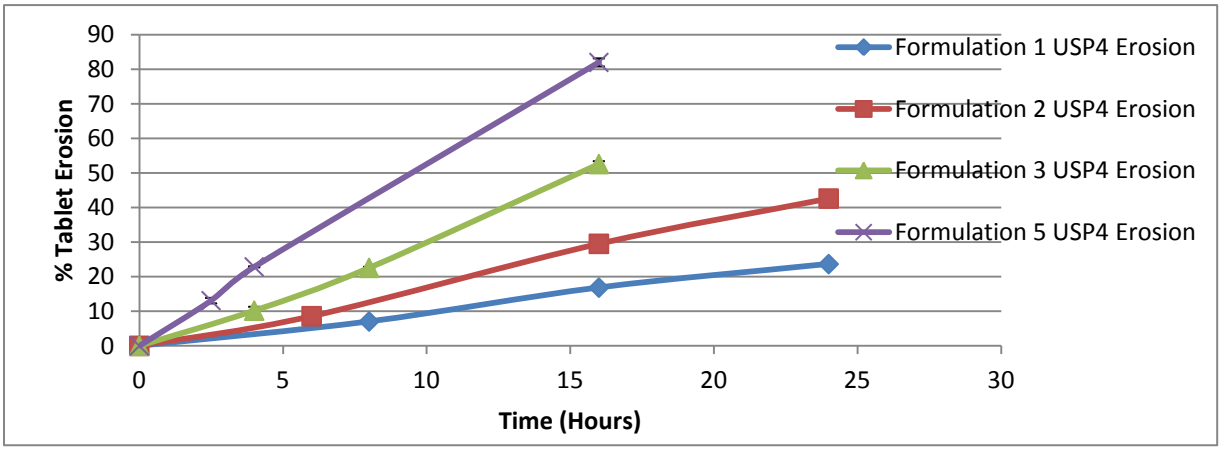

Figure 6. 1. Experimental tablet erosion profiles of the 4 different formulations tested using the USP 4 apparatus at a flow rate of 25ml/min

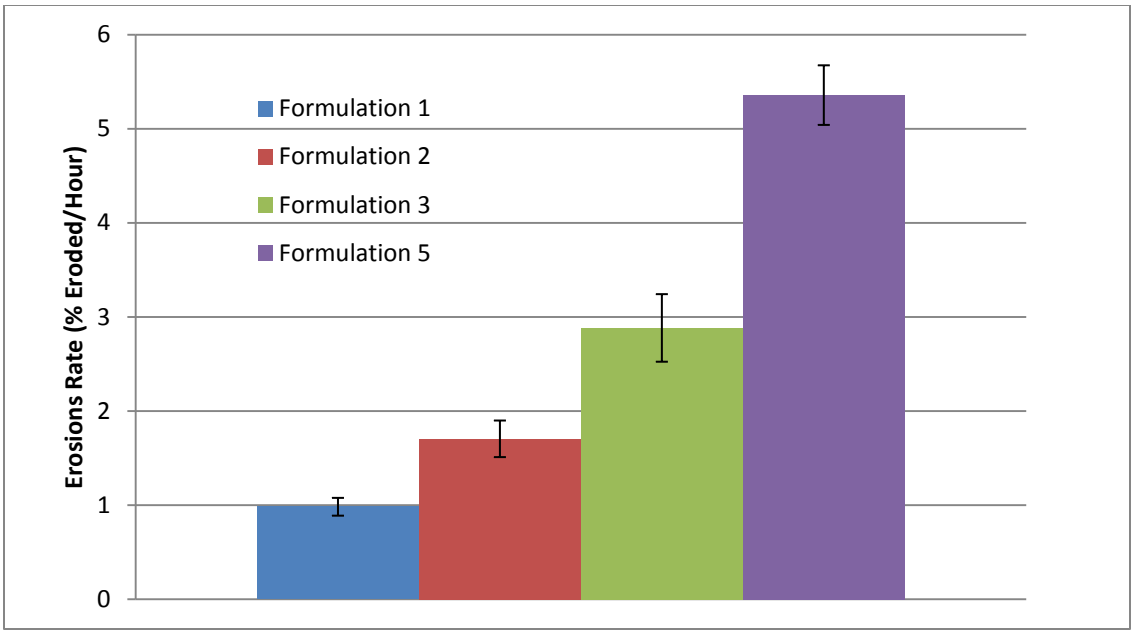

Figure 6. 2. Experimental erosion rates of the 4 different formulations tested using the USP 4 apparatus at a flow rate of 25ml/min

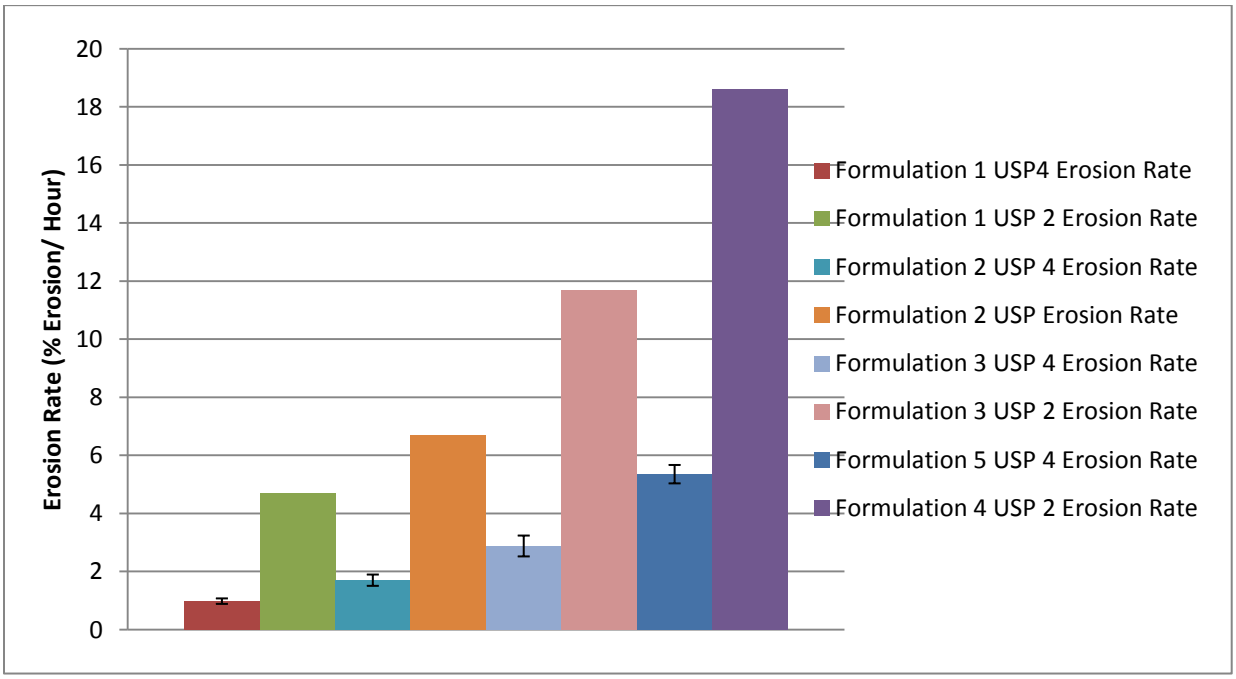

Figure 6. 3. Comparison of the tablet erosion rates for the 4 different formulations tested in vitro using the USP 4 apparatus and the USP 2 apparatus

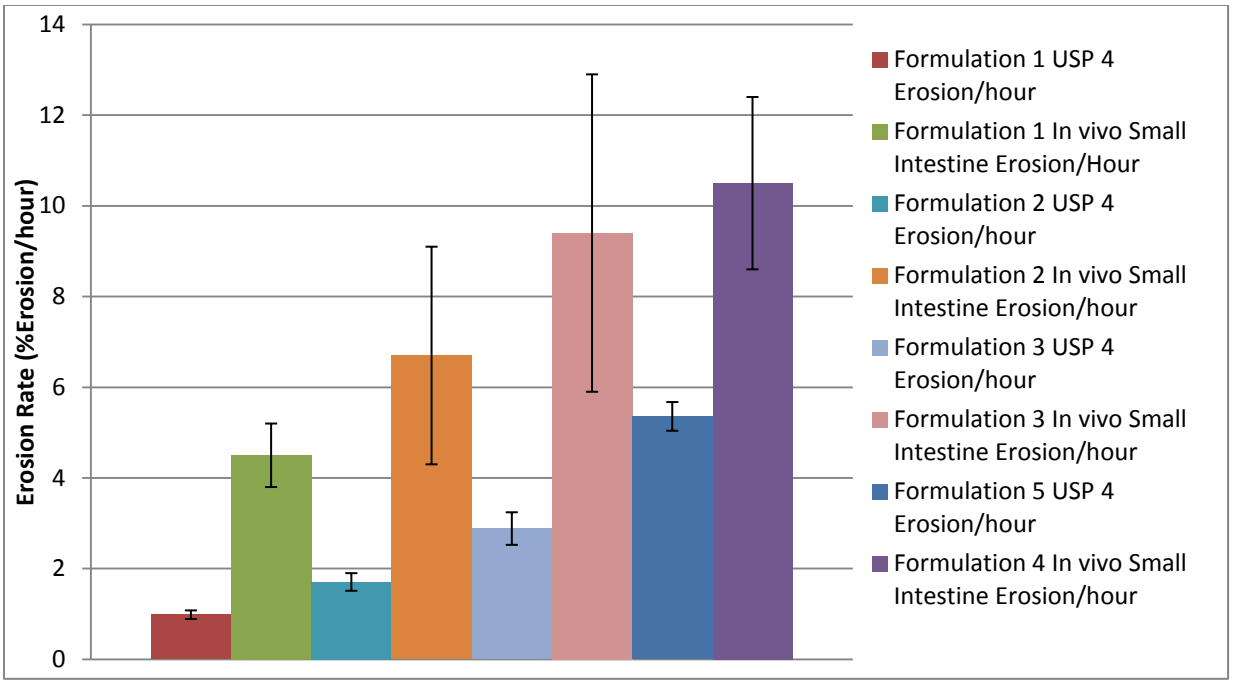

Figure 6. 4. Comparison of the tablet erosion rates for the 4 different formulations tested in vitro using the USP 4 apparatus and in vivo in the small intestine.

References

1. Jain AK, Soderlind E, Viriden A, Schug B, Abrahamsson B, Knopke C, Tajarobi F, Blume H, Anschutz M, Welinder A, Richardson S, Nagel S, Abrahamsen-Alami S, Weitschies W 2014. The influence of hydroxypropyl methylcellulose (HPMC) molecular weigth, concentration and effect of food on *in vivo* erosion behavior of HPMC matrix tablets. Journal of Controlled Release 187:50-58.
2. Abrahamsson B, Alpsten M, Bake B, Larsson A, Sjogren J 1998. In vitro and in vivo erosion of two different hydrophilic gel matrix tables. European Journal of Pharmaceutics & Biopharmaceutics 46(1):69.
3. Ghmire M, Hodges LA, Band J, O'Mahony B, McInnes FJ, Mullen AB, Stevens HNE 2010. In-vitro and in-vivo erosion profiles hydroxypropylmethylcellulose (HPMC) matrix tablets. Journal of Controlled Release 147:70-75.
4. Asare-Addo K, Levina M, Rajabi-Siahboomi AR, Nokhodchi A 2011. Effect of ionic strength and pH of dissolution media on theophylline release from hypromellose matrix tablets - Apparatus USP III, simulated fasted and fed conditions. Carbohydrate Polymers 86:85-93.
5. Akhgari A, Abbaspour MR, Razaee S, Kuchak A 2011. Evaluation of the Swelling, Erosion, and Drug Release From Polysaccharide Matrix Tablets Based on Pectin and Inulin. Jundishapur Journal of Natural Pharmaceutical Products 6(1):51-58.
6. Asare-Addo K, Conway BR, Larhrib H, Levina M, Rajabi-Siahboomi AR, Tetteh J, Boateng J, Nokhodchi A 2013. The effect of pH and ionic strength of dissolution media on in-vitro release of two model drugs oof different solubilities from HPMC matrices. Colloids and Surfaces B: Biointerfaces 111:384-391.
7. Gao P, Meury RH 1996. Swelling of hydroxypropyl methylcellulose matrix tablets. Part 1. Characterization of swelling using a novel optical imaging method. Journal of Pharmaceutical Sciences 85(Jul):725-731.
8. Tajarobi F, Abrahmsén-Alami S, Hansen M, Larsson A 2009. The Impact of Dose and Solubility of Additives on the Release from HPMC Matrix Tablets—Identifying Critical Conditions. Pharmaceutical Research 26(6):1496-1503.
9. Zeng A, Yuan B, Fu Q, Wang C, Zhao G 2009. Influence of sodium dodecyl sulfate on swelling erosion and release behavior of HPMC matrix tablets containing a poorly water-soluble drug. Pharmacetical Development and Technology 14(5):499-505.
10. Asare-Addo K, Levina M, Rajabi-Siahboomi A, Nokhodchi A 2010. Study of dissolution hydrodynamic conditions versus drug release from hypromellose matrices: The influence of agitation of sequence. Colloids and Surfaces B: Biointerfaces 81:452-460.
11. Kavanagh N, Corrigan OI 2004. Swelling and erosion properties of hydroxypropylmethylcellulose (hypromellose) matrices - influence of agitation rate and dissolution medium composition. International Journal of Pharmaceutics 279:141-152.
12. Klancar U, Markun B, Baumgartner S, Legen I 2013. A Novel Beads-Based Dissolution Method for the In Vitro Evaluation of Extended Release HPMC Matrix Tablets and the Correlation wiith the In Vivo Data. The AAPS Journal 15(1):267-277.
13. Asare-Addo K, Kaialy W, Levina M, Rajabi-Siahboomi A, Ghori MU, Supuk E, Laity PR, Conway BR, Nokhodchi A 2013. The influence of agitation sequence and ionic strength on in vitro drug release from

hypromellose (E4M and K4M) ER matrices - The use of the USP III apparatus. Colloids and Surfaces B: Biointerfaces 104:54-60.
14. Wu Y, Ghaly ES 2006. Effect of Hydrodynamic Environment on Tablet Dissolution Using the Flow-Through Dissolution Apparatus. Pharmacology 25(1):75-83.
15. Williams HD, Nott KP, Barrett DA, Ward R, Hardy IJ, Melia CD 2011. Drug Release from HPMC Matrices in Milk and Fat-Rich Emulsions. Journal of Pharmaceutical Scienes 100(11):4823-4835.
16. Meulenaar J, Keizer RJ, Beijnen JH, Schellens JHM, Huitema ADR, B N 2013. Development of an Extended-Release Formulation of Capecitabine Making use of in-vitro. J Pharm Sci 103:478-484.
17. Macha S, Yong C-L, Darrington T, Davis MS, MacGregor TR, Castles M, Krill SL 2009. I*n Vitro - In Vivo* Correlation for Nevirapine Extended Release Tablets. BiopharmDrug Dispos 30:542-550.
18. Gutzeit A, Patak MA, Weymarn Cv, Graf N, Doert A, Willemse E, Binkert CA, Froehlich JM 2010. Feasibility of Small Bowel Flow Rate Measurement With MRI. Journal of Magnetic Resonance Imaging 32:345-351.
19. Diebold SM. 2005. Chapter 6. Physiological Parameters Relevant to Dissolution Testing: Hydrodynamic Considerations. Pharmaceutical Dissolution Testing, ed.